UNIVERSITÀ DEGLI STUDI DI SALERNO

DIPARTIMENTO DI CHIMICA E BIOLOGIA "A. ZAMBELLI"

Towards new catalysts for polymerization of ethylene and copolymerization of ethylene with carbon monoxide: a rational design approach.

Doctoral thesis

Submitted by:

Maria Voccia

Supervisor:

Prof. Lucia Caporaso

Co-Tutor

Dr. Laura Falivene

Coordinator:

Prof. Claudio Pellecchia

Salerno, November 2022

Alla mia metà:

Quella che riempie il bicchiere semipieno.

Abstract

The steric and the electronic environment are the fundamental parameters that define the catalytic properties of any active site. For late transition metal catalysts, they determine polymer molecular weight and branching in ethylene polymerization as well as in the ethylene-CO copolymerization, and consequently the final properties of the resulting materials. Among the late transition metal catalysts active in the ethylene polymerization, an interesting class of compounds is represented by Ni(II) salicylaldiminato complexes. Moreover, more recently Ni(II) phosphine phenolate complexes revealed to be interesting for both ethylene polymerization and ethylene-CO copolymerization reactions.

For salicylaldiminato complexes, although a rather conclusive picture on the importance of substituents bulk that already exists, designing the target active site was still a challenge.

To this end, a defined steric environment of the active site and the controlled manipulating of the electronic properties for new emerging catalytic systems is essential for a complete understanding of the catalysts' behaviour.

For salicylaldiminato complexes, these aims were achieved:

- by means of the introduction of a further ancillary imine donor that serves also as an additional binding site;
- through the incorporation of a bridging proton N···H^+···O between the two binding sites;
- by means of a cage around the metal centre.

The resulting catalysts proved to be promising candidates to obtain products whose microstructure is strictly dependent on the catalyst structure, ranging from high- molecular-weight polyethylene to oligomers.

For the Ni(II) phosphine phenolate complexes, the same issues were addressed:

- by means of the introduction of a bis-phenyl substituent on the ancillary ligand that provides a suitable and modulable steric and electronic contribution;
- through different nature of remote substituents on the bis-phenyl moiety.

These complexes in addition to being promising candidates to obtain polyethylene-based products with different microstructures, proved to have a peculiar structure. It favours the formation of in-chain-functionalized polyethylenes with a desirable property profile (i.e. low content of CO) for the unique ethylene-CO co-polymerization reaction.

The aims of this thesis were reached by means of quantum mechanical DFT (Density Functional Theory) calculations and by a close collaboration with the experimental group of Prof. Stefan Mecking at the University of Konstanz, which provided the synthesis and characterization of catalysts and of polymerization reactions.

Publications.

Parts of this thesis have been published. Journal Publications:

- Voccia M.; Schiebel E.; Falivene L.; Caporaso L.; Mecking, S. ACS catalysis, 2021, 11, 5358-5368 "*The Impact of Charge in a Ni(II) Polymerization Catalyst*"
- Voccia M.; Schiebel E.; Falivene L.; Schnetmann I. G.; Caporaso L.; Mecking, S. ANIE, 2021, 11, 5358-5368 "*Neutral Unsymmetrical Coordinated Cyclophane Polymerization Catalysts*"
- Voccia M.; Odenwold L.; Li F.; Baur M.; Falivene L.; Caporaso L.; Mecking, S. JACS,2022, "*Mechanistic Insights into Ni(II)-Catalyzed Non-alternating Ethylene–Carbon Monoxide Copolymerization*"

Parts of this thesis not yet published. Journal Publications:

- Voccia M.; Lin F.; Odenwald L.; Schnetmann I. G.; Falivene L.; Caporaso L.; Mecking S. Manuscript in preparation "*Beyond Axial Shielding: Role of Weak Interaction in Ethylene Polymerization by Phosphinophenolato Ni(II) Catalyst*"

Other type of publications:

- Pierri G.; Corno M.; Macedi E.; Voccia M.; Tedesco C.; *Cryst. Growth Des.* 2021, 21, 2, 897–907 "*Solid-State Conformational Flexibility at Work: Energetic Landscape of a Single Crystal-to Single Crystal Transformation in a Cyclic Hexapeptoid.*"
- Paderni D.; Giorgi L.; Voccia M.; Formica M.; Caporaso L.; Macedi E.; Fusi V.; Chemosensors 2022, 10, 188. "*A new benzoxazole-based fluorescent macrocyclic chemosensor for optical detection of Zn^{2+} and Cd^{2+}*"
- Ritacco I.; Voccia M.; Impemba S.; Camellone M. F.; Milione S.; Caporaso L.**;** EurJIC 2022. Accepted. "*Electronic and steric effects on L-Lactide Ring-Opening polymerization with NSSN-type Zr(IV) Complexes*"

Poster Presentations:

- Poster Presentation on CIS2019: Chemistry meets Industry and Society, 28-30 August 2019 Salerno. Title: "Control of chain walking by tailoring the strength of neighboring group interactions switches polymerization to dimerization catalysis";
- Poster presentation on XXI National congress of Industrial chemistry division 27 August 2019 Salerno. Title: "Mechanistic insights into the Pd-catalyzed intermolecular alkyne hydroarylation reaction: the role of the ligand on activity and selectivity unveiled."

Oral Communications:

- Oral communication as Invited Speaker at "2nd 2021 Global Conference on Polymers, Plastics and Composites (PPC-2022)" 04-05 October 2022 London, UK (Online). Title: "Mechanistic Insights on Ethylene Polymerization with Ni(II) Catalysts: the impact of the ligand on the polymer microstructure.";
- Oral communication on "Macrogiovani 2021" 22-23 July 2021 Genova. Title: "The Impact of Charge in a Ni(II) Polymerization Catalyst";

- Oral communication on “Online Workshop I Giovani e la Chimica in Abruzzo" 5-6 July 2021 (Online). Title:” The Impact of Charge in a Ni(II) Polymerization Catalyst”.

Table of Contents

List of Abbreviations

AN acrylonitrile
BAr_{F4}- B-(3,5-$(F_3C)_2C_6H_3)_4$
BHE β-H elimination
CO carbon monoxide
CV cyclic voltammetry
DFT density functional theory
DSC differential scanning calorimetry
early-TM early transition metal
GC gas chromatography
GPC gel permeation chromatography
h hours
HDPE high-density polyethylene
late-TM late transition metal

LDPE low-density polyethylene
LLDPE linear low-density polyethylene
MA methyl acrylate
min minute(s)
MMA methyl methacrylate
M_n number average molecular weight
M_w weight average molecular weight
M_w/M_n molecular weight distribution
M_v viscosity average molecular weight
NBO natural bond orbital
Ni(II) Nickel
NMR nuclear magnetic resonance
ORTEP oak ridge thermal ellipsoid plot
Pd(II) Palladium
PE polyethylene
py pyridine
PS polystyrene
rds rate determining step
r.t. room temperature
T_g glass transition temperature
THF tetrahydrofuran
T_m melting temperature
TON turnover number
TOF turnover frequency
TS transition state
Vac vinyl acetate

vdW van der Waals
vs. Versus

Chapter 1
General introduction

1.1 Polyethylene and polyketones.

Plastics are essential in our modern civilization due to their versatility.[1] Frequently, they are the materials of choice for a wide range of applications because of their adaptability, low cost, and bioinertness.[1] Actually, in the last decade, the world plastic production has grown by 265 Mt (2011) to 368 Mt (2021), with polyethylene (PE) accounting for more than 100 million tons.[2-3] The versatility of polyethylene is the result of the accessibility of different microstructures of the polymeric chain. In fact, polyethylene is produced in three main forms: low density polyethylene (LDPE) (< 0.930 g cm^{-3}), linear low-density polyethylene (LLDPE) (ca 0.915-0.940 g cm^{-3}) and high-density polyethylene (HDPE) (ca 0.940-0.965 g cm^{-3}), Scheme 1.1.[4]

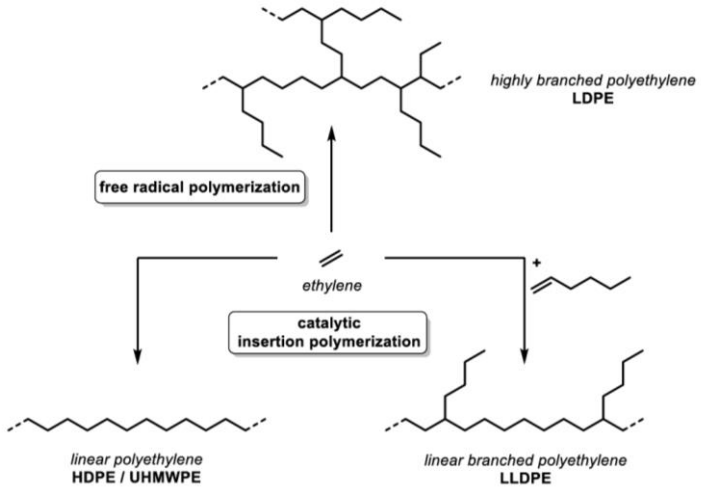

Scheme 1.1: Schematic microstructure of different types of polyethylene.

LDPE is produced since 1940 by free-radical polymerization of ethylene at high pressure (1000-3000 atm) and moderate temperature (420-570 K).[5] Due to inter- and intramolecular radical transfer reactions, LDPE ($T_m \approx$ 110°C, $T_g \approx$ -110°C)[4] contains short and long-chain branches (Scheme 1.1), hence, a precise microstructure control cannot be achieved in these conditions.[5] The crystallinity of the material strongly depends on the branching which in turn affects the density of the produced species.[4] As a result, the LDPE is a soft material with a low melting point and low density. In contrast to radical polymerization, for the first time the synthesis of linear polyethylene, i.e. HDPE ($T_m \approx$ 131°C, $T_g \approx$ -110°C)[4], was achieved by using Ziegler-Natta catalytic systems[6] *via* an insertion polymerization process under mild reaction conditions. The controlled chain growth leads to a highly linear microstructure, resulting in high crystallinity, mechanical strength and high density of the obtained polymer.[6]

If α-olefins, like 1-butene, 1-hexene or 1-octane, are used as comonomers, the latter are incorporated in the linear polymeric chain giving short-chain branches and resulting in a different material, namely LLDPE (in Scheme 1.1, $T_m \approx$ 122°C, $T_g \approx$ -110°C)[4]. The type and ratio

of the comonomer enables custom-made properties like flexibility, chemical resistance, ductility and durability.[4,7] Due to its high ductility and low production cost, LLDPE is largely used for short lived plastics like packaging, foils, plastic-bags. According to a recent market research,[8] its sales will increase by an average of 4.1% per year worldwide through 2026.

Despite of the remarkable qualities of these materials, in the current time an improper use of plastics is politically discussed due to their negative impact on the environment:[9–14] PE is a material hydrophobic, nonpolar and poorly degradable in the environment.[15] Over the last 20 years there is a growing interest both in academia and industry to discover cheap and eco-friendly alternatives for PE. The introduction of polar groups in the hydrocarbon chains could help overcome problems related to the environmental resistance and enhance the polymer reactivity. Keto-modified polyethylenes with a non-alternating distribution of the comonomers (see Scheme 1.2-B) might be an interesting alternative, since, as demonstrated by Hartley and Juliet in 1967, they are photochemically degradable through type I and II Norrish reactions.[16,17]

It was reported that low contents of carbon monoxide (CO) in the polyethylene chain allow to improve the photodegradability but otherwise retaining characteristic PE properties, such as the crystallinity.[18]

In detail, for the products of the ethylene-carbon monoxide (E-CO) copolymerization two possible polymeric structures can be obtained, alternating polyketone, Scheme 1.2-A, and non-alternating polyketone, Scheme 1.2-B.[19-20]

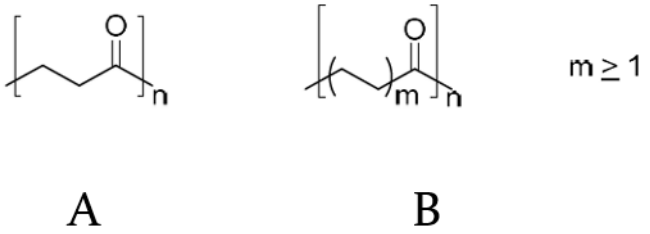

Scheme 1.2: Structure motifs of alternating and non-alternating polyketones.

Alternating polyketones show a microstructure largely different from that of PE resulting in different properties.[19] Due to their crystallinity, they are highly brittle and suffer from low processability because of a high melting point ($T_m \approx 260$ °C).[19] Thus, to obtain a melt-processible material, a third monomer like propylene or higher 1-alkene can be added leading to the formation of terpolymers.[20-21]

Alternatively, the problem of processibility of alternating polyketones as well as the drawbacks of crystalline polyethylene materials can be considerably overcome by reducing the CO content in the copolymer, i.e. producing non-alternating copolymers, Scheme 1.2-B. The resulting isolated keto groups in the polyethylene chain (non-alternating polyketones) provide an improvement of the reactivity in terms of degradability, both for branched low-density polyethylenes and for linear polyethylenes.[22-25]

A radical process could be employed for the synthesis of such non-alternating copolymers, however, it provides branched chains.[26] In fact, in free-radical growth, the low reactivity of the acyl radicals formed upon incorporation of CO hinders further chain growth and favours

the formation of oligomers rather than PE materials.[27] Thus, a precise microstructure and the control of the content of incorporated CO functions is difficult to achieve using a radical process.[28] Alternatively, as for other type of copolymers,[29] the keto- modified PE could be obtained with a post-functionalization of PE by an additional partial oxidation step performed after the ethylene polymerization. Nevertheless, it requires a further synthetic step in which it is difficult to control both the incorporation of CO and the selection of the ketone functional groups.[30-32] Finally, PEs with in-chain keto groups can be generated through a one-step reaction by incorporation of carbon monoxide comonomer via a catalytic insertion polymerization of ethylene.[33-34] This method has the advantage to allow a better control over the microstructure and molecular weights of produced polymers. The study of polymerization catalysis of these materials is one of the focus of this thesis.

1.2 Transition Metal Catalysts for Ethylene Homo-polymerization.

The first catalytic systems active in the synthesis of high molecular weight polyethylene via insertion polymerization were based on early Transition Metal (early-TM).[35-36] The origin of this finding dates back to 1955 when Ziegler discovered that some transition-metal compounds, i.e. $TiCl_4$, used in combination with aluminum alkyls, polymerize ethylene into linear polyethylene at unprecedented low pressures.[6] Nowadays, both HDPE and LLDPE are produced by catalytic insertion polymerization with early transition metals (Zr, Ti, Cr, V) based on the Ziegler-Natta and Phillips catalysts.[36-38]

Although on an industrial scale the polyolefins are principally produced using these multi-site catalysts, there is a growing market for single-site catalysts for polyolefins, i.e. metallocenes, post and non-metallocenes early-TM catalysts, which lead to products with a more defined microstructures, controlled molecular weight distributions and superior mechanical properties.[39-40]

In contrast to the early-TM, the late transition metal (late-TM) catalysts usually yield dimers or oligomers because of the propensity of the complexes for chain transfer reactions via β-Hydride Elimination (BHE) reaction, see Scheme 1.3. A prominent example is the Shell Higher Olefin Process (SHOP) that leads to linear α-olefins by nickel-catalyzed oligomerization of ethylene (for more detail on SHOP process see section 1.2.5).[41-42]

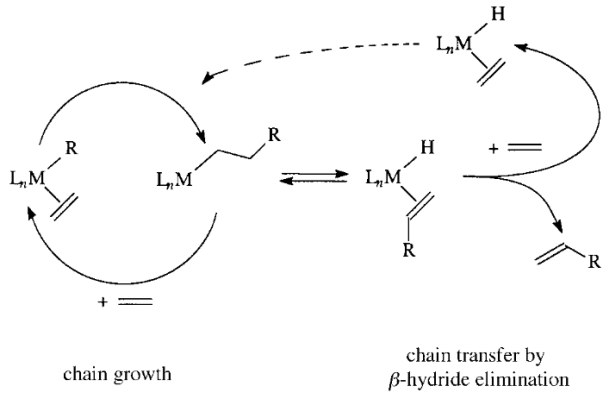

Scheme 1.3: Simplified schematic representation of ethylene oligomerization and polymerization promoted by transition metal (M) complexes (R= growing polymer/oligomer chain).

However, it is important to underline that early-TM catalysts exhibit a very high oxophilicity. As a result, they are extremely sensitive towards any monomer containing heteroatoms like oxygen or nitrogen. Therefore, much effort is devoted to the development of new types of catalytic systems based on late-TMs, e.g. palladium and nickel complexes.[43-44]

1.2.1 Pd(II) and Ni(II) complexes.

Late-TM complexes such as palladium (Pd(II)) and nickel (Ni(II)) based catalysts (see Scheme 1.4) proved to be the most promising ones due to their ability to tolerate functional-groups. This allows for the synthesis of functionalized polyolefins with various polymer architectures,[45-55] with a less sophisticated purification of feed and solvent needed, and the possibility to use polar media.[56]

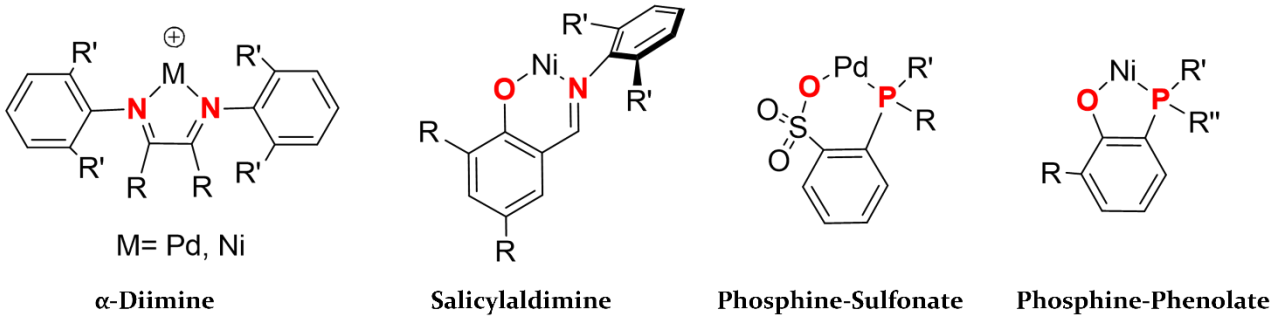

Scheme 1.4: Late TM catalysts used as (Co)-Polymerization reactions.

Among the most used systems, the cationic catalytic systems α-diimine Ni(II) and Pd(II) should be mentioned. However, in recent years, Ni(II) neutral salicyladiminate N,O catalysts and P,O-type neutral catalysts mainly comprising Pd(II) phosphine-sulfonate and Ni(II) phosphine-phenolate catalysts, have received more attention, see Scheme 1.4.[45]
These catalysts have been extensively studied both in the homo-polymerization of ethylene and in copolymerization of ethylene with polar monomers, such as methyl acrylate (MA), methyl methacrylate (MMA), vinyl acetate (Vac), acrylonitrile (AN) and vinyl halides.[45]
As for the non-alternating ethylene-CO copolymerization, Pd phosphine-sulfonate and Ni phosphine-phenolate complexes gave remarkable results.[57,86,98]
In this thesis an in-depth mechanistic study on the polymerization of E-CO in the presence of these catalytic systems will be discussed with the aim of understanding the relationship between the polymer microstructure and the electronic and steric features of the catalyst.

1.2.2 Cationic Pd(II) and Ni(II) α-Diimine catalysts for homo-polymerization of ethylene.

In 1995 Brookhart reported a series of cationic Pd(II) and Ni(II) α-diimine complexes extremely active in the homo-polymerization of ethylene (Scheme 1.5). These late-TM catalysts show a reactivity in line with that of early-TM catalysts, giving polymers with high molecular weight.[57-58]

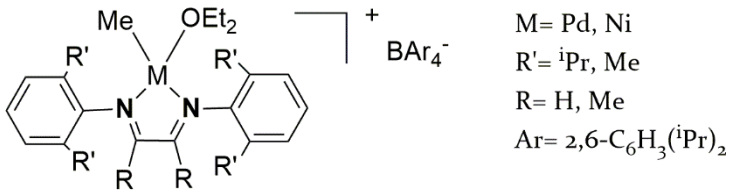

Scheme 1.5: Cationic Pd(II) and Ni(II) α-diimine complexes reported by Brookhart.

The overall mechanism for ethylene polymerization is depicted in Scheme 1.6.[59] Under Brookhart conditions, the olefin alkyl complex **A1** was found to be the resting state, whereas the rds of the polymerization is the insertion of ethylene in the nickel alkyl bond. This barrier is highly dependent on the steric bulk of the ligand: a great steric bulk increases the energy of the resting state **A1**, resulting in a lower barrier for insertion.[60-61] Overall the mentioned barrier for ethylene insertion results to be significantly lower for the nickel complexes than for the palladium analogues accounting for their much higher activity in ethylene polymerization.[60]
Following the migratory insertion step, a 14-electron alkyl complex **A2** with a β-agostic interaction is formed. Coordination and insertion of a second molecule results in linear chain propagation. Alternatively, the β-agostic complex **A2** can also undergo β-hydride elimination resulting in the formation of the hydride olefin complex **A3**. After rotation of the olefin and reinsertion in a 2,1-fashion, i.e. from **A2** to **A4**, subsequent insertion of ethylene introduces a methyl branch, see **A5** complex. A series of β-hydride elimination, rotation, and reinsertion results in a 'walking' of the metal centre along the polymer chain and introduces longer alkyl branches, e.g. **A6** and **A7** species.
Depending on the ligand structure, the nature of the metal and the reaction conditions, the polyethylene microstructure can exhibit short or long chain branches as well as branches on branches, i.e. a so-called 'hyperbranched polymer'.[58-59]

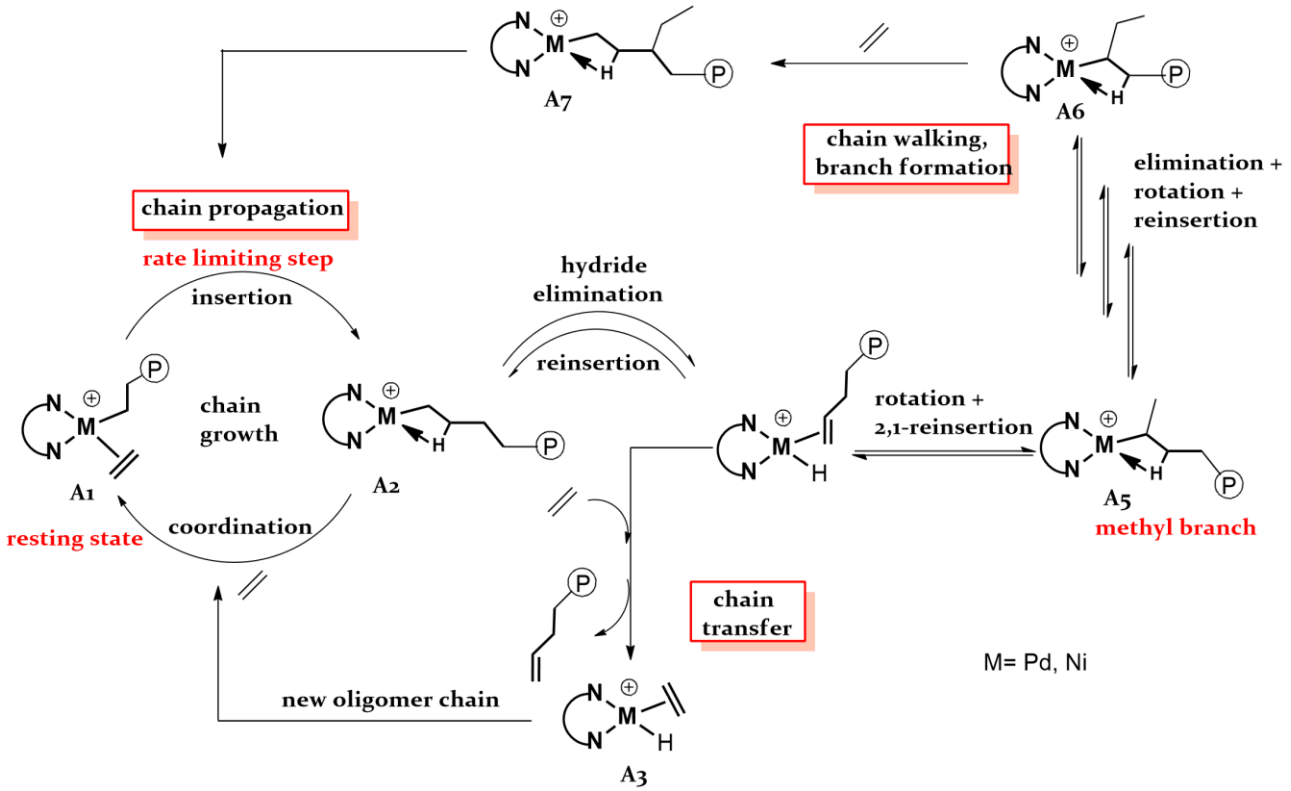

Scheme 1.6: Mechanism of ethylene polymerization in presence of α-diimine catalysts.

Thus, for the first time, these Ni(II) and Pd(II) α-diimine catalysts made possible the access to highly branched, amorphous polyethylene *via* a controlled catalytic insertion mechanism. Additionally, due to their lower oxophilicity and higher functional group tolerance than early-TMs, these catalysts allowed the copolymerization of ethylene with polar vinyl monomers, such as methyl acrylate.[58] Nevertheless, one limitation is their high sensitivity to temperature, i.e. the Pd(II) α-diimine complexes[62] decompose at 50 °C and the Ni(II) α-diimine ones[63] at 70°C. The M_W of the PEs formed by Ni(II) catalysts also decreases precipitously as the temperature of polymerization is raised.[7] Since gas phase olefin polymerizations typically take place at temperatures between 80–100°C,[64] these issues hindered the commercialization of these catalysts.

1.2.2.1 Cyclophane based catalysts.

The α-diimine based catalysts can be easily modified by changing the nature of its substituents on the two *N*-donors, Scheme 1.7. Since it was reported that bulky *N*-aryl substituents suppress chain transfer reactions by blocking axial positions at the metal centre,[45,57,65] PE with high molecular weights were obtained through a cyclophane structure, see Scheme 1.7-B.[66-67] Cyclophanes are ring structures consisting of alkyl chain and phenyl units.[68-69] The first α-diimine cyclophane complex was synthesized by the group of Guan and has two methylene groups bridging the outer aryl units of the two terphenyl groups, see again Scheme 1.7-B.[70]

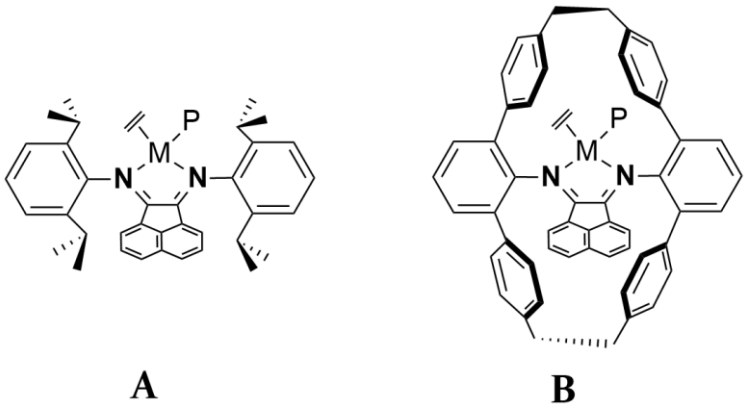

Scheme 1.7: Comparison of the acyclic with cyclophane based Ni(II) α-diimine catalysts.

Compared to the acyclic α-diimine based catalyst (Scheme 1.7-A), the Ni(II) cyclophane catalyst (Scheme 1.7-B) showed an increased stability at higher temperatures producing polymers with slightly increased molecular weight and a significantly higher branching density.[70-71] The unexpected result related to the microstructure was explained with a different chain transfer process.[71] The generally accepted mechanism for chain transfer for square-planar d^8 complexes consists in an associative olefin substitution process. In detail, a free olefin monomer coordinates to the alkyl intermediate giving a pentacoordinate species, and then in a second step the polymeric chain bound to the metal centre is displaced, see Scheme 1.8.

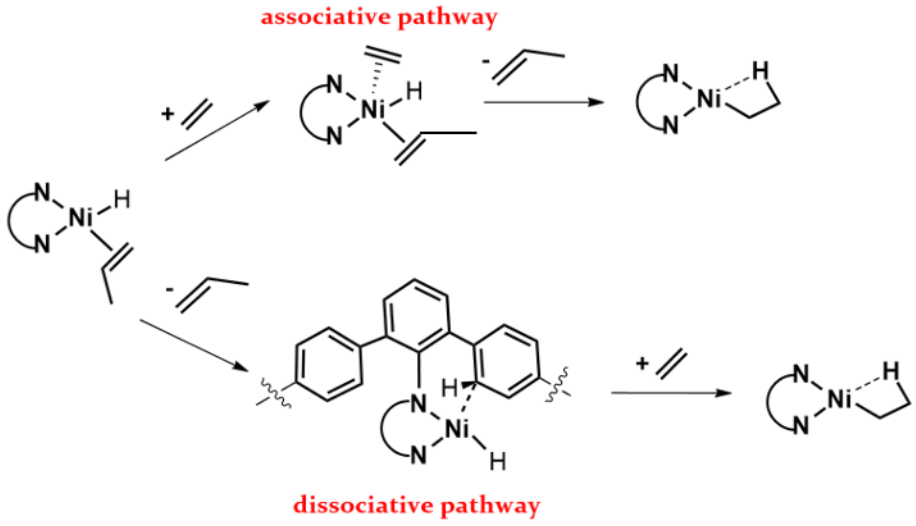

Scheme 1.8: Schematic representation of the chain transfer mechanisms operating for the acyclic (associative pathway) and cyclophane-based α-diimine catalysts (dissociative pathway).

Alternatively, cyclophane α-diimine catalysts can promote a dissociative pathway (Scheme 1.8). This event is thermodynamically favoured by electronic stabilization of the coordinatively unsaturated M-hydride intermediate via an axial agostic interaction from the ligand to the metal, see Scheme 1.9.[71]

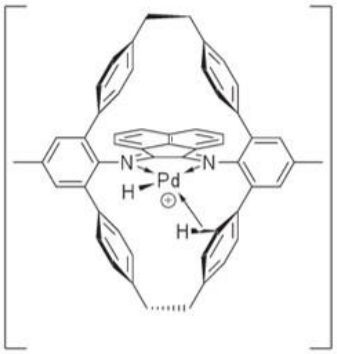

Scheme 1.9: Intermediate related to the dissociation of the olefin-terminated polymer along the chain transfer reaction via a dissociative pathway.

1.2.3 Neutral Ni(II) Salicyaldiminate catalysts for homo-polymerization of ethylene.

Driven by the potential of the α-diimine ligands, Johnson at the DuPont and Grubbs, independently, reported a series of neutral nickel complexes with anionic *N,O*-ligands that showed to be very active in the polymerization of ethylene.[72-74]

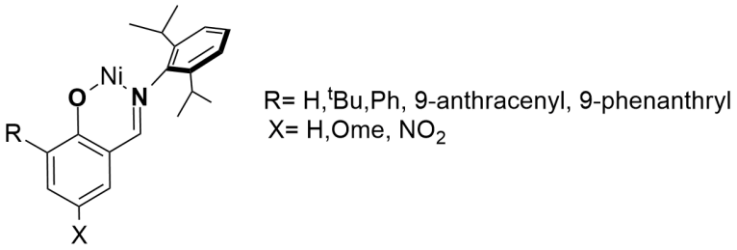

Scheme 1.10: Neutral Ni(II) salicyaldiminate complexes.

At low temperature and pressure (7 °C and 10 bar), salicyaldiminate-based catalysts (see Scheme 1.10)[75] promote the formation of linear polymers with a high tolerance for solvents containing heteroatoms, i.e. diethyl ether, THF, and for H_2O or other protic compounds,[75-77] allowing also the advantageous polymerization in aqueous emulsion. The latter process consists in the dissolution of the catalytic precursor in water with the formation of a lipophilic active species that undergoes a phase transfer favouring the polymerization into a micelle.[77]
Recent studies on the ethylene polymerization promoted by Ni(II)-salicilaldiminate compounds have revealed a significant impact of the nature of the ligand substituents. From these studies it emerges that the catalytic behaviour and the properties of the obtained materials can be finely tuned tailoring the steric and electronic properties of the ligands.[78-79]
In detail, it was demonstrated that the remote substituents on the terphenyl moiety of the 2,6-diphenylanilines influence both the molecular weight and the microstructure of the polymer severely: electron-donating substituents (e.g. R = $-CH_3$ or $-OCH_3$) lead to low molecular weight branched polymers or oligomers, whereas electron-withdrawing

substituents, such as R = -CF_3 or -NO_2, give polymers with high molecular weights and low amount of branching, Scheme 1.11.[80-84]

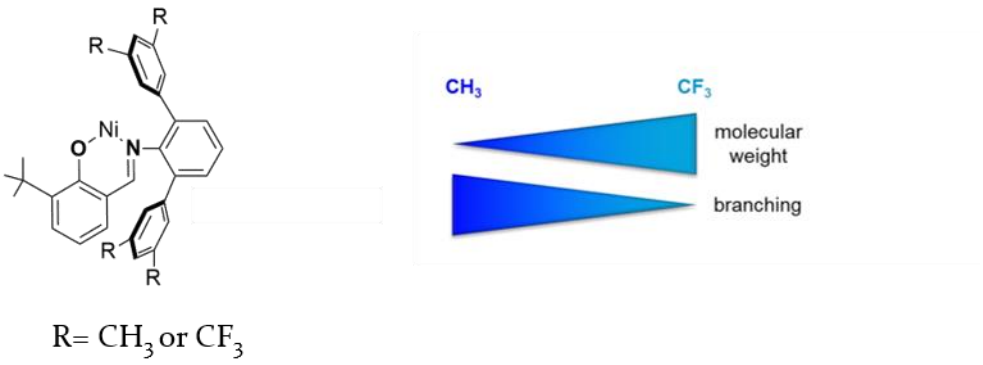

Scheme 1.11: (A) Neutral salicyaldiminato Ni(II) complexes, containing a substituted terphenyl moiety and (B) influence of the remote substituents on polymer microstructure obtained in ethylene polymerization.

In conclusion, these catalysts allowed the access to a wide range of PE microstructures under identical reaction conditions. The origin of the so-called '*remote substituent effect*' was extensively investigated by DFT calculations, as reported in Scheme 1.2.[83-84]

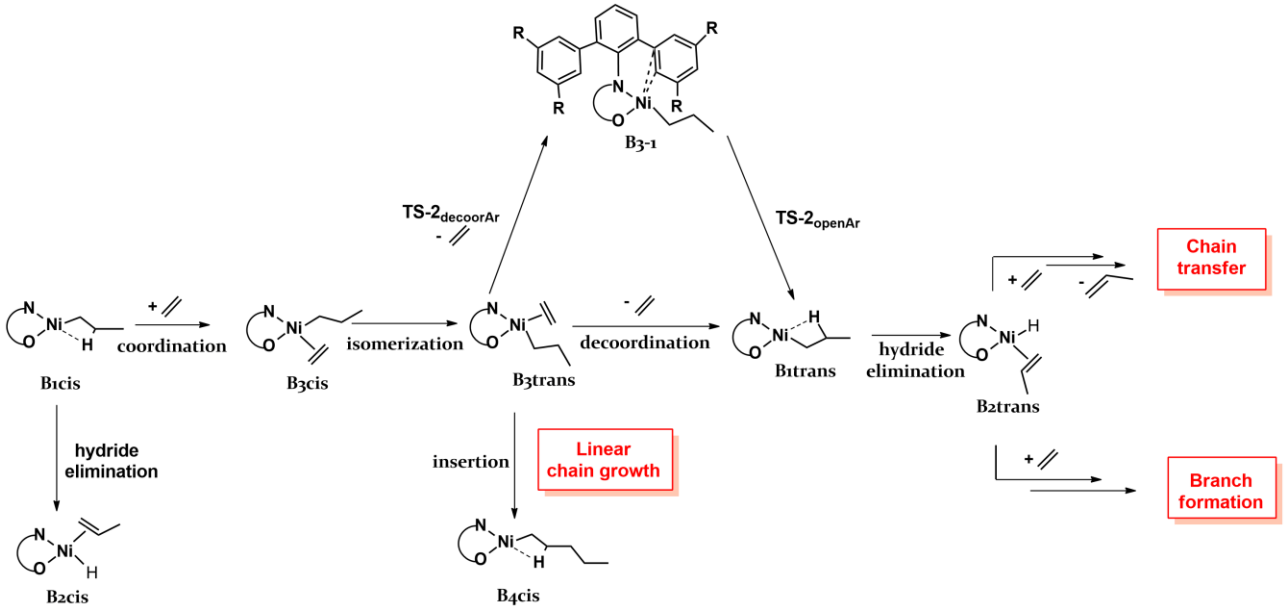

Scheme 1.12: Mechanism of ethylene polymerization for N,O salicyaldiminate Ni(II) complexes.

The Ni-alkyl species with a β-agostic interaction (**B1cis**) obtained from the first ethylene insertion into the Ni-Me bond of the precatalyst, was considered as the reference intermediate. From this intermediate with the alkyl group *trans* to the oxygen atom, BHE (Beta-Hydrogen Elimination reaction) leads to **B2cis** species that is disfavoured due to a high energy barrier. Instead, ethylene coordination and isomerization to **B3trans** is preferred.

From **B3trans** species, ethylene insertion, and therefore linear chain growth, takes place leading to **B4cis**. Ethylene insertion results to be the rate determining step (rds) of this pathway.
Alternatively to the linear chain growth pathway, ethylene decoordination leading to **B1trans** is also possible opening the way to BHE reaction. The dissociation step can take place in one step reaction or alternatively in two-step reaction assisted by a Ni-aryl interaction (see **B3a** species). The preference between the two paths depends on the remote substituents present on the terphenyl moiety. The two-step reaction is favoured for electron-rich terphenyl groups, i.e. in presence of groups like -CH_3 and -OCH_3. For electron-poor terphenyls with R = -CF_3, -NO_2, the Ni-aryl interaction is not strong enough and the direct pathway is favoured.
Considering that the insertion reaction is not affected by the substituents on the terphenyl ring, when the two-step decoordination pathway takes place, the formation of the **B1trans** isomer is favoured.
From **B1trans**, BHE can take place enabling branch formation and chain transfer pathways. Overall, the Ni-aryl interaction gives a low energy decoordination pathway and thus, the catalysts with electron-rich terphenyls are more prone to give BHE and consequently branch formation and chain transfer reactions compared to electron poor ligand substituted catalysts. This directly explains the low molecular weight and highly branched products obtained for the catalyst with -CH_3 (or -OCH_3) groups and consequently the linear, high molecular weight products for catalyst with electron-poor terphenyl groups.[84]

1.2.4 Neutral Pd(II) Phosphine Sulfonate catalysts for homo-polymerization of ethylene.

In the same years in which Brookhart reported the cationic Pd(II) and Ni(II) α-diimine complexes, several patents have been filed for Pd(II) phosphine-sulfonate ligand-based polymerization catalysts, see Scheme 1.13.[45,85-87]

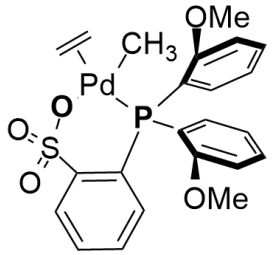

Scheme 1.13: Neutral Pd(II) phosphine sulfonate complex.

Following the initial academic report by Drent in 2002,[85] these catalysts have attracted a lot of interest from numerous research groups. These catalysts produce highly linear structures with only a few branches and are active also into the copolymerization with polar comonomers, such as acrylates, producing linear copolymers.[45,87-88]
The mechanism of ethylene homo-polymerization was extensively studied[45,89-90] by Ziegler and Nozaki-Morokuma by DFT calculations, see Scheme 1.14.

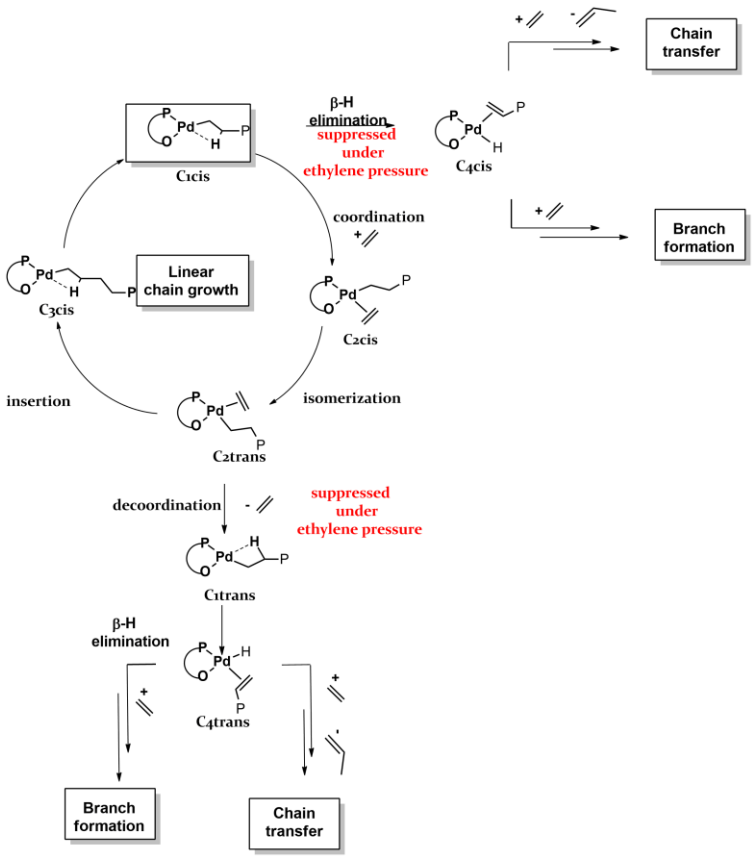

Scheme 1.14: Mechanism for ethylene homo-polymerization with Pd(II) phosphine-sulfonate complexes.

As previously reported for the Ni(II) salycialdiminato complexes, starting from the Pd-alkyl chain species **C1$_{cis}$**, with a β-agostic interaction, the catalyst can access the linear chain growth pathway, with the ethylene insertion that represents the rds.

Alternatively, it can promote the BHE elimination, favouring the branch formation and chain transfer pathways. DFT calculations showed that for these Pd(II) phosphine-sulfonate complexes, the energy barrier for ethylene insertion from **C2$_{trans}$**, the BHE elimination from **C1$_{cis}$** and the route to obtain **C1$_{trans}$** *via* ethylene decoordination, are comparable in energy; thus, high concentrations of ethylene favour ethylene insertion, in line with the experimental results.[89-90]

1.2.5 Neutral Ni(II) phosphine phenolate catalysts for homo-polymerization of ethylene.

Another late TM catalyst successfully employed in the homo-polymerization of ethylene is based on the neutral Ni(II) phosphine phenolate complex. These systems are at the base of the Shell Higher Olefin Process, which is still used industrially today. In the SHOP process, a κ^2-P,O Ni(II) complex developed by Keim catalyses the oligomerization of ethylene to α-olefins, Scheme 1.15-A.[91-93]

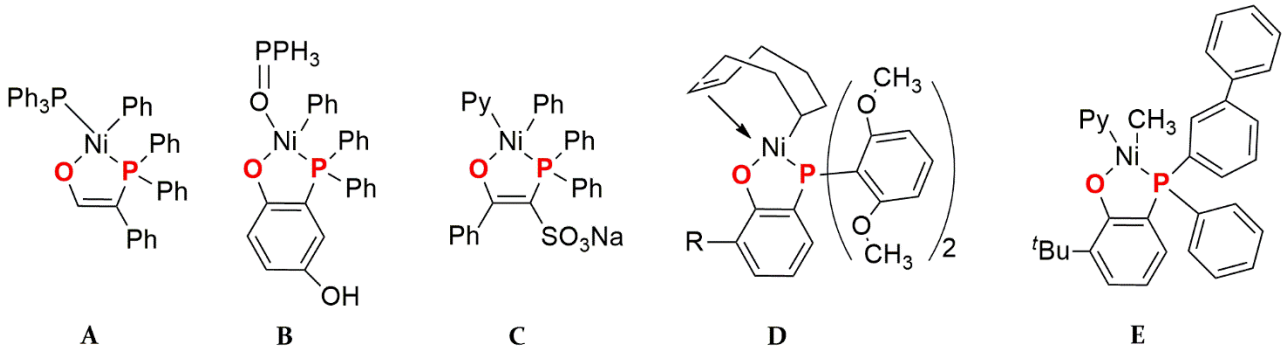

Scheme 1.15: Late transition metal catalysts for ethylene oligomerization and polymerization: SHOP catalyst (left) and modified SHOP catalysts.

As reported in Scheme 1.16, the nickel hydride complex is the active species that can coordinate and insert ethylene to give a nickel alkyl species. After repeated chain growth steps, the system undergoes a chain transfer step, producing the oligomeric product and regenerating the nickel hydride species.[91]

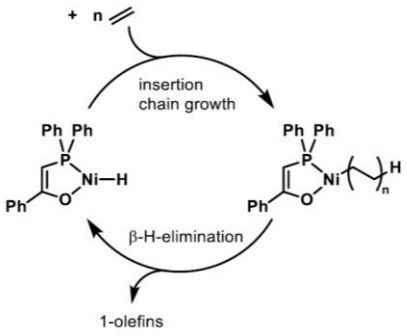

Scheme 1.16: Shell Higher Olefin Process for the synthesis of linear 1-olefins.

Later, Klabunde and Ostoja-Starzewski reported the synthesis of other κ²-P,O ligand Ni(II) catalysts able to favour chain growth over chain termination reactions leading to high molecular weight PE, Scheme 1.15-B and C.[94-96]
Recently, Shimizu team reported a new strategy for obtaining catalysts that disadvantages the BHE reactions, thanks to the interactions between the nickel centre and oxygen atoms on the P-bound ligand, see Scheme 1.15-D.[97] These complexes gave highly linear and high molecular weight copolymers with alkyl acrylates. The microstructure of the resulting copolymers is highly influenced by the structure of the ligand.
Additionally, Li and coworkers[98] reported that the inclusion of a sterically bulky group in the axial position of the metal, see Scheme 1.15-E, reduces the associative chain transfer reactions favouring the linear growth of the polymeric chain, as proposed in Scheme 1.17.[98] The latter complexes showed very high catalytic activities for ethylene polymerization even at high temperature, giving linear polymers with high Mw up to 10^5 g mol^{-1}.[98] Furthermore, they yield high molecular weight linear copolymers with incorporation of various polar monomers, i.e. acrylate and acrylamide, into the polymer chain. The potential of these complexes recently

was also tested for the copolymerization of ethylene with CO. More details are given in the section 1.3.2 and chapter 6.[99]

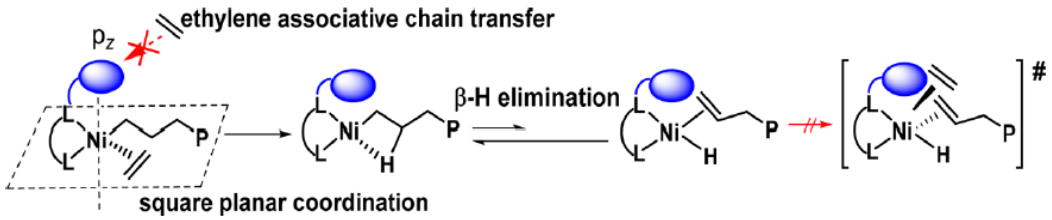

Scheme 1.17: Suppression of chain transfer reaction by introduction of an axially oriented bulky group.[98]

1.3 Transition Metal Catalysts for Ethylene Copolymerization with Carbon Monoxide.

In 1951 was reported for the first time the use of a Ni(II) catalyst for ethylene and CO alternating copolymerization.[100] Since this seminal finding, 40 years of research have passed until the discovery and commercialization by Shell of a class of highly active cationic palladium catalysts.[101-102]

Although numerous studies on the late-TMs mediated copolymerization of ethylene and CO have been reported, most of them afforded strictly alternating copolymers, see Scheme 1.2-A.[102-104] Until recently, there was basically no catalyst providing non-alternating ethylene-CO copolymers, see Scheme 1.2-B.

Only in 2002 Drent reported the first example of non-perfectly alternating copolymerization of ethylene with carbon monoxide via the coordination-insertion mechanism. He demonstrated that a mixture of $Pd(OAc)_2$ and a phosphine-sulfonate ligand led to ethylene-CO non-alternating copolymers with CO contents in the range between 42-49%.[86]

Numerous studies have been carried out since this finding.[105-109] As mentioned above, early-TM catalysts have been excluded as they deactivate in presence of CO. In fact, quenching with CO is an established method for deactivating precisely such olefin polymerization catalysts.[110]

Considering the classes of catalysts mentioned in the previous sections, the cationic Pd(II) and Ni(II) α-diimine catalysts were used for the ethylene copolymerization with CO but the obtained copolymers have a perfectly alternating structure.[111] Thus, in this thesis a detailed discussion of the mechanism for this class of catalysts will be not considered.

As for the Ni(II) salicyaldiminate catalysts, very recently, the catalyst with CF_3 groups as remote substituents has been used also for the ethylene copolymerization with CO.[99] Since that only alternating polyketones were obtained also in this case, a detailed discussion of mechanism for this class of catalysts will be not considered as well.

Conversely, the behaviour of the neutral Pd(II) phosphine-sulfonate and of the Ni(II) phosphine-phenolate catalysts turned out to be unique in ethylene-CO copolymerization reactions.More details are reported in the sections 1.3.1 and 1.3.2 and in the Chapter 6.

1.3.1 Neutral Pd(II) Phosphine Sulfonate catalysts for copolymerization of ethylene with CO.

Until 2021, the Pd(II) phosphine sulfonate complexes, see Scheme 1.13, were the only catalysts suitable for obtaining non-alternating ethylene-CO copolymers with a low content of CO (< 49%).[86] Pd(II) complexes bearing both a phosphinoarylsulfonate (1.18-A) and a phosphinoalkylsulfonate (1.8-B) ligand were found to be active for this type of copolymerization.

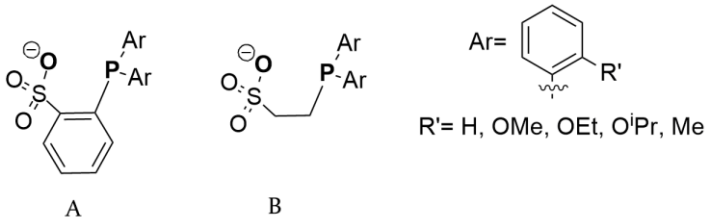

Scheme 1.18: Pd(II) phosphine-sulfonate catalysts employed for the non-alternating copolymerization of ethylene with carbon monoxide.

By altering the reaction conditions, the desired ethylene incorporation ratio can be obtained. For instance, the multiple insertion of ethylene is enhanced by an increase in the ethylene-CO ratio, although the catalytic activity is reduced.[86] The amount of ethylene incorporated into the copolymer was also significantly increased by a tailored modification of the ligand skeleton, i.e. by adding a bulky *o*-alkoxy group such as the *o*-methyl group on the aryl substituent. As a result, it has been possible to produce non-alternating copolymers with as little as 10 mol % CO incorporation with this class of catalysts.[112]

These catalysts gave low molecular weight brittle waxes and no high molecular weight polyketones were obtained despite extensive studies by different joint industrial and academic ventures.

The mechanism of ethylene-CO copolymerization was investigated through experimental[107] and theoretical[108-109] studies. It was demonstrated that it comes *via* a coordination-insertion mechanism in a similar way to what was previously reported for the homo-polymerization of ethylene.[107]

In the study Ziegler compared two systems, i.e. the neutral Pd(II) phosphinoarylsulfonate catalyst (named **Drent** catalyst, Scheme 1.19-A) and the cationic bidentate diphosphine 1,3-bis(diphenylphosphino)propane ligand (**dppp**) based catalyst, see Scheme 1.19-B.[108] For these two systems, the two competitive ways, i.e. alternating (from **D1** to **D5** in Scheme 1.20) and non-alternating pathways (from **D1** to **D3** in Scheme 1.20), were studied.

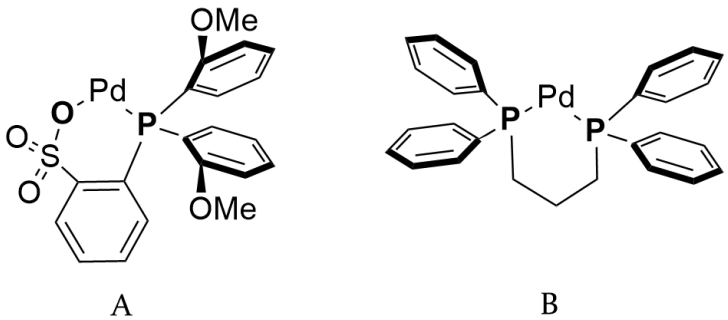

*Scheme 1.19: Schematic representation of the neutral Drent catalyst **A** and the cationic palladium catalyst **B**.*

The stable five membered chelate **D1** obtained *via* a CO insertion followed by an ethylene insertion is the resting state of the ethylene-CO copolymerization reactions. From **D1** formation of multiple ethylene units, i.e. non-alternating copolymers, can be understood as a result of the favored ethylene insertion into this five-membered palladacycle species **D1**, leading to the β-agostic intermediate **D3**. On the contrary, alternating copolymers could be obtained if from **D1** the CO insertion is favored over the ethylene insertion to form the six-membered chelate **D4**. From **D4** only the coordination and insertion of the ethylene unit is possible because the double insertion of CO is thermodynamically and kinetically unfavored.[108-109]

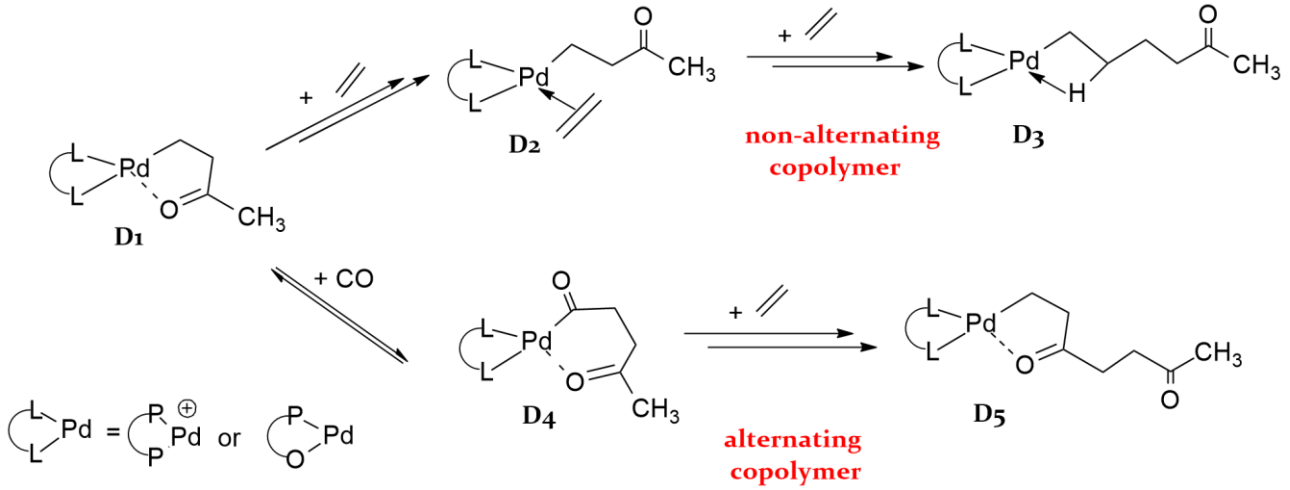

*Scheme 1.20: Mechanism of the alternating and non-alternating copolymerization of ethylene with CO for catalysts **A** and **B**.*

For the **Drent** catalyst, the Pd···O interaction in **D1** and **D4** intermediates is weaker compared to the cationic complex, due to the increased back-donation from the palladium to the monomer for the neutral complex.[108-109] Consequently, the opening of the chelate structures **D1** and **D4** becomes easier for the neutral Pd(II) catalyst compared to the cationic complex.[113] Furthermore, for **Drent** catalyst, the decarbonylation reaction, i.e. CO elimination from **D4** toward **D1**, is more favorable than for the cationic complex. This was also supported by experimental results, i.e. the formation of **D4** was not observed by NMR analyses.[107] In conclusion, the multiple ethylene insertion is possible only for the neutral Pd(II) catalyst, while the cationic Pd(II) **dppp** complex produces strictly alternating polyketone.[108-109]

1.3.2 Neutral Ni(II) phosphine phenolate catalysts for copolymerization of ethylene and CO.

Despite the literature consensus that phosphine-phenolate catalysts are rapidly deactivated by CO[110] and at most form only alternating polyketones with low activity[110], in the last year, the group of Prof. Mecking reported a series of phosphine-phenolate catalysts with bulky substituents on the phenolate moiety (Scheme 1.15-E) able to copolymerize ethylene E-CO mixtures with a very low partial pressure of CO.[99] A substantial amount of high Mw

polyethylene was obtained with the desired low content of keto groups in the chain. The high molecular weights of the keto-modified PEs and the complete absence of branches suggest that the incorporation of CO does not promote any problematic chain transfer reaction.[99]
In this thesis a detailed mechanistic study for this class of catalysts for the E-CO copolymerization reactions is discussed, for more details see Chapter 6.

Chapter 2

Objectives

The steric environment and the electrical properties of the active catalytic sites are the fundamental parameters which define and modulate the catalytic behaviour of a catalyst. Late-TM catalysts allow in most of the cases to achieve a good control of the molecular weight and branching microstructure of the polymers, and consequently of the properties of the obtained materials, both for ethylene polymerization and for ethylene and carbon monoxide copolymerization.
To this end, tailoring the steric environment of the active site and manipulating the electronic properties for new emerging catalytic systems is challenging but also essential for a complete understanding of the catalyst behaviour.
This doctoral thesis addresses some of the essential open issues to rationalize the behaviour of catalysts in development, using molecular descriptors to build structure-activity relationships as a guide toward the rational design of outperforming catalysts.
The aim is reached by means of quantum mechanical DFT calculations and in a close collaboration with the experimental group of Prof. Stefan Mecking at University of Konstanz. In particular, the attention has been focused mainly on two different classes of catalysts, i.e. Ni(II) salicyaldiminato and Ni(II) phosphine-phenolate complexes.

The mechanistic studies carried out are described as the objectives of this thesis

- Chapter 3: Mechanistic study of the homo-polymerization of ethylene promoted by four new 2,6-Bis(arylimino)phenoxy catalysts. The aim of this work was to understand the role of the second imine donor in the ligand and the impact of the charge on the corresponding protonated cationic catalysts.

- Chapter 4: Mechanistic study of the homo-polymerization of ethylene promoted by new neutral bis(imino)phenoxy complex bearing an asymmetrical cyclophane ligand. The aim of this study was to understand if the steric environment of the peculiar cyclophane architecture plays a key role in affecting the polymer microstructure.

- Chapter 5: Mechanistic study of the homo-polymerization of ethylene promoted by two Ni(II) phosphine phenolate complexes which differ in the remote substituents present on the bis-phenyl moiety. The aim of this study was to understand how the electronic nature of the substituents influences the microstructure of the polymers.

- Chapter 6: Mechanistic study of the copolymerization of ethylene with carbon monoxide promoted by several Ni(II) phosphine phenolate complexes. The aim was to understand the mechanism that leads to the formation of in-chain polyketones and to rationalize the role of a peculiar Ni-ligand interaction.

All the complexes studied in this thesis were synthetized and characterized by the experimental group of Prof. Stefan Mecking. The experimental results will be described in the introduction of the following chapters.

Chapter 3

Results and discussion

Theoretical study by DFT of the ethylene polymerization promoted by neutral and cationic Ni(II) Bis(imino)phenoxy Catalysts: rationalization of the role of the second imine donor and the impact of the charge.

3.1 Introduction

Salicylaldiminato complexes with a second imine donor in *ortho*-position to the oxygen atom of the ligand are known as 2,6-bis(arylimino)phenoxy complexes. Based on such a ligand structure, several nickel catalysts for the polymerization of ethylene have been synthesized.[114-115] The peculiar structure of this ligand gives rise to two potential binding sites for metal species, and consequently offers the possibility for the nickel centre to switch between them, as reported in Scheme 3.1.[114-117]

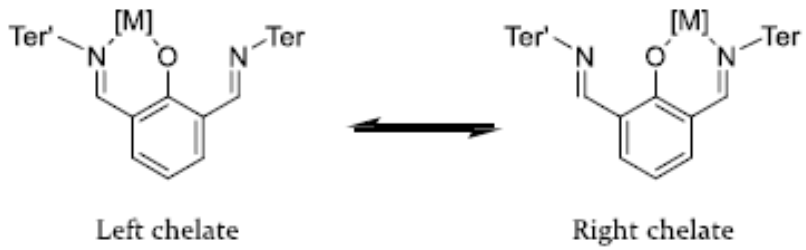

Scheme 3.1: Generic structure of bis(imino)phenoxy complexes with two binding sites.

Neutral bis(imino)phenoxy complexes with a single site of binding occupied by the nickel ion and with different remote substituents on the imine donors were synthetized, namely $\mathbf{CH_3}$ and $\mathbf{CF_3}$ catalysts in Scheme 3.2, and their catalytic properties were tested in ethylene polymerization experiments.[118]

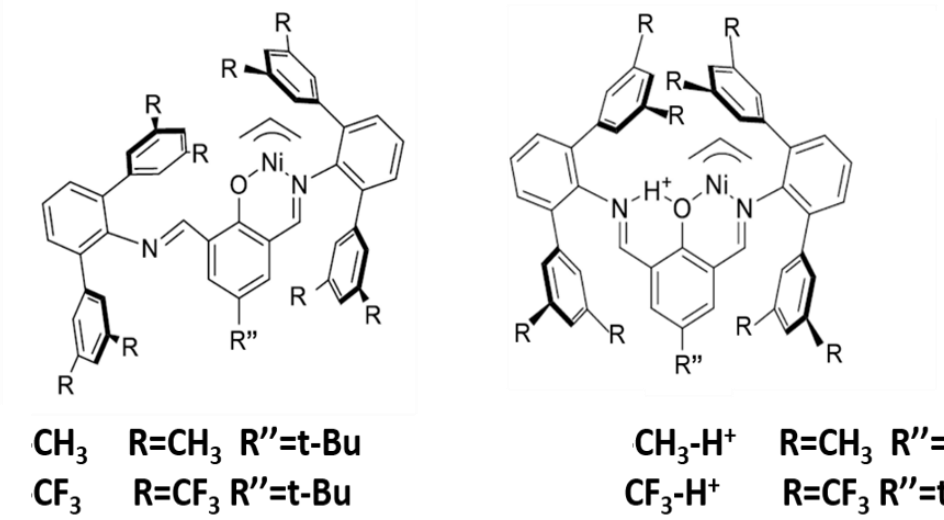

Scheme 3.2: Structure of catalysts ***CH_3, CF_3, CH_3-H^+*** *and* ***CF_3-H^+****.*

It has been reported that for Ni(II) salicylaldiminato catalysts a distinctive difference in catalysis exists between trifluoromethyl- or methyl substituted terphenyl group due to the so-called "remote substituent effect" (see section1.2.3 and Scheme 1.11).[85,119-120]

Similarly,[85] for the 2,6-bis(arylimino)phenoxy complexes, it was observed that in the same experimental conditions, catalyst **CH_3** produces hyperbranched oligomers (for more details see supplementary file Table 3.1: entry 1-2), whereas catalyst **CF_3** produces HDPE with high molecular weights (see supplementary file Table S3.1: entry 6-8).

Additionally, in the second binding site an added proton was incorporated creating a N···H^+···O bridge next to the nickel atom with the central oxygen atom, namely **CH_3-H^+** and **CF_3-H^+** catalysts in Scheme 3.2. Studies of two different remote substituents on the *N*-terphenyl distal rings, varying their electronic nature, shed more light on the role of the added proton other than the second imine donor.

Additionally, the second nitrogen binding site for this class of complexes has been shown to be well suited for the incorporation of a single proton with the formation of a N···H^+···O bridging motif, see Scheme 3.2.[118] The proton was incorporated by addition of Brookhart's acid $[H(OEt_2)_2][BAr^F{}_4]$ (Ar^F = 3,5-$(F_3C)_2C_6H_3$). The anion introduced in such way, i.e. $BAr^F{}_4$, is noncoordinating, and, thus, this will have a scarce influence on the catalytic properties. For this reason, it was not considered in the computational studies. Also in this case, complexes with two different remote substituents on the *N*-terphenyl distal rings were tested, i.e **CH_3-H^+** and **CF_3-H^+.**

It was observed that the presence of a bridging proton in the cationic complexes dramatically alters the catalytic properties (see supplementary files, Table S3.1 entry 3-5 and 9-11). This effect is most pronounced for **CF_3-H^+**. In fact, while the parent neutral complex **CF_3** affords HDPE, this protonated complex yields low molecular weight branched oligomers (Mn < 3 kg mol^{-1} by NMR, 23–27 branches/1000 C atoms by $^{13}C\{^1H\}$ NMR). As for **CH_3-H^+** *vs*. **CH_3**, the type and amount of branches differ significantly with the neutral non-protonated catalyst being capable of extensive chain walking resulting in hyperbranched structures (Mn < 2 kg mol^{-1} by

NMR, 94–96 branches/1000 C atoms by $^{13}C\{^1H\}$ NMR) and the protonated complex producing oligomers with a rather low degree of branching and exclusively methyl branches (Mn < 1 kg mol^{-1} by NMR, 23–25 branches/1000 C atoms by $^{13}C\{^1H\}$ NMR).[118]
All the experimental results reported herein on the ethylene polymerization catalyzed by neutral and cationic bis(imino)phenoxy complexes were performed by Dr. Eva Schiebel in the group of Prof. Stefan Mecking at the University of Konstanz (Germany).[118]
The DFT approach was used in this study to clarify the role of the non-coordinated imine donor lying on the new **CH_3** and **CF_3** nickel complexes and the impact of the charge in the cationic counterpose catalysts **CH_3-H^+** and **CF_3-H^+** during ethylene polymerization.

The distinctly different catalytic behaviour of the neutral and cationic complexes was further investigated through detailed mechanistic studies analysing both the steric and electronic influence of the protonation, i.e. through the comparison of the energies involved along the linear chain growth, chain transfer and branching formation pathways. An isolated analysis of the steric impact alone is given by topographic steric maps, whereas a detailed analysis of the energies of the intermediates and transition states during catalysis captures both the electronic and steric impact. The computed free energies are expressed as ΔG in kcal mol^{-1} (the computational details are reported in the supplementary files).

3.2 Results and discussion.

3.2.1 Detailed analysis of the catalyst precursors: Allyl-CH_3, Allyl-CF_3, Allyl-CH_3-H^+ and Allyl-CF_3-H^+.

3.2.1.1 Structural analysis.

At first, to determine the most favored orientation of the second imine arm, a conformational analysis was performed on **Allyl-CH_3**, **Allyl-CF_3**, **Allyl-CH_3-H^+** and **Allyl-CF_3-H^+** pre-catalysts. For both **Allyl-CH_3** and **Allyl-CF_3** pre-catalysts the conformer with the non-coordinated imine donor lying away from the nickel centre is lower in energy of about 3 kcal mol^{-1}, (see Scheme 3.3). This conformation turns out to be more stable also for all intermediates and transition states involved in the mechanistic study discussed below.

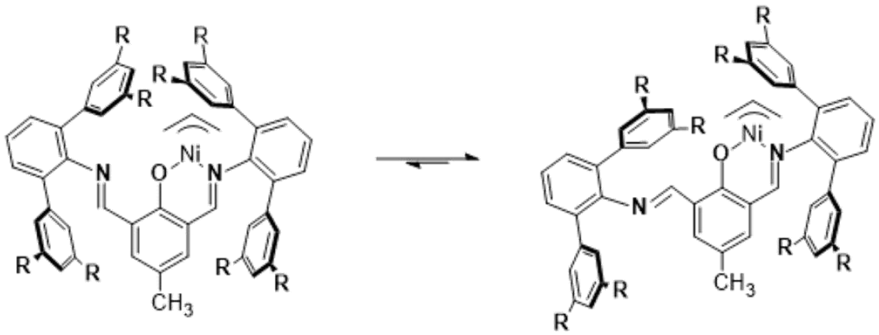

R=CH_3	Allyl-CH_3	0.0	- 3.0 kcal/mol
R=CF_3	Allyl-CF_3	0.0	- 3.0 kcal/mol

*Scheme 3.3: Model of the two isomeric structures for **Allyl-CH_3** and **Allyl-CF_3** precatalysts. Note that for all systems, the calculations are performed on the catalysts with a methyl substituent in para position on the phenoxy ligand rather than the ^{t}Bu group. The microstructure formed is independent of this substituent (see supplementary*

files, section 3.3.2) which allows the replacement of the ^{t}Bu group for a methyl group for reduced computational effort.[118]

By contrast, the second imine arm points in the direction of the nickel atom for the protonated complexes (**Allyl-CH_3-H^+** and **Allyl-CF_3-H^+**) and it is bridged to the phenoxy O-donor.
It this worth noting that the favoured conformations were also observed in the X-ray structure for all the four allyl pre-catalysts, for more details see section 3.3.3 in supplementary files.

3.2.1.2 Steric analysis.

For the four allyl pre-catalysts, the steric analysis performed by computing the steric maps[121] showed that the most sterically hindered area coincides with the position of the nitrogen atom coordinated to Ni projecting the upper terphenyl group towards the coming substrates (see north-east quadrant in Figure 3.1), as already observed in presence of the mono(imino)phenoxy ligands.[85] On the contrary, the opposite hemisphere around the nickel is occupied by the non-coordinated *N*-terphenyl donor that lies more far from the metal centre. However, in case of **Allyl-CH_3-H^+** and **Allyl-CF_3-H^+** catalysts, as discussed above, the second imine ligand is rotated towards nickel centre generating a new hindered area around the metal (see red spots in the south-west quadrant in Figure 3.1). Finally, in all cases, the fluorinated complexes are more hindered due to the presence of the -CF_3 groups.

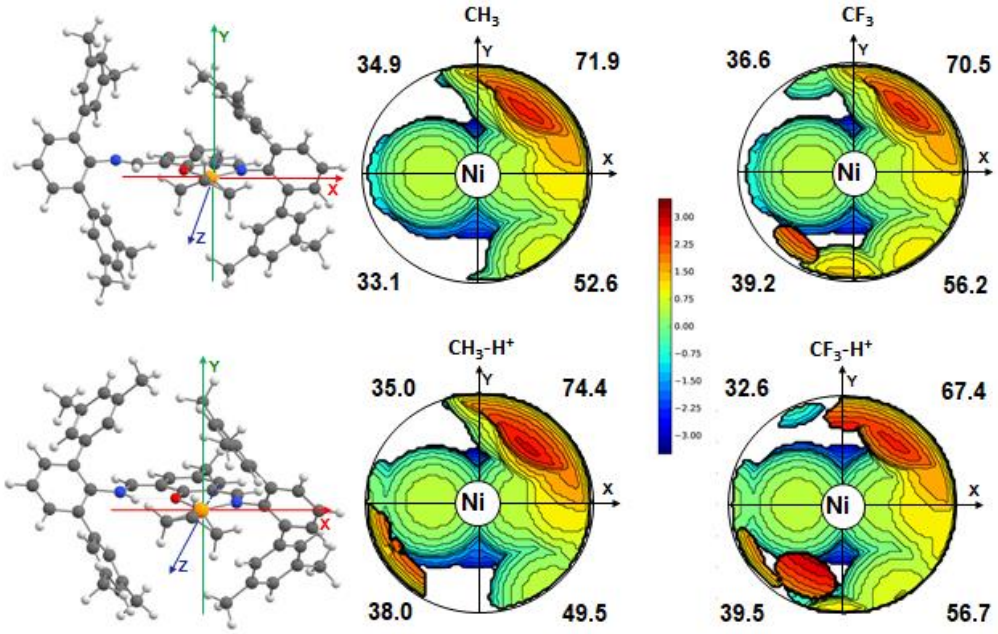

*Figure 3.1: Topographic steric maps and %V_{Bur} divided by quadrants of the **Allyl-CH_3**, **Allyl-CF_3**, **Allyl-CH_3-H^+**, **Allyl-CF_3-H^+** systems. The complexes are oriented as shown for **Allyl-CH_3** (above on the left) and **Allyl-CH_3-H^+** (below on the left).*

3.2.1.3 Electronic analysis.

The natural bond population analysis (NBO) performed on the four allyl catalytic precursors showed that the protonated catalysts exhibit a higher positive charge on Ni due to the weaker Ni-O bond, as consequence of the incorporation of the proton into the second binding site giving rise to H···O interaction (for more detail see supplementary files, section3.3.3). These results agree with the lower electron density on the protonated complexes than on the neutral ones as experimentally observed by cyclic voltammetry analysis (i.e. the forward peak potential obtained by cyclic voltammetry analysis reported in supplementary files, Table S3.6).

3.2.2 Mechanistic investigation.

In line with our previous studies on the mono(imino)phenoxy analogue complexes,[85] the Ni-propyl species **1-β-T** (stabilized by a β-agostic interaction with the metal centre), showing an alkyl chain in *trans* position with respect to the oxygen, models the product of the ethylene insertion into the Ni-growing chain bond. For this reason, it is considered as the zero point energy reference for all the reaction pathways studied.

For the protonated catalysts, the starting species **1-β-T** seems to have a weaker Ni-O bond (longer Ni-O bond) and a stronger Ni-H interaction (shorter Ni-H bond) than their non-protonated counterparts as a consequence of the established O···H interaction, see the Figure 3.2 in which the Ni–$^{\beta}$H, Ni–$^{\beta}$C and Ni-O distances of the neutral $\mathbf{CH_3}$ catalyst are compared with the distances of the analogue protonated complex $\mathbf{CH_3\text{-}H^+}$.

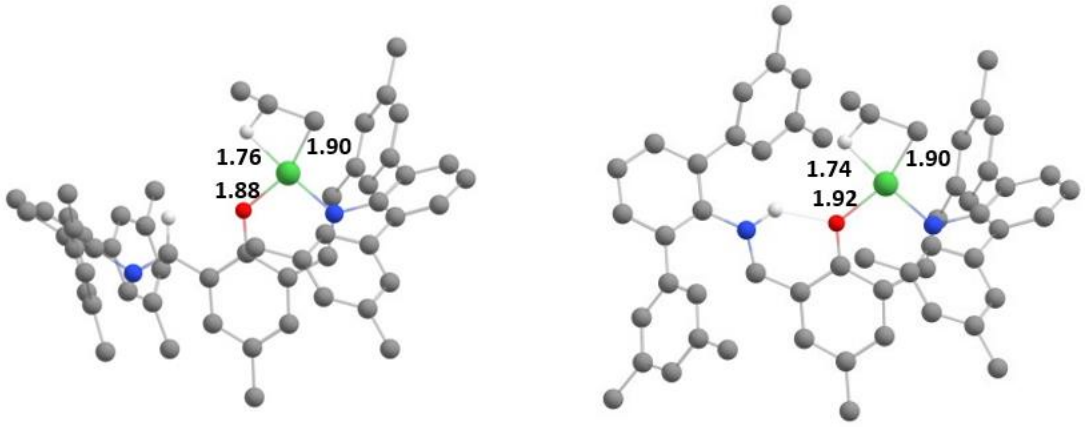

*Figure 3.2: Intermediate **1-β-T** for **CH3** (on the left) and **CH3-H**$^+$ (on the right). The distances are reported in Å.*

From **1-β-T**, the complete mechanism of the linear propagation reaction, the termination and the branches formation reactions were studied, Scheme 3.4. In detail, the red and green numbers account for $\mathbf{CH_3}$ and $\mathbf{CF_3}$ neutral catalysts and black and blue numbers for $\mathbf{CH_3\text{-}H^+}$ and $\mathbf{CF_3\text{-}H^+}$ cationic catalysts, respectively.

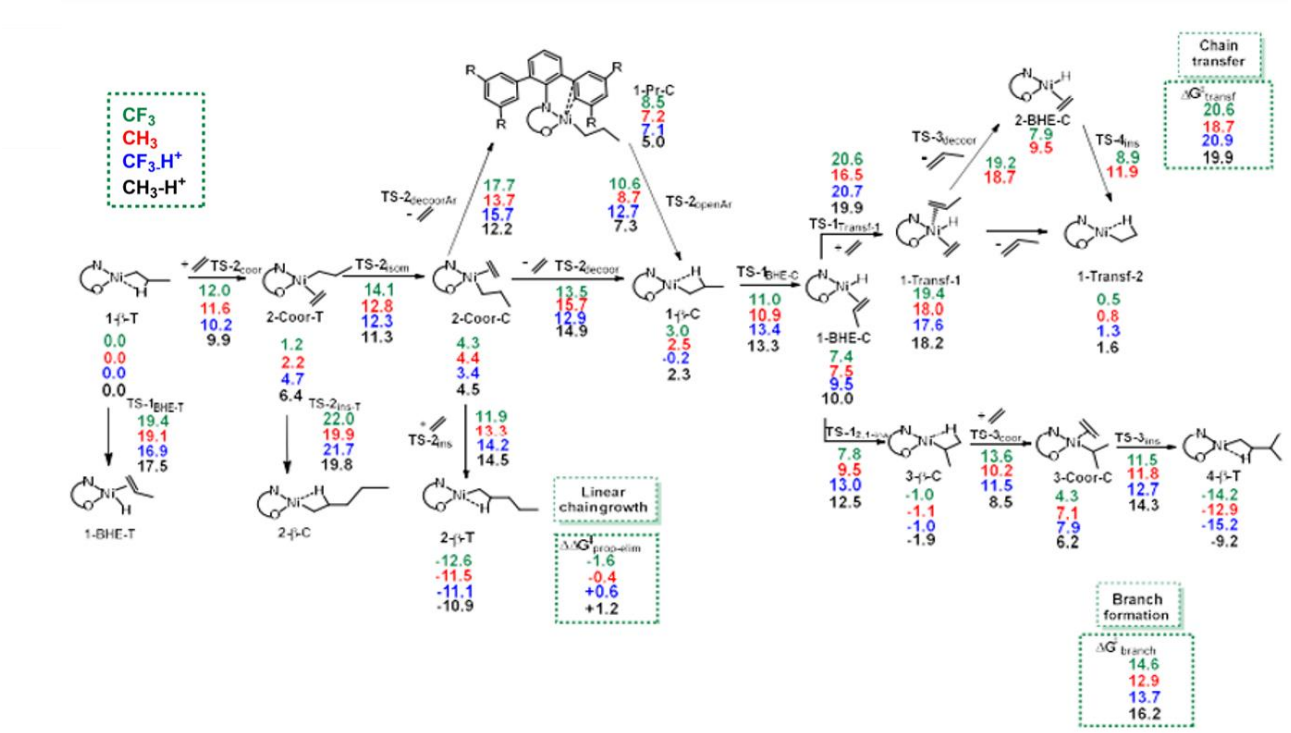

*Scheme 3.4: Gibbs free energies (ΔG_{Tol} in kcal mol^{-1}) of key species for linear chain growth, chain transfer and branch formation with **CF_3** (green), **CH_3** (red), **CF_3-H^+** (blue) and **CH_3-H^+**(black).*

3.2.2.1 Linear chain growth pathway.

In the first step during catalysis, ethylene coordinates yielding **2-Coor-T**, a complex with the alkyl chain *trans* to the oxygen atom. The energies of this intermediate are higher for the protonated complexes (4.7 kcal mol^{-1} for **CF_3-H^+** and 6.4 kcal mol–1 for **CH_3-H^+**) compared to the neutral complexes (1.2 kcal mol^{-1} for **CF_3** and 2.2 kcal mol^{-1} for **CH_3**) reflecting a further increase of the Ni–O bond length and indicating the relatively less favourable nature of ethylene coordination (compared to a β-agostic interaction) in the cationic systems. The next step during catalysis is an isomerization to **2-Coor-C**, where the olefin is coordinated *trans* to the oxygen atom, an intermediate with overall similar energies for all four complexes. Starting from **2-Coor-C**, either ethylene insertion or chain transfer can take place. Ethylene insertion occurs via **TS-2$_{ins}$** to **2-β-T**. The energies for the transition states for the protonated complexes are significantly higher in this case (14.2 kcal mol^{-1} for **CF_3-H^+** and 14.5 kcal mol^{-1} for **CH_3-H^+**) compared to the energies for the neutral complexes (11.9 kcal mol^{-1} for **CF_3** and 13.3 kcal mol^{-1} for **CH_3**), coinciding with an increased Ni–O bond length as well as higher Ni-olefin distances in the transition state. It this worth noting that the energies required for the insertion step arm are similar to those observed for the mono(imino)phenoxy systems (compare the energy barriers of 11.9 kcal mol^{-1} for **CF_3** and 13.3 kcal mol^{-1} for **CH_3** with those calculated for analogues mono(imino) complexes with **CF_3** and **CH_3** groups, respectively) and thus not affected by the presence of the non-coordinated imine.[85]

3.2.2.2 BHE elimination pathway.

Branch formation and chain transfer starts with the formation of a β-agostic complex, **1-β-C**, followed by BHE giving **1-BHE-C**. In the first step, ethylene decoordination can take place either directly in a single step (via **TS-2$_{decoor}$**) or *via* an intermediate with a Ni-aryl interaction (**1-Pr-C**) in a two-step decoordination process. The single-step process is favoured for the complexes with an electron-poor terphenyl group (**CF$_3$** and **CF$_3$-H$^+$**), whereas the two-step process is viable for the complexes with electron-rich terphenyl groups (**CH$_3$** and **CH$_3$-H$^+$**), similar to mono(imino)phenoxy systems.[85] The observed difference in catalysis between the two neutral complexes arises from this step: while for the **CH$_3$**, the Ni-aryl interaction opens a low energy pathway toward branch formation and chain transfer, this pathway is unlikely for **CF$_3$** due to a higher energy barrier. Therefore, hyperbranched oligomers are obtained for **CH$_3$**, while **CF$_3$** gives HDPE in pressure reactor experiments. The pathway including a Ni-aryl interaction via **1-Pr-C** is also accessible for the protonated, methyl substituted complex. The electron-donating properties of the methyl substituted terphenyl groups seem to overrule the electronic change by protonation. However, the effect of this Ni–aryl interaction is irrelevant for the protonated complexes, as in the next step toward chain transfer or branch formation, the BHE itself shows higher energy barriers compared to (Ni-aryl assisted) ethylene decoordination forming the first intermediate (**2-Coor-C** to **1-β-C**).The intermediate **1-β-C** is, as a β-agostic complex, more stable for the protonated complexes than for the non-protonated ones, and in the case of **CF$_3$-H$^+$** it can be considered as a resting state. For the following BHE, the higher energies for **TS-1$_{BHE-C}$** are attributed to the cationic complexes (13.4 kcal mol^{-1} for **CF$_3$-H$^+$** and 13.3 kcal mol^{-1} for **CH$_3$-H$^+$**) compared to the neutral complexes (11.0 kcal mol^{-1} for **CF$_3$** and 10.9 kcal mol^{-1} for **CH$_3$**), reflecting the forming Ni-olefin complex **1-BHE-C**.
Starting from **1-β-T**, BHE could lead to the nickel hydride species **1-BHE-T** with a propene molecule coordinated trans to the oxygen atom. Due to the unfavorable kinetics this possibility was ruled out for all the complexes. Hence, BHE has to occur from the cis isomer **1-β-C**, leading to the sterically less crowded and energetically favored isomer **1-BHE-C**. All potential pathways for a direct *cis*/*trans* isomerization of the β-agostic complex were calculated to involve transition states with extremely high free energies and therefore they have also been ruled out.
Comparing the two possible pathways starting from **2-Coor-C**, either ethylene decoordination and BHE or linear chain growth, the neutral complexes are more likely to undergo linear chain growth when compared to the cationic complexes; a measure for that is the energy difference between the highest energy barrier for each pathway ($\Delta\Delta G_{prop\text{-}elim}^{\ddagger}$: calculated from the energy attributed to **TS-2$_{ins}$** for ethylene insertion and the energy for the transition state with the highest energy toward **1-BHE-C** en route to chain transfer and branch formation). Whereas **CF$_3$** has the highest tendency for ethylene insertion ($\Delta\Delta G_{prop\text{-}elim}^{\ddagger}$ = –1.6 kcal mol^{-1}), **CH$_3$-H$^+$** has the highest tendency toward BHE ($\Delta\Delta G_{prop\text{-}elim}^{\ddagger}$ = +1.2 kcal mol^{-1}). This agrees with the experimentally observed high molecular weight polymer for **CF$_3$**, while for **CH$_3$-H$^+$** short chain oligomers are obtained.

3.2.2.4 Chain transfer pathway.

The chain transfer reaction occurs prevalently through a two steps mechanism consisting in monomer coordination and then chain decoordination leading to the β-agostic complex **1-Transf-2** that starts a new polymer chain.
From **1-BHE-C** the ethylene coordination leads to a five-coordinated intermediate, **1-Transf-1**. For $\mathbf{CF_3}$ and $\mathbf{CH_3}$ starting from **1-Transf-1**, the following release of propene occurs *via* **TS-3**$_{\mathbf{decoor}}$ leading to the **2-BHE-C** intermediate with the monomer coordinated in *cis* position with respect to the oxygen atom. After displacement of propene, ethylene insertion in the Ni-H bond via **TS-4**$_{\mathbf{ins}}$ yields to the stable β-agostic complex, **1-Transf-2**. Instead for $\mathbf{CF3\text{-}H^+}$ and $\mathbf{CH_3\text{-}H^+}$, the decoordination of the unsaturated chain is concerted with monomer insertion and **1-Transf-2** product is obtained through a barrierless mechanism for which it was not possible to locate the corresponding TS. This difference can be ascribed to the effect of the bridge and of the species lying *trans* to the oxygen atom for $\mathbf{CH_3\text{-}H^+}$ and $\mathbf{CF_3\text{-}H^+}$ systems.
The overall energy barriers ($\Delta G_{transf}^{\ddagger}$, this is the overall energy barrier for the whole process; resting states like **1-β-C** for $\mathbf{CF_3\text{-}H^+}$ must be considered) for this process do not differ significantly both neutral or cationic complexes. However, compared to the overall energy barriers of ethylene insertion, chain transfer is less likely for the neutral complexes.

3.2.2.4 Branch formation pathway.

Branch formation from **1-BHE-C** proceeds *via* **TS-1**$_{\mathbf{2,1\text{-}ins}}$ (2,1-insertion of the propyl chain) to form the resting state **3-β-C**. Finally, monomer coordination and insertion into the Ni-isopropyl bond *via* **TS-3**$_{\mathbf{ins}}$ form the methyl branched product **4-β-T**. The overall energy barriers for branch formation ($\Delta G_{branch}^{\ddagger}$) are 12.9 and 14.6 kcal mol^{-1} for $\mathbf{CH_3}$ and $\mathbf{CF_3}$ and 16.2 and 13.7 kcal mol^{-1} for $\mathbf{CH_3\text{-}H^+}$ and $\mathbf{CF_3\text{-}H^+}$, respectively. Comparing these energy barriers to the ones of chain propagation and chain transfer, it is more likely for $\mathbf{CH_3}$ and $\mathbf{CF_3\text{-}H^+}$ to form branches than $\mathbf{CF_3}$ and $\mathbf{CH_3\text{-}H^+}$.

3.2.2.5 Comparison of CH_3, CF_3, CH_3-H^+ and CF_3-H^+ catalysts.

Overall, for the neutral complexes, the second imine donor does not influence catalysis significantly; it is rotated away from the nickel atom and thus does not interfere in catalysis. The catalytic properties are similar to those of mono(imino)-phenoxy catalysts. For the protonated complexes, this imine forms a chelate with the incoming proton thereby slightly increasing steric pressure. The proton itself reduces the donor properties of the oxygen atom and decreases the Ni–O bond strength for all modelled transition states and intermediates, as reflected by higher Ni–O bond lengths. As the most decisive effect, β-agostic interactions are more favourable relative to olefin coordination. This results in a higher energy of the ethylene insertion transition state, which ultimately leads to a higher preference of the cationic complexes to undergo monomer decoordination and BHE compared to the neutral complexes.

3.2.2.6 Summary and conclusion.

In this chapter the DFT study performed on the ethylene polymerization mechanism in presence of the new reported bis(imino)phenoxy complexes was discussed for both the neutral systems and the cationic ones obtained by addition of a proton. For the protonated complexes, the additional imine donor in the ligand forms a chelate with the incoming proton. This interaction slightly raises the steric pressure around the Ni centre respect to the corresponding neutral systems. On the other hand, the proton itself reduces the charge donation of the oxygen atom to the metal and consequently the Ni–O bond weakens. In fact, from calculations it is observed an elongation of the Ni–O bond in all transition states and intermediates geometries, in agreement with X-ray structural analysis and oxidation potentials results. In the parent non-protonated complexes, the second imine donor is directed away from the active site and has little influence on the catalytic properties. This enables a comparison of the catalytic behaviour of cationic protonated species and reference neutral species, with otherwise essentially identical coordination environments of the active site. Studies of two different remote substituents on the *N*-terphenyl distal rings varying in their electronic nature, which are known to impact polymer microstructures in neutral catalysts, further illuminate the role of protonation. The presence of a bridging proton in the cationic complexes dramatically alters the catalytic properties. This is more pronounced for $\mathbf{CF_3}$-$\mathbf{H^+}$. While the parent neutral complex $\mathbf{CF_3}$ affords HDPE, this protonated complex yields low molecular weight oligomers (Mn < 1 kg mol^{-1}). This indicates a much higher rate for chain transfer for the protonated complex. For $\mathbf{CH_3}$-$\mathbf{H^+}$ vs $\mathbf{CH_3}$, the type and amounts of branches differ significantly. The neutral non-protonated catalyst is capable of extensive chain walking, resulting in hyperbranched structures. In contrast, the protonated complex produces oligomers with a rather low degree of branching and exclusively methyl branches. Theoretical studies showed that olefin coordinated intermediates and transition states of protonated complexes are relatively more destabilized compared to the neutral complexes when referenced to β-agostic intermediates. Ultimately, this results in a higher tendency for the cationic complexes to undergo BHE compared to ethylene insertion. More precisely, the energy barriers of the two steps leading to the BHE product, ethylene decoordination and BHE itself, compared to the energy barrier for ethylene insertion give a relative tendency of the system to either undergo BHE or chain propagation. The neutral complex $\mathbf{CF_3}$ always favours ethylene insertion, leading to HDPE. For the neutral complex $\mathbf{CH_3}$, ethylene decoordination and ethylene insertion are similar in energy, but BHE itself is favoured over ethylene insertion, which consequently leads to frequent chain walking. For both cationic complexes ($\mathbf{CF_3}$-$\mathbf{H^+}$ and $\mathbf{CH_3}$-$\mathbf{H^+}$), ethylene decoordination and BHE itself is favoured over ethylene insertion, which accounts for the similar, low molecular weight products for both cationic complexes. These findings provide a rationale for the impact of electron density on the active site on late transition metal catalysed polymerization, an important parameter that is usually difficult to unravel. This is helpful for understanding catalysts' behaviour, and for design of catalysts with unsymmetrical chelating ligands with two different donors.

3.3 Supplementary files.

3.3.1 Polymerization experiments.

Table S3.1: Ethylene polymerization results for ***CH_3, CF_3, CH_3-H^+ and CF_3-H^+*** *catalysts.*[a]

#	pre-catalyst	T [°C]	ethylene uptake [g]	isolated yield [g]	M_n (NMR) [kg mol^{-1}][b]	M_n (GPC) [kg mol^{-1}]	PDI	T_m [°C][h]	B[j,k]	% Me[k]
1	**CH_3**	30	1.5	1.6	1.5	2.9[d]	1.7[d]	i	94	86
2	**CH_3**	50	4.1	4.0	1.1	2.2[d]	1.6[d]	i	96	82
3	**CH_3-H^+**	30	0.7	0.3	0.76	0.72[e]	1.4[e]	30	23	99
4	**CH_3-H^+**	50	2.1	1.8	0.58	0.61[e]	1.3[e]	50	33	92
5	**CH_3-H^+**	70	1.3	1.4	0.52	0.55[e]	1.3[e]	50	35	91
6	**CF_3**	30	3.0	3.1	/[c]	126[f]	4.6[f]	127	5	100
7	**CF_3**	50	9.2	9.0	/[c]	37[f]	1.9[f]	114	15	99
8	**CF_3**	70	14.9	14.2	/[c]	20[f]	1.8[f]	108	20	97
9	**CF_3-H^+**	30	0.8	0.55	2.4	2.9[e,g]	2.4[e,g]	113	27	99
10	**CF_3-H^+**	50	1.1	1.27	4.5	5.0[e,g]	2.8[e,g]	113	23	100
11	**CF_3-H^+**	70	1.2	1.18	3.6	4.1[e,g]	2.1[e,g]	106	24	99

[a] Polymerization conditions: 5 µmol precatalyst, t = 30 min, 40 bar C_2H_4, 100 mL toluene. [b] From ^{1}H NMR; determined by comparing the olefinic signals to the backbone. [c] No olefinic end groups detectable. [d] Determined by gel permeation chromatography (GPC) at 50 °C in THF vs polystyrene standards. [e] Determined by GPC at 160 °C in dichlorobenzene vs linear PE standards. [f] Determined by GPC at 160 °C, universal calibration against polystyrene. [g] Bimodal molecular weight distribution. [h] From DSC, second heating cycle, heating rate: 10 K min^{-1}. [i] Fully amorphous material. [j] Branches/1000 C atoms. [k] Determined by ^{13}C{^{1}H} NMR (inverse gated).

3.3.2 Influence of a substituent *para* to the Phenol-O.

An analogue of complex **CF_3** with a ^{t}Bu substitution in *para* position to the phenolic oxygen atom (**CF_3-^{t}Bu**; Scheme S3.1) was also prepared.

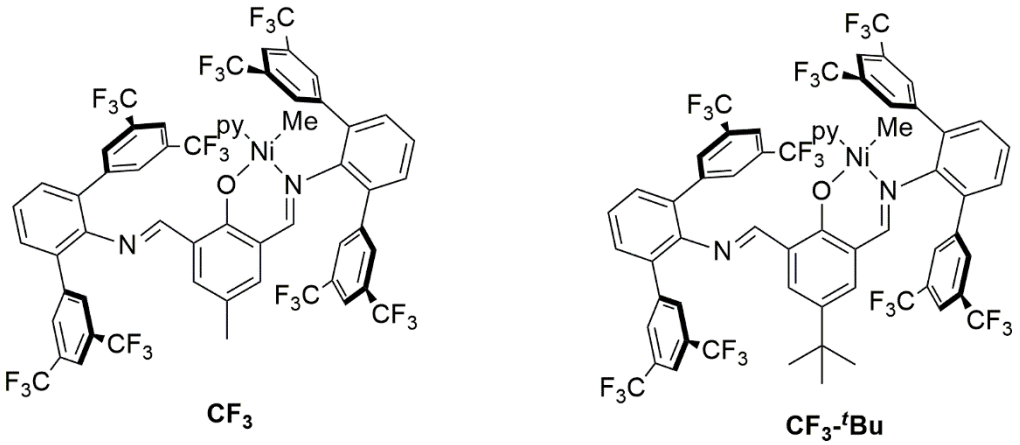

*Scheme S3.1: Structures of catalysts **CF₃** and **CF₃-ᵗBu**.*

This complex (**CF₃-ᵗBu**) was tested in ethylene polymerization experiments using the same conditions as for **CF₃** (Table S3.2). The productivity, activity and the microstructure of the obtained polymer does not depend significantly on the substituent *para* to the phenolic oxygen atom.

*Table S3.2: Ethylene polymerization results for **CF₃** and **CF₃-ᵗBu**.*

#	Precatalyst	n (precat) [µmol]	T [°C]	Isolated yield [g]	M_n (NMR) [kg mol^{-1}]	M_n (GPC) [kg mol^{-1}][a]	PDI	T_m [°C][d]	B[e,f]	% Me[c]
1	CF_3	5	30	3.1	/[b]	126[c]	4.6[c]	127	5	100
2	CF_3	5	50	9.0	/[b]	37[c]	1.9[c]	114	15	99
3	CF_3	5	70	14.2	/[b]	20[c]	1.8[c]	108	20	97
4	CF_3-ᵗBu	10	30	7.5	/[b]	59.1[c]	3.1[c]	127	8	99
5	CF_3-ᵗBu	10	50	14.6	11.6	10.9[c]	1.9[c]	121	22	98

Polymerization conditions: 40 bar C_2H_4, 100 mL toluene, 1000 rpm, t = 30 min; a) from ^1H NMR; determined by comparing the olefinic signals to the backbone; b) no olefinic end groups detectable c) determined by GPC in dichlorobenzene, universal calibration against polystyrene; d) determined by DSC, second heating cycle, heating rate: 10 K min^{-1}; e) Branches/ 1000 C atoms; f) determined by $^{13}C\{^1H\}$ NMR (inverse gated).

3.3.3 Crystal Structure Analysis.

For the complexes, including two of the protonated complexes, crystals suitable for single crystal X-ray crystallography could be obtained (Figure S3.1, S3.2, S3.3 and S3.4). The nickel atom is coordinated square planar with a slight distortion in all structures. For the non-protonated complexes (**Allyl-CH₃** and **Allyl-CF₃**) the non-coordinated imine donor is rotated away from the nickel centre. By contrast, this imine points in the direction of the nickel atom for the protonated complexes (**Allyl-CH₃-H⁺** and **Pyr-CF₃-H⁺**) and is bridged to the phenoxy

O-donor by the proton originating from the Brookhart's acid. For both crystal structures, the characteristic proton in the N,O-chelate was found by its electron density.

Figure S3.1: Schematic structure and ORTEP-plots of ***Allyl-CH$_3$*** *(30 % probability ellipsoids, hydrogens are omitted for clarity) determined by X-ray diffraction from different perspectives.*

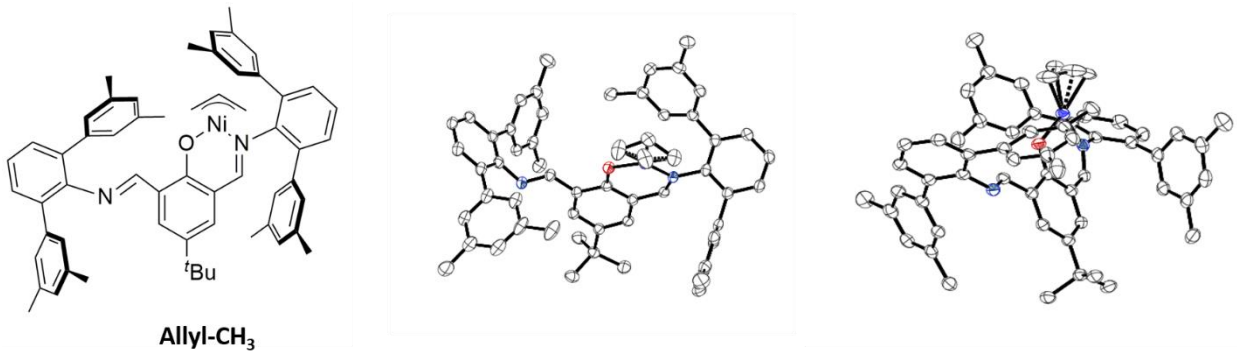

Figure S3.2: Schematic structure and ORTEP-plots of ***Allyl-CF$_3$*** *(30 % probability ellipsoids, all hydrogens are omitted for clarity) determined by X-ray diffraction from different perspectives. For the Ni Allyl group is and some of the CF$_3$ groups disorders are modelled.*

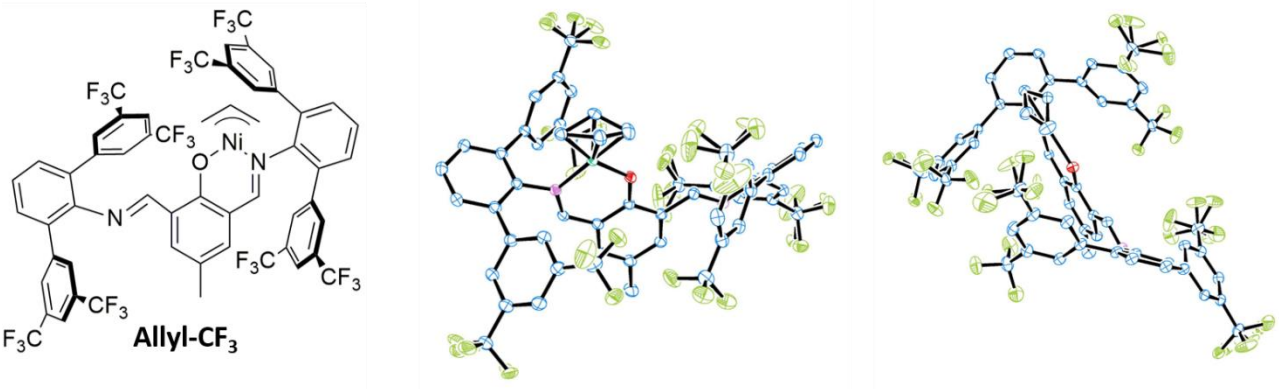

Figure S3.3: Schematic structure and ORTEP-plots of ***Allyl-CH$_3$-H$^+$*** *(30 % probability ellipsoids, all hydrogens are omitted for clarity) determined by X-ray diffraction from different perspectives.*

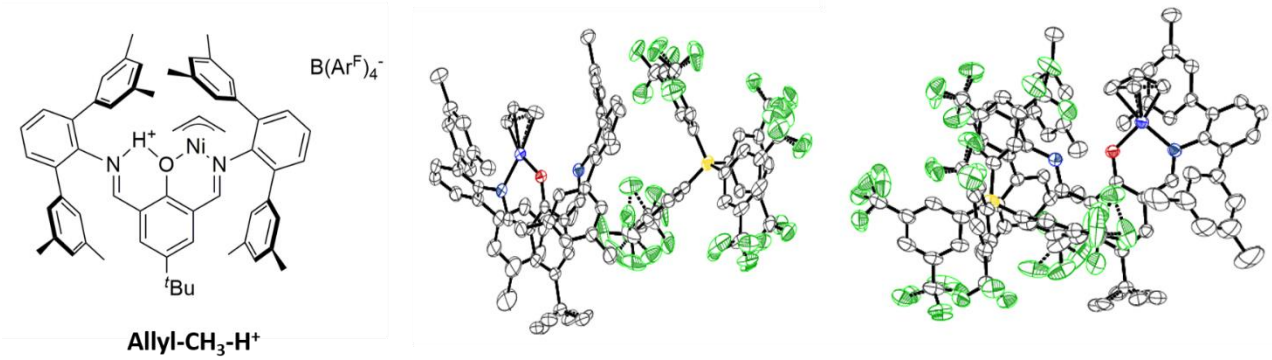

Figure S3.4: Schematic structure and ORTEP-plots of ***Pyr-CF3-H+*** *(30 % probability ellipsoids, all hydrogens are omitted for clarity) determined by X-ray diffraction from different perspectives.*

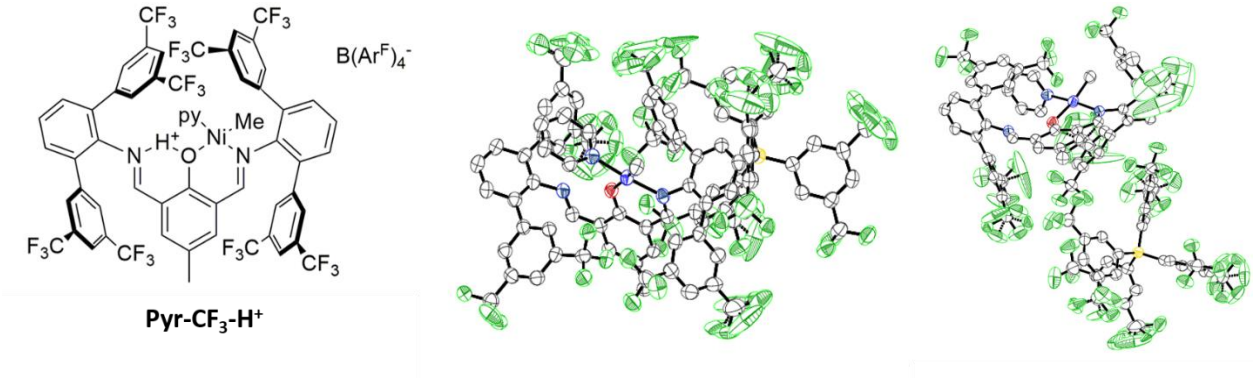

The bridging proton in **CH_3-H$^+$** and **CF_3-H$^+$** is clearly N-bonded, but also interacts with the oxygen atom. The distances between the N-atom and the proton of d = 0.75(5) Å (**Pyr-CF_3-H$^+$**) and d = 0.88(4) Å (**Allyl-CH_3-H$^+$**) are close to the respective covalent radii.

3.3.4 Natural Bond Population Analysis.

3.3.4.1 Complexes CF_3, CH_3, CF_3-H$^+$ and CH_3-H$^+$.

Natural bond population analysis (NBO) was performed for **Allyl-CF_3**, **Allyl-CH_3**, **Allyl-CF_3-H$^+$** and **Allyl-CH_3-H$^+$**. Due to the protonation, the Ni–O bond is weakened, as indicated by the increased Ni-O bond distances for the protonated systems respect to the non-protonated ones, (**Allyl-CH_3**: Ni–O 1.885 Å, **Allyl-CF_3**: Ni–O 1.882 Å, **Allyl-CF_3-H$^+$**: Ni–O 1.919 Å, **Allyl-CH_3-H$^+$**: Ni–O 1.913 Å). These results agree with the structures obtained by X-ray crystallography. Moreover, the protonated systems exhibit a lower positive charge on Ni and a greater negative charge on the oxygen atom. The two nitrogen atoms are electronically different in these complexes. In details, for the non-protonated **Allyl-CH_3** and **Allyl-CF_3** systems the greater electron density is localized on N1 that coordinates to the metal. On the contrary, even though N2 is protonated in case of **Allyl-CH_3-H$^+$**and **Allyl-CF_3-H$^+$**, a greater

electron density is present on N2 than on N1. This unusual result can be ascribed to the presence of the π-conjugated system that is able to delocalize the iminium positive charge.

Table S3.3: NBO Charges for **Allyl-CH_3**, **Allyl-CF_3**, **Allyl-CH_3-H^+**and **Allyl-CF_3-H^+**.

	N1 (N coordinated to Ni)	N2	O	Ni
Allyl-CH_3	-0.47939	-0.44514	-0.58414	0.40857
Allyl-CH_3-H^+	-0.45075	-0.48306	-0.60651	0.42562
Allyl-CF_3	-0.49483	-0.45978	-0.58128	0.39998
Allyl-CF_3-H^+	-0.46028	-0.49156	-0.60716	0.41722

An electronic analysis with a natural bond population analysis (NBO) has been performed on the discussed intermediates and transition states for the two protonated complexes **CH_3-H^+** and **CF_3-H^+**.

Table S3.4: NBO Charges and (O···H and Ni-O) distances for complexes **CH_3-H^+**.

Catalyst CH_3-H^+	Distances O···H (Å)	Distances Ni—O (Å)	Charges on Ni (NBO)	Charges on O (NBO)	Charges on H (NBO)
2-Coor-T	1.94339	2.04372	0.43332	-0.61770	0.46153
2-Coor-C	1.87536	1.97887	0.44627	-0.61148	0.46635
TS-2_{ins}	1.93332	2.01371	0.42573	-0.61699	0.45828
1-β-T	1.85939	1.92229	0.43529	-0.63567	0.46884
TS-1_{BHE-C}	1.90752	1.95767	0.28444	-0.61941	0.46490

1-BHE-C	1.93220	1.96992	0.28031	-0.61778	0.46330

Table S3.5: NBO Charges and (O···H and Ni-O) distances for complexes $\mathbf{CF_3\text{-}H^+}$.

Catalyst CF_3-H^+	Distances O···H (Å)	Distances Ni—O (Å)	Charges on Ni (NBO)	Charges on O (NBO)	Charges on H (NBO)
2-Coor-T	1.85645	2.02809	0.43666	-0.62309	0.46279
2-Coor-C	1.84915	1.97380	0.43470	-0.61181	0.46585
TS-2_{ins}	1.98200	2.01420	0.42109	-0.61700	0.46313
1-β-T	1.80895	1.92411	0.42475	-0.63416	0.46984
TS-$1_{BHE\text{-}C}$	1.83693	1.95556	0.27526	-0.61926	0.46483
1-BHE-C	1.85730	1.96900	0.27282	-0.61870	0.46458

NBO performed on protonated and non-protonated complexes showed that, as consequence of the incorporation of the proton on the second imine arm and of the H-O interaction, the protonated systems exhibit a higher positive charge on Ni in agreement with the experimental results obtained by CV.

Table S3.6: Halve-wave potentials of $\mathbf{CH_3}$, $\mathbf{CF_3}$, $\mathbf{CH_3\text{-}H^+}$ **and** $\mathbf{CF_3\text{-}H^+}$ in DCM referenced against $[Cp^*_2Fe]/[Cp^*_2Fe]^+$ ($Cp^* = C_5(CH_3)_5$-), $^nBu_4PF_6$ as electrolyte and a sweep rate of 100 mV s^{-1}.

	R = CH_3	R = CF_3
E by CV [mV], non-protonated complexes **R**	27	283
E by CV [mV], Protonated complexes **R-H^+**	508	624

For the non-protonated complexes half wave potentials of E = 27 mV ($\mathbf{CH_3}$) and E = 283 mV ($\mathbf{CF_3}$), respectively, were measured. These values differ only slightly from reported values for

similar Ni(II) salicylaldiminato complexes without a second imine function. The forward peak potentials for the protonated complexes are significantly higher, E = 508 mV (**CH_3-H^+**) and E = 624 mV (**CF_3-H^+**). This clearly shows that protonation reduces the electron density at the Ni site. The electron densities are not only lower, the difference between the CF_3- and CH_3-substituted complexes is also less pronounced. In this sense, protonation dominates the electronic nature as observed by electrochemistry.

3.3.5 Computational Details

3.3.5.1 General Methods

All the DFT geometry optimizations were performed at the GGA BP86[122-124] level of theory with the Gaussian 09 package.[125] The electronic configuration of the systems was described with the 6-31G(d) basis set for H, C, N, F, and O while for Ni the quasi-relativistic LANL2DZ ECP effective core potential was adopted.[126] All geometries were characterized as minimum or transition state through frequency calculations. The reported free energies were built through single point energy calculations on the BP86/6-31G(d) geometries using the M06 functional and the triple-ζ TZVP[127-129] basis set on main group atoms. Solvent effects (toluene) were included with the PCM model.[130-131] To this M06/TZVP electronic energy in solvent, thermal corrections were included from the gas-phase frequency calculations at the BP86/6-31G(d).

Chapter 4

Results and discussion

Theoretical study by DFT of the ethylene polymerization promoted by Neutral Unsymmetrical Coordinated Cyclophane Polymerization Catalyst: rationalization of the steric environment.

4.1 Introduction

The steric environment of a catalytically active site experienced by the substrates is key to determine favorable reaction pathways. Square planar coordinated active sites, as encountered in innumerable d^8-metal catalysts, are particularly challenging in this regard due to the relatively low coordination number and the consequently large open spaces in the apical direction. A prominent example are late-TM olefin polymerization catalysts.[132-133] Compared to early-TM catalysts,[134] the less electron deficient and less oxophilic nature of such d^8-metal sites results in functional group tolerance. At the same time, the propensity for BHE reactions enables the formation of unique branching structures,[57,135] but the BHE pathway also needs to be controlled as it determines not only the branching microstructure but also the polymer molecular weights. A sophisticated approach to generate a defined rigid environment also in those spatial positions remote to the coordination plane and to the donor atoms of square-planar coordinated catalysts is provided by cyclophanes. Guan devised an elegant strategy to generate two alkane bridges between the two identical *N*-terphenyl groups of an α-diimine catalyst, Scheme 4.1-A.[71,136-139] The effective blocking of the axial sites enhanced the control of molecular weight in ethylene polymerization as well as temperature stability of the catalysts. However, this approach is restricted to symmetrically coordinated catalysts. Means to introduce cyclophane motifs also to unsymmetrical coordinated catalysts with different types of donors are desirable. This can unlock a large diversity of possible structures in principle, which can provide unique properties. For example, polymerization catalysts with an unsymmetrical κ^2-*N,O*-chelate are known to stand out in their tolerance towards polar reaction media.[53,140-142] In this chapter, the polymerization mechanism of ethylene in presence of the Ni catalyst bearing an asymmetrically coordinated cyclophane motif (see Scheme 4.1-B) will be discussed and how the cyclophane environment affects the reaction pathways will be shown.

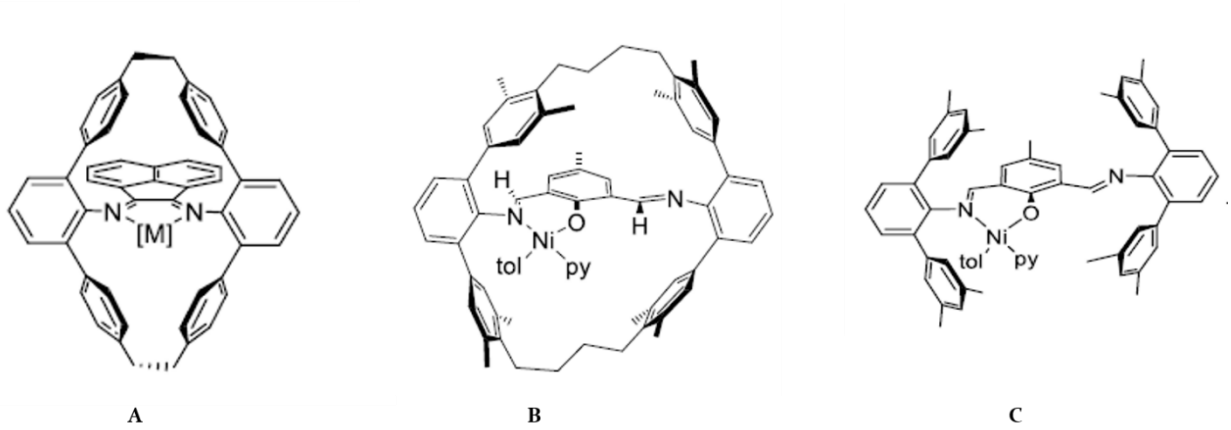

Scheme 4.1: A) Cyclophane structure in symmetrical κ²-N,N-coordinated catalyst, B) Cyclophane structure in unsymmetrical κ²-N,O-coordinated Ni(II) complex, ***cyclophane-Ni*** *, C) Bis(imino)phenoxy κ²-N,O-coordinated Ni(II) complex,* ***CH₃****.*

In order to exploit this elegant and proven ring closing chemistry to realize an unsymmetrically coordinated complexes, a second catalytically inert imine function on the salicyl ring of κ²-N,O-coordinated Ni(II) salicylaldiminato complexes was introduced.[143] Finally, the cyclophane ligand has been obtained introducing two alkane bridges between these two imine functions on the salicyl ring of bis(imino)phenoxy catalyst, yielding the desired complex, named **cyclophane-Ni** see Scheme 4.1-B. A non-bridged reference complex **CH_3** already discussed in the Chapter 3, was reported here for comparison (Scheme 4.1-C).
It was observed that in pressure reactor polymerization experiments (see supplementary files, Table S4.1), the **cyclophane-Ni** catalyst is considerably more temperature stable than the reference **CH_3**. For all temperatures, branching density of the products obtained with **cyclophane-Ni** as catalyst are significantly lower compared to those obtained in presence of the reference catalyst **CH_3**, which produced hyperbranched oligomers (Mn 1.7 kg mol^{-1} by ^1H NMR, 48 branches/1000 C atoms by $^{13}C\{^1H\}$ NMR for **cyclophane-Ni**, whereas Mn ≈ 1 kg mol^{-1},97 branches/1000 C atoms by $^{13}C\{^1H\}$ NMR for **CH_3** when T= 50°C, see Table S4.1 entry 2 and 5).[143]
All the experimental results reported herein for the **cyclophane-Ni** and the **CH_3** complexes and experimental studies of their catalytic properties in ethylene polymerization were performed by Dr. Eva Schiebel in the group of Prof. Stefan Mecking at the University of Konstanz (Germany).
The DFT approach was used here to clarify the effect of the cage around the active centre on the product microstructure for this new complex, **cyclophane-Ni,** Scheme 4.1-B, comparing its behavior with that of the **CH_3** complex, Scheme 4.1-C.
The impact of the cyclophane structure on catalysis was elucidated by detailed DFT mechanistic studies. An isolated analysis of the steric impact alone is given by topographic steric maps, whereas a detailed analysis of the energies of the intermediates and transition states during catalysis captures both the electronic and steric impact. The computed free

energies are expressed as ΔG_{Tol} in kcal mol^{-1} (the computational details are reported in the supplementary files).

4.2 Results and discussion.

4.2.1 Structural properties and steric analysis of the Ni-cyclophane catalyst.

Conformational analysis of both pre-catalysts showed that the conformers with the non-coordinated imine rotated away are about 3 kcal mol^{-1} more stable compared to the conformers with the imine rotated towards the nickel atom, due to a lower steric pressure of the terphenyl group on the second imine, and an attractive imine–CH···O interaction.
Therefore, the most sterically hindered area is in the left hemisphere of topographic steric maps[121] (Figure 4.1). Notably, the cyclophane structure also introduces steric pressure in the apical positions and in the right hemisphere.
The geometries showing this preferred orientation of the non-coordinated imine are lower in energy for all intermediates and transition states (see mechanistic investigation section 4.2.2).

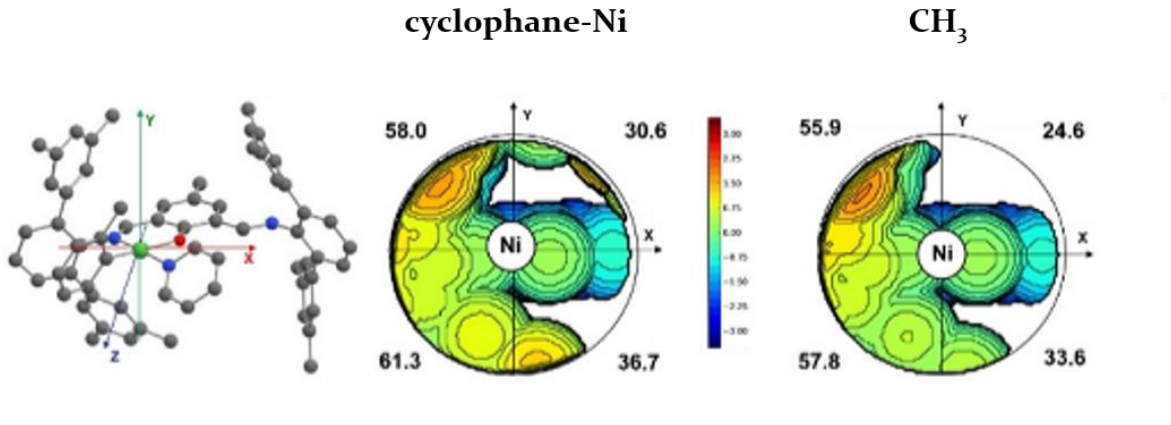

Figure 4.1: Topographic steric maps and %V_{Bur} divided by quadrants of ***cyclophane-Ni*** *(centre) and* ***CH_3*** *(right). The complexes are oriented as shown for* ***CH_3*** *on the left. Distance in the colour scale is in Å.*

It is worth to note that this favoured conformation was also observed in the X-ray structure of the **cyclophane-Ni** catalyst, for more details see section 4.3.2 in supplementary files. For **CH_3** it was already reported in chapter 3, see Figure 3.1.

4.2.2 Mechanistic investigation.

In line with our previous studies on the mono(imino)phenoxy analogue complexes[85] and on the bis(imino)phenoxy complexes previously reported, the Ni-propyl species **1-β-T** (stabilized by a β-agostic interaction with the metal centre) with the alkyl chain in *trans* position with respect to the oxygen, models the product of the ethylene insertion into the Ni-growing chain bond. For this reason, it is considered as the zero point energy reference for all the reaction pathways studied, Scheme 4.2. From **1-β-T**, the complete mechanism of the linear propagation

reaction, the termination and the branches formation reactions were studied, Scheme 4.2. In detail, the red and green numbers account for **CH_3** and **cyclophane-Ni** catalysts, respectively.

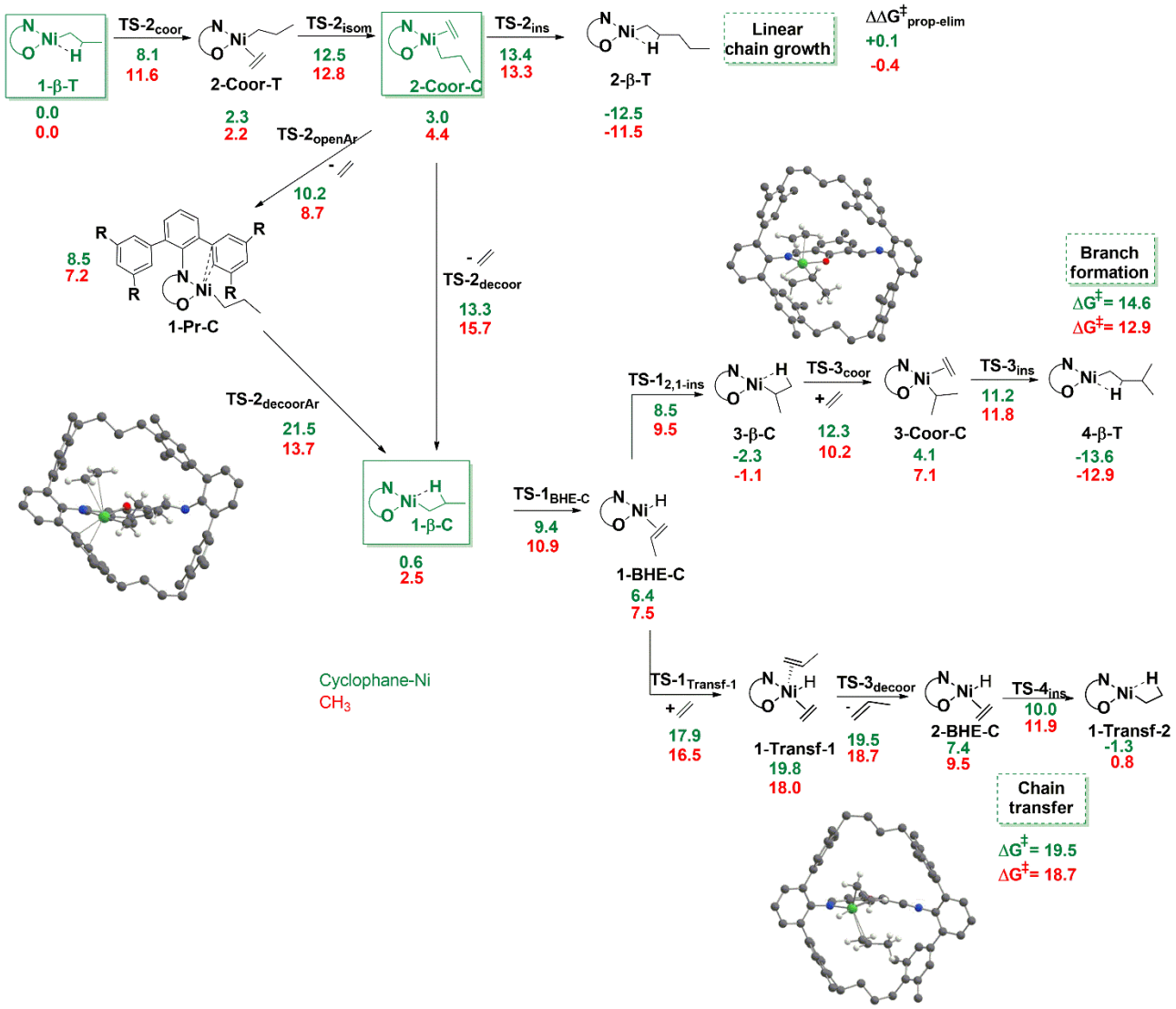

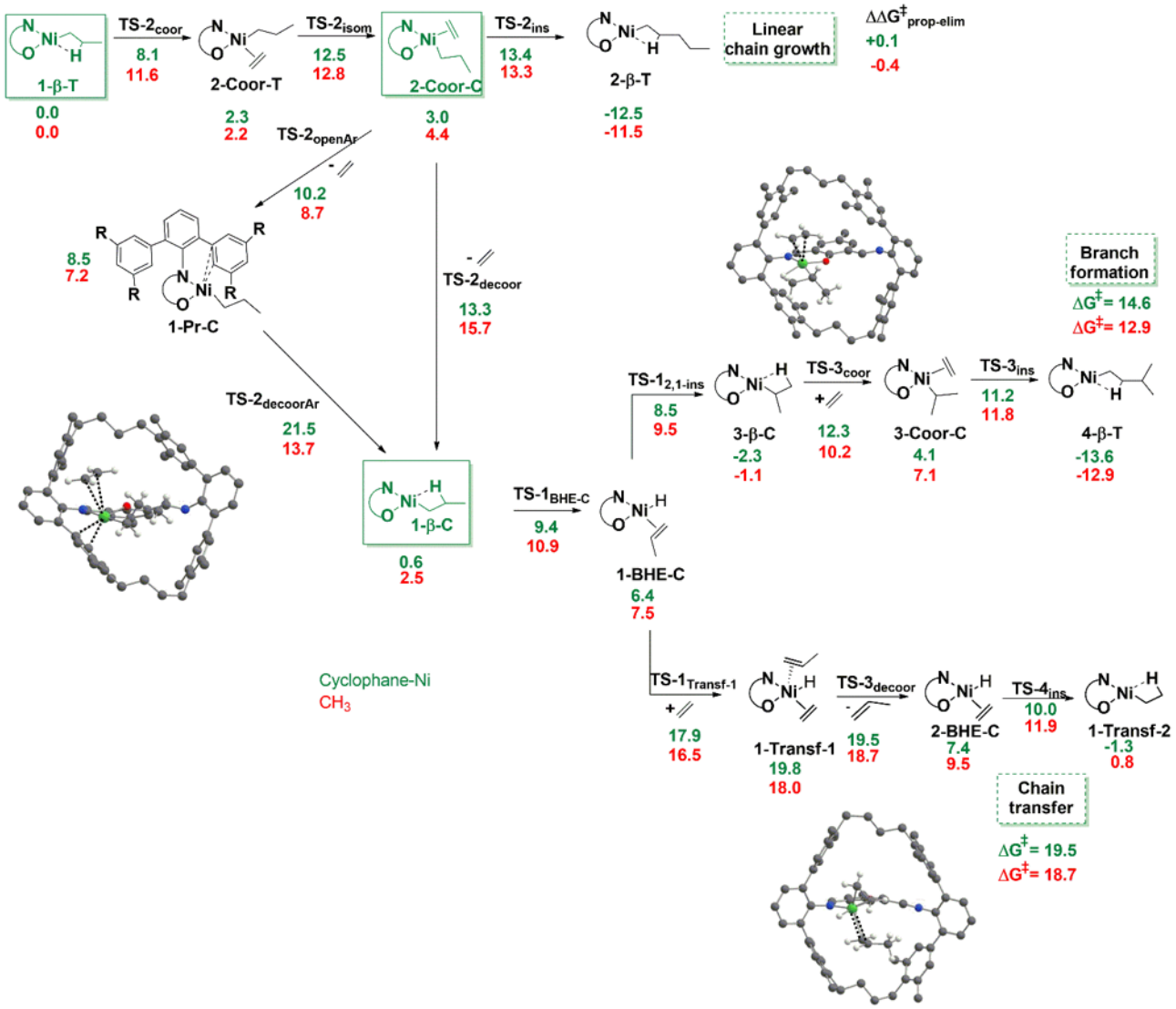

Scheme 4.2: Gibbs free energies (ΔG_{Tol} in kcal mol^{-1}) of key species for linear chain growth, chain transfer and branch formation with ***cyclophane-Ni*** *(green) and* ***CH$_3$*** *(red). Optimized geometries of* ***TS-2$_{decoorAr}$****,* ***TS-3$_{decoor}$****, and for* ***TS-3$_{coor}$*** *for* ***cyclophane-Ni*** *are shown. For more detail on these TSs and the related distances see section 4.3.4 in supplementary files.*

4.2.2.1 Linear chain growth pathway.

The first step is an ethylene coordination to **2-Coor-T**, followed by isomerization to **2-Coor-C**. The energies for the intermediates and the rds for this process are similar for both catalysts (**cyclophane-Ni** and **CH$_3$**), and do not differ from mono(imino)phenoxy catalysts.[85] Starting from **2-Coor-C**, either chain propagation (ethylene insertion to **2-β-T**) or branch formation and chain transfer (through ethylene decoordination and BHE to **1-BHE-C**) are possible. Ethylene insertion via **TS-2$_{ins}$** to **2-β-T** is attributed with similar energies for both systems (**cyclophane-Ni** and **CH$_3$**). The entire ethylene insertion process is not influenced by the C_4 bridges or the non-coordinating imine donor.

4.2.2.2 BHE elimination pathway.

The energy barriers associated with BHE (overall: going from **2-Coor-C** via **1-β-C** to **1-BHE-C**) are similar for the cyclophane and reference catalyst. In detail, ethylene decoordination from **2-Coor-C** to **1-β-C** can proceed either directly *via* **TS-2$_{decoor}$**, or in a two-step pathway as assisted ethylene decoordination with a Ni-aryl complex (**1-Pr-C**) as an intermediate (a typical process for electron-rich mono(imino)phenoxy catalysts)[85]. The direct isomerization from **1-β-T to 1-β-C** and the direct BHE elimination to **1-BHE-T** are not favoured as previously reported. For complex **CH$_3$**, the two-step pathway is 2.0 kcal mol^{-1} lower in energy compared to the direct pathway. For the cyclophane complex, the transition state to reach **1-Pr-C** *via* **TS-2$_{decoorAr}$** is very high in energy (21.5 kcal mol^{-1}) due to a high steric pressure between the rigid terphenyl group and the released ethylene. The direct ethylene decoordination via **TS-2$_{decoor}$** is significantly lower in energy (13.3 kcal mol^{-1}) and thus preferred for complex **cyclophane-Ni**. The energy barriers for ethylene decoordination, are comparable for both catalyst systems, despite the different pathways. The energy barriers for the next step yielding **1-BHE-C** are similar for both catalysts.

4.2.2.3 Branch formation pathway.

The rigid cyclophane ligand impedes branch formation. This pathway starts with the formation of a β-agostic complex **3-β-C** *via* **TS-1$_{2,1\text{-}ins}$** followed by ethylene coordination *via* **TS-3$_{coor}$** yielding **3-Coor-C**. Then, ethylene is inserted via **TS-3$_{ins}$** to give **4-β-T**. Here, the energy barrier for the **cyclophane-Ni** (14.6 kcal mol^{-1}, see difference from **3-β-C** to **TS-3$_{coor}$**) is 1.7 kcal mol^{-1} higher compared to the not-bridged catalyst **CH$_3$** (12.9 kcal mol^{-1}, see difference from **3-β-C** to **TS-3$_{ins}$**), explaining the lower branching density of the products obtained by **CH$_3$** in the experimental studies.

4.2.2.4 Chain formation pathway.

The rds of the chain transfer pathway (which occurs *via* two steps consisting of monomer coordination followed by chain decoordination) is sterically demanding and, again, higher in energy for the cyclophane complex (19.5 kcal mol^{-1} for **cyclophane-Ni** *vs*. 18.7 kcal mol^{-1} for **CH$_3$**). The ethylene molecule and the leaving propyl group are close to the left terphenyl group, which cannot rotate away due to the C_4 bridges. Ultimately, the energy barriers for this transition state can account for the higher molecular weights obtained with **cyclophane-Ni** when compared to **CH$_3$**, as chain transfer becomes slightly less favored compared to ethylene insertion ($\Delta\Delta G^{\neq}_{transf\text{-}prop}$ = 6.1 kcal mol^{-1} for **cyclophane-Ni** and $\Delta\Delta G^{\neq}_{transf\text{-}prop}$=5.4 kcal mol^{-1} for **CH$_3$**).

4.2.2.5 Summary and conclusion.

In this chapter the DFT study performed on the ethylene polymerization in presence of new square-planar cyclophane complexes with two different chelating donors (*N,O*) was discussed and the results compared with those obtained with the corresponding acyclic complex. In

agreement with the experimental results, the theoretical studies show that the second imine moiety is directed away from the active sites and consequently it does not significantly affect the reaction. The distinct effect of the cyclophane motif on product molecular weight and branching microstructure can be traced to the increased energy of sterically demanding transition states. This affects the rds towards chain transfer and branch formation, while chain propagation remains highly effective.

4.3 Supplementary files.

4.3.1. Polymerization reaction.

Table S4.1: Ethylene polymerizations with **cyclophane-Ni** and **CH_3**.

#	precatalyst	T [°C]	n_{precat} [µmol]	t [h]	yield [g]	Productivity [TON] [b]	M_n (NMR) [kg mol^{-1}] [c]	M_n (GPC) [kg mol^{-1}]	M_w/M_n	B [f,g]	% Me [g]
1	**cyclophane-Ni**	30	5	7.0	6.3	4.5	1.8	5.8[d]	4.4[d]	26	99
2	**cyclophane-Ni**	50	10	1.0	4.0	1.4	1.7	1.9[d]	4.4[d]	48	94
3	**cyclophane-Ni**	70	5	1.0	2.9	2.1	1.1	1.5[d]	3.0[e]	61	92
4	**CH_3**	30	5	2.0	/[a]	/[a]	/[a]	/[a]	/[a]	/[a]	/[a]
5	**CH_3**	50	5	1.0	0.6	0.4	1.3	3.0[e]	1.6[e]	97	82
6	**CH_3**	70	5	1.0	0.7	0.5	1.0	2.1[e]	1.5[e]	95	75

Polymerization conditions: 40 bar C_2H_4, 100 mL toluene. a) No product obtained. b) 10^4 x mol [C_2H_4] x mol^{-1} [Ni]. c) From ^1H NMR; determined by comparing the olefinic resonances to the backbone resonance intensity. d)Determined by gel permeation chromatography (GPC) at 160 °C in dichlorobenzene, universal calibration (with polystyrene). e) Determined by GPC at 50 °C in THF, linear calibration against PS. f) Branches per 1000 C atoms. g) Determined by $^{13}C\{^1H\}$ NMR (inverse gated).

4.3.2 X-ray structure.

*Figure S4.1: Schematic structure and ORTEP plot (20% probability ellipsoids, hydrogen atoms omitted for clarity) of Pyr-**cyclophane-Ni**. Note: The complex crystallized as two isomers, with a disorder of the pyridine and toluoyl group.*

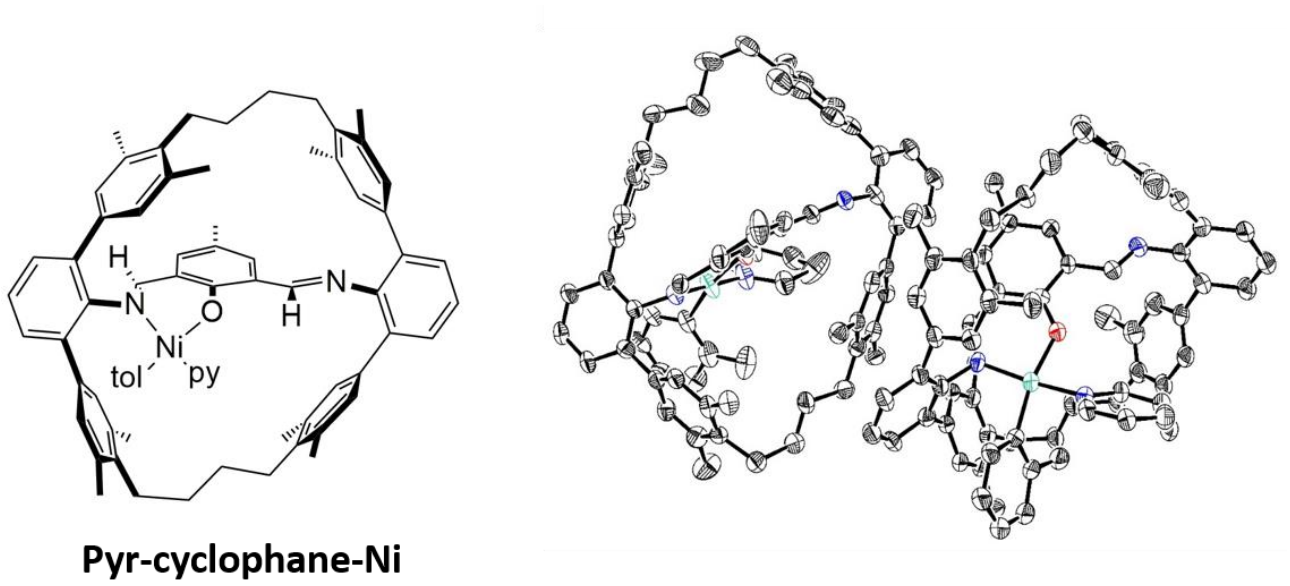

Pyr-cyclophane-Ni

4.3.3 Computational details.

All the DFT geometry optimizations were performed at the GGA BP86[122-124] level with the Gaussian09 package.[125] The electronic configuration of the systems was described with the 6-31G(d) basis set for H, C, N, F, and O while for Ni the quasi relativistic LANL2DZ ECP effective core potential was adopted.[126] All geometries were characterized as minimum or transition state through frequency calculations. The reported free energies were built through single point energy calculations on the BP86/6-31G(d) geometries using the M06 functional and the triple-ζ TZVP[127-129] basis set on main group atoms. Solvent effects were included with the PCM model using toluene as the solvent. [130-131] To this M06/TZVP electronic energy in solvent, thermal corrections were included from the gas-phase frequency calculations at the BP86/6-31G(d).

4.3.4 Mechanistic insight.

4.3.4.1 Structures of selected transition states.

Figure S4.2: Optimized geometries of ***TS-2***$_{decoorAr}$, ***TS-3***$_{decoor}$, *and for* ***TS-3***$_{coor}$ *for* ***Cyclophane-Ni*** *are shown, relevant distances are included.*

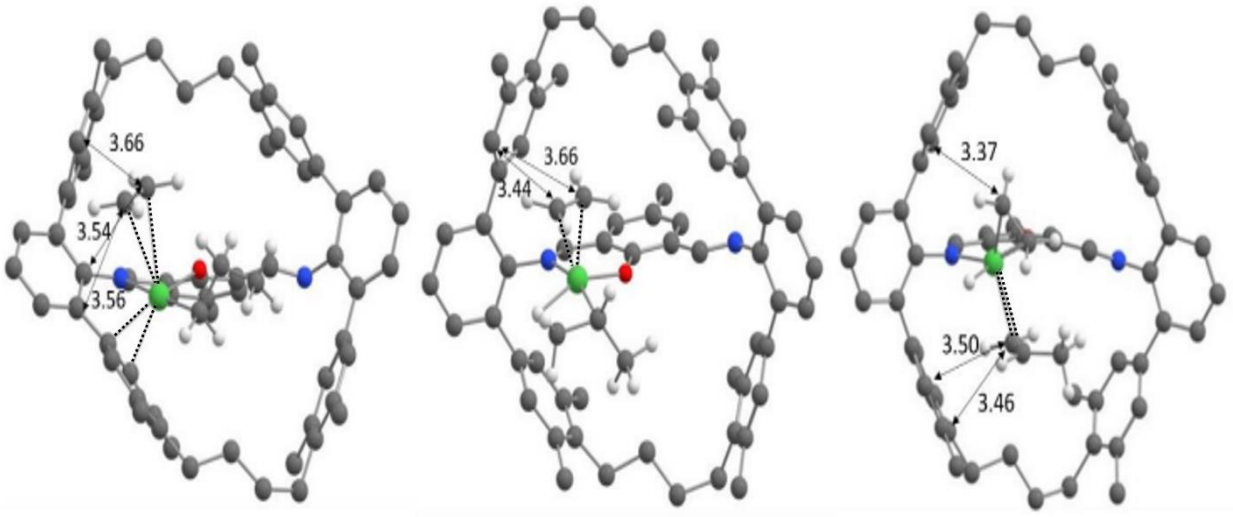

TS-$2_{decoorAr}$ TS-3_{coor} TS-3_{decoor}

Chapter 5

Results and discussion

Theoretical study by DFT of the ethylene polymerization promoted by Neutral Ni(II) Phosphine Phenolate Complexes: rationalization of the role of the weak and apical metal-ligand interaction.

5.1 Introduction

Considering possible approaches for the synthesis of different polymeric materials, the known capability of late-TM catalysts to produce a wide range of products appears attractive. As mentioned in Chapter 1, one of the most recognized pioneer in late-TM catalysts for olefin polymerization was Brookhart's reports on Pd(II) and Ni(II) diimine complexes.[144-146] Owing to the relatively low coordination number and the consequently large open space in the apical direction of the square planar coordinated active sites, these catalysts showed a great trend for BHE reaction which determines not only the branching microstructure but also the low molecular weights. As previously mentioned, the introduction of bulky substituents on the aryl groups of the diimine ligand to block the axial sites and thus effectively retard chain transfer was revealed as the most efficient way to unfavour BHE reaction.[66,70,143,147] Similar to Brookhart's catalyst, also SHOP catalysts[148-149] and other [P,O] catalysts[150] gave PE with low molecular weights of several 10^3 g mol^{-1} due to the propensity for BHE reaction. The catalyst structures have been adjusted through steric and electronic variations to enhance the catalytic performance. For the ortho-phosphinobenzenesulfonate Pd(II) catalyst, the substitutions of naphthyl, anthracenyl, or 1-methoxynaphthalene moieties appeared to reduce the polymerization activity and molecular weight.[151-152] In contrast, the catalytic activities and molecular weight of the obtained polyethylene were boosted significantly by the incorporation of very bulky 2-{2',6'-$(MeO)_2C_6H_3$}C_6H_4 moieties.[153] Nozaki's group synthesized a series of alkylphosphine-sulfonate ligands and correlated the steric bulk of the ligands with the molecular weight of (co)polymers, highlighting the need of blocking the axial position for the inhibition of chain transfer and the production of high-molecular weight polymers.[154] With respect to phosphinophenolato Ni(II) complexes, by Shimizu[155] and Li[98] reported the introduction of 2-C_6H_5-C_6H_4 or 2-{2',6'-$(MeO)_2C_6H_3$}C_6H_4 (Scheme 5.1-A)[98] substitution as strategy to increase remarkably the catalyst activity and ethylene molecular weights, up to 10^7 g mol_{Ni}^{-1} h^{-1} and 6.53×10^5, respectively. Very recently, Agapie reported a series of Ni(II) complexes derived from phosphine enolate SHOP catalyst to highlight the importance of axial steric hindrance for improve the catalyst activity, thermal stability, and polyethylene molecular weight.[156] A similar behaviour was also found for phosphinobenzenesulfonate Ni(II) catalyst,[157] in which a weak interaction between Ni and the aryl C_{ipso} was proposed to contribute to the increase of the polymer molecular weight in analogy to dialkyl(biaryl)phosphine ligands in Pd-catalyzed coupling catalysts where metal–arene interactions are observed.[158-160]

These reports asked for more mechanistic elucidations. As already reported in this thesis, the combined theoretical and experimental study on salicylaldiminato Ni(II) catalysts[85,161], revealed that a weak η^2 coordination of the electron-rich distal aryl rings with the Ni(II) centre in the equatorial direction can promote decoordination of ethylene and hereby favour BHE and consequently chain transfer and branch formation.[85,140,161] In this chapter a conclusive picture elucidating, the impact of this weak interaction between aryl and Ni centre in *P,O* Ni(II) catalysts on chain transfer reactions for ethylene polymerization reactions was reported. This study was conducted for two new catalysts, namely **2-CF_3** and **2-CH_3** in Scheme 5.1-B and C, bearing an electron-withdrawing 3,5-bis(trifluoromethyl)phenyl substitution for **2-CF_3** (Scheme 5.1-B) and an electron-donating 3,5-bis(methyl)phenyl substituent for **2-CH_3** (Scheme 5.1-C).

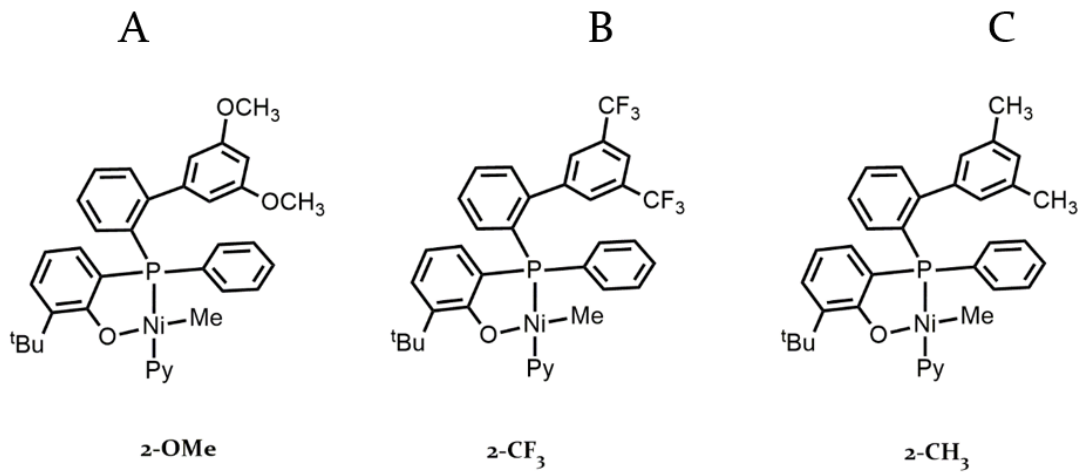

*Scheme 5.1: Structures of phosphinophenolato Ni(II) complex **2-OCH_3**[98] compared to phosphinophenolato Ni(II) **2-CF_3** and **2-CH_3** complexes.*

Experimentally, depending on the electronic nature of the remote substituents on the bidentate ligand, products with different microstructure were obtained with these two catalysts. In detail, it is worth to note that, differently from the Ni(II) salicyilaldiminate complexes,[85,118] catalyst **2-CH_3** with electron-donating substituents produces higher molecular weight polymers (M_n > 800 kg mol^{-1} at 30 °C by GPC) than **2-CF_3** catalyst. Furthermore, it is evidenced by a relatively low number of chains formed per nickel atom also at high temperatures for **2-CH_3** as a catalyst (switching from ≈ 5 to 15 chains for nickel at 30°C and 70° respectively, Table S5.1: entry 4-6). By contrast catalyst **2-CF_3** gives polymers with lower molecular weight (Mn ≈ 60 kg mol^{-1} at 30 °C by GPC and a number of chains that switch from ≈ 8 to 124 chains respect to nickel from 30°C to 70°, respectively), see Table S5.1: entry 1-3.
All the experimental results reported herein on the **2-CF_3** and **2-CH_3** complexes and on their catalytic properties in ethylene polymerization were obtained by Dr. Fei Lin in the group of Prof. Stefan Mecking at the University of Konstanz (Germany).
The impact of the ligand modification on the mechanistic pathways was elucidated by DFT calculations. An isolated analysis of the steric impact of the ligand is given by topographic steric maps, whereas a detailed analysis of the energies of the intermediates and transition

states during catalysis captures both the electronic and steric aspects. The computed free energies are expressed as ΔG_{Tol} in kcal mol^{-1} (the computational details are reported in the supplementary files).

5.2 Results and discussion.

5.2.1 Structural properties of the catalyst precursors.

5.2.1.1 Steric analysis.

Analysis by SambVca 2.1 program[121] provided topographical steric maps and percent buried volume data (%V_{Bur}) related to ligands space filling properties (see Figure 5.1). The most sterically hindered areas for both the complexes are in the axis position of nickel centre, which come from the *ortho*-aryl groups. The comparable %V_{Bur} reveals that the variation of substitutions on *ortho*-aryl groups gives insignificant influence on the steric environment of nickel centre. Remarkably, the distance between the aryl *ipso*-carbon and nickel centre in the complex with electron-donating axis aryl group (3.301, Å for **2-CH$_3$**) is smaller than or close to the sum of van der Walls radii (r_w, 3.33 Å) of carbon and nickel atom,[162] indicating there is a weak interaction between the *ipso*-carbon and nickel centre (as reported in Figure 5.1). This weak interaction can be unfavoured by the electron-withdrawing substitutions on the axis aryl groups, which is evidenced by the larger distances of *ipso*-carbon to Ni in complexes **2-CF$_3$** (3.406 Å). In addition, the presence of a stronger weak interaction in complexes **2-CH$_3$** is also verified by the smaller distance between centre of axis aryl group and nickel atom (3.545 Å) respect to that present in complex **2-CF$_3$** (3.627 Å), see Figure 5.1.

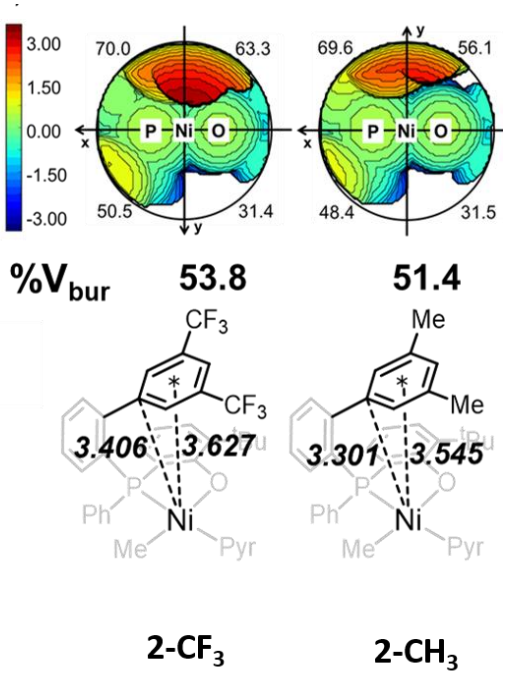

*Figure 5.1: Topographical steric maps with %V_{Bur} of complexes **2-CF$_3$** and **2-CH$_3$**, distance in the colour scale is in Å, H atoms were included in the calculations.*

5.2.2 Mechanistic investigation.

In line with the previous studies on Ni(II) salycilaldiminate complexes,[85,118] modelling starts with **1-β-T** (referenced as the zero point energy, Scheme 5.2), with the growing alkyl chain *trans* to the oxygen atom and a stabilizing η^2 interaction of the aryl ring with the metal centre. From **1-β-T**, the complete mechanisms of the linear propagation reaction and chain transfer reactions were studied, as reported in Scheme 5.2. In detail, the blue and red values account for **2-CF$_3$** and **2-CH$_3$** catalysts, respectively.

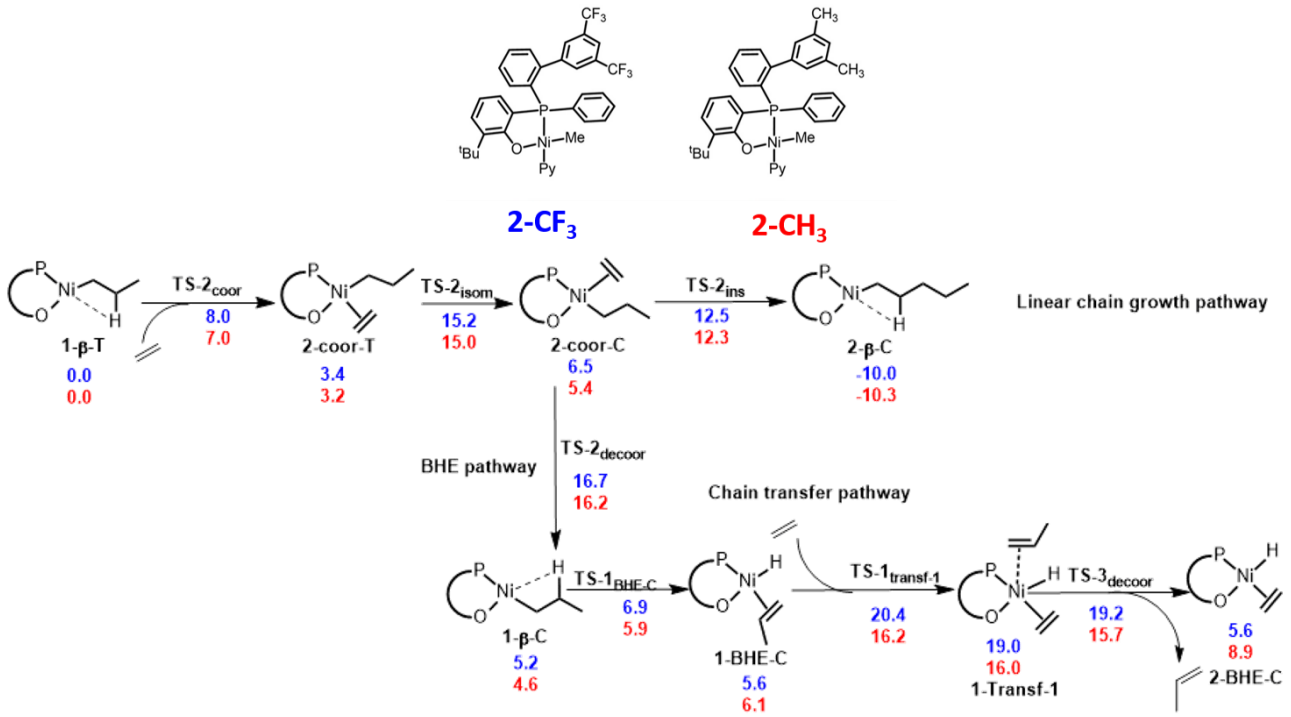

*Scheme 5.2: Gibbs free energies (ΔG_{Tol} in kcal mol^{-1}) of key species along the linear chain growth and chain transfer reactions with catalysts **2-CF$_3$** (blue) and **2-CH$_3$** (red).*

5.2.2.1 Linear chain growth pathway.

From **1-β-T**, the coordination of ethylene to form **2-Coor-T** occurs by opening of the β-agostic interaction through **TS-2$_{coor}$** with a similar free energy barrier for both **2-CF$_3$** and **2-CH$_3$** complexes, i.e. 7.0-8.0 kcal mol^{-1}. The following intermediate is slightly higher in energy relative to **1-β-T** + C_2H_4 and isoenergetic for both catalysts. From **2-Coor-T**, the favoured linear chain growth pathway consists in the isomerization *via* **TS$_{Isom}$** to the less stable *π*-complex **2-Coor-C**, followed by the monomer insertion *via* **TS-2$_{ins}$** leading to **2-β-T**. The two catalysts behave similar along the whole linear chain growth pathway, with the determining isomerization energy barrier of about 15 kcal mol^{-1}, in conformity with the comparable polymerization activities, for more details see Table S5.1 in the supplementary files.

5.2.2.2 BHE elimination.

From the key intermediate **2-Coor-C** (see Figure S5.1), the monomer decoordination reaction competes with the monomer insertion reaction leading to the β-agostic intermediate **1-β-C**

which still features the Ni-aryl interaction mentioned above. Ethylene dissociation takes place *via* a single step (**TS-2**$_{decoor}$) process with a similar energy barrier for the two catalysts (16.2 and 16.7 kcal/mol for 2-$\mathbf{CF_3}$ and **2-**$\mathbf{CH_3}$, respectively).

As consequence, the ethylene decoordination step is no longer the decisive step for the microstructure and molecular weights of the polyethylene obtained.[163]

From **1-β-C**, BHE occurs with an energy barrier of about 6 kcal mol^{-1} for both catalysts leading to the Ni-H intermediate **1-BHE-C**. All the competitive pathways to reach **1-β-C** and **1-BHE-T** were ruled out for kinetic reasons, as already observed for the Ni-salicylaldiminate complexes.

5.2.2.3 Chain transfer pathway.

Starting from **1-BHE-C**, the favoured chain transfer pathway consists in the coordination of a new monomer *via* **TS-1**$_{Transf-1}$ with the formation of a pentacoordinate intermediate **1-Transf-1** that quickly releases propene, *via* **TS-3**$_{Decoor}$, yielding complex **2-BHE-C**. The first step is rds along the chain transfer pathway for both catalysts with an energy barrier 4.2 kcal mol^{-1} higher for **2-**$\mathbf{CF_3}$ than for **2-**$\mathbf{CH_3}$ (Scheme 5.2). In **TS-1**$_{Transf-1}$ the new monomer coordinates in the apical position above the metal displacing the aryl ring-Ni interaction present in all the main species along the considered pathways. As consequence, the stronger Ni-aryl interaction in **2-**$\mathbf{CH_3}$ ascribed to the presence of electron donating groups on the ring (as evidenced also by the shorter Ni-aryl distances in **2-**$\mathbf{CH_3}$ than in **2-**$\mathbf{CF_3}$) is more difficult to break with the energy of **TS-1**$_{Transf-1}$ increasing, in agreement with the higher PE molecular weight obtained experimentally in presence of **2-**$\mathbf{CH_3}$**,** for more details see Table S5.1 in supplementary files.

In conclusion, it is worth to note that the strength of the Ni-aryl interaction increases with the electron density on the aryl ring, that is higher for **2-**$\mathbf{CH_3}$ than **2-**$\mathbf{CF_3}$, with a consequent suppression of the chain transfer reaction to a greater extent, in agreement with the experimental results.

5.2.2.4 Summary and conclusion.

A DFT study on the ethylene polymerization mechanism in presence of the two new Ni(II) phosphinophenolate catalysts was performed with the aim of understanding how a suitable axial shielding of the catalytic site can influence the polymerization behavior. Surprisingly, differently from the common idea that an axial shielding is sufficient to suppress chain transfer reaction to produce high molecular weight polyethylene, despite both the catalysts in this study were adequately shielded in the axial direction, only catalyst **2-**$\mathbf{CH_3}$, bearing electron-donating substituents, can lead to high molecular weight polyethylene. These DFT calculations showed how the combination of the peculiar geometry with the right electronic and steric nature of the ligands for the phosphinophenolato Ni(II) catalysts affects the chain transfer reaction, providing a rationalization of the different microstructure of the polyethylene obtained: the more electron donating are the substituents on the aryl ring of the ligand, the more energetically costly is the releasing of the favorable Ni-aryl apical interaction along the chain transfer reaction and, as a consequence, the higher are the molecular weights of the PE produced. This work sheds new light on polymerization catalyst design to well

control the polymerization performance, the deeper works on living polymerization and copolymerization are currently in progress.

5.3 Supplementary files.

5.3.1. Polymerization reaction.

Table S5.1 Ethylene polymerization by complexes **2-CF$_3$** and **2-CH$_3$**.[a] All the experimental results reported herein for these complexes and experimental studies of their catalytic properties in ethylene polymerization were performed by Dr. Fei Lin in the group of Prof. Stefan Mecking at the University of Konstanz (Germany).

Entry	Complex	T (°C)	Yield (g)	Activity[b]	M_n[c] (× 10^3)	M_w/M_n[c]	chains per nickel	T_m[d] (°C)	cryst.[d] (%)
1	**2-CF$_3$**	30	0.47	0.94	57	2.00	8.2	135	66
2	**2-CF$_3$**	50	2.43	4.86	49	1.66	49.6	136	76
3	**2-CF$_3$**	70	3.36	6.72	27	1.77	124.4	135	76
4	**2-CH$_3$**	30	4.38	8.76	816	1.96	5.4	139	50
5	**2-CH$_3$**	50	4.96	9.92	430	2.03	11.5	141	54
6	**2-CH$_3$**	70	2.87	5.74	187	2.11	15.3	138	55

a) Polymerization conditions: 1 μmol of complex in 100 mL of toluene, 10 bar ethylene pressure, 30 min polymerization time, 1000 rpm. *b*) Given in 10^6 g_{PE} mol_{Ni}^{-1} h^{-1}. c*)* Determined via GPC at 160 °C in 1,2-dichlorobenzene. *d)* Determined by DSC with 10 K min^{-1} heating/cooling rate (data from second heating cycle), crystallinities were determined assuming a melt enthalpy of 293 J g^{-1} for 100% crystalline polyethylene.

5.3.2 Mechanistic investigation.

5.3.2.1 Selected Intermediates and Transition States.

*Figure S5.1: Optimized geometries of **2-Coor-C** for **2-CF$_3$** and **2-CH$_3$** (top), **TS-2$_{decoor}$** and **TS-2$_{decoorAr}$** for **2-CH$_3$** (middle), and **TS-1$_{Transf-1}$** for **2-CF$_3$** and **2-CH$_3$** (bottom) are shown, relevant distances are included.*

2-Coor-C

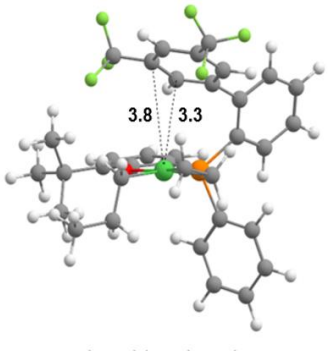

2-CF_3

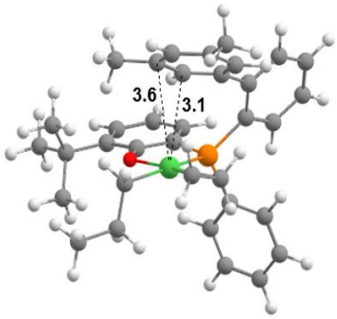

2-CH_3

TS-2_{decoor}

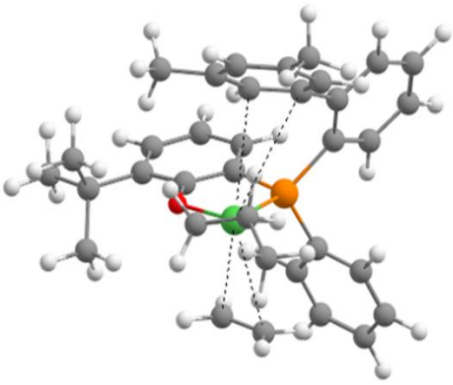

2-CH_3

TS-$2_{decoorAr}$

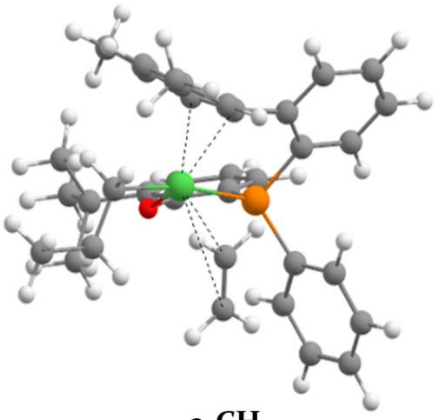

2-CH_3

TS-$1_{Transf-1}$

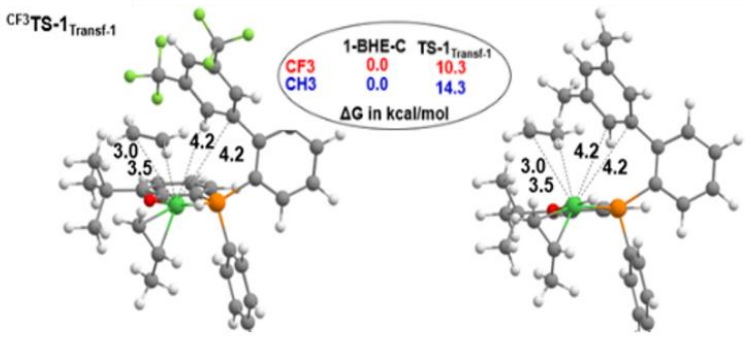

2-CF_3

2-CH_3

5.3.3 Computational details

5.3.3.1 General Methods

All the DFT geometry optimizations were performed at the GGA BP86[122-124]level with the Gaussian 09 package.[125] The electronic configuration of the systems was described with the 6-31G(d) basis set for H, C, N, F, P and O while for Ni the quasi-relativistic LANL2DZ ECP effective core potential was adopted.[126] All geometries were characterized as minimum or transition state through frequency calculations. The reported free energies were built through single point energy calculations on the BP86/6-31G(d) geometries using the M06 functional and the triple-ζ TZVP[127-129] basis set on main group atoms. Solvent effects (toluene) were included with the PCM.[130-131] To this M06/TZVP electronic energy in solvent, thermal corrections were included from the gas-phase frequency calculations at the BP86/6-31G(d).

Chapter 6

Results and discussion

Theoretical study by DFT of the ethylene-CO copolymerization promoted by Neutral Ni(II) Phosphine Phenolate Complexes: rationalization of the steric and electronic effects.

6.1 Introduction.

An access to polyethylenes with in-chain keto units by incorporation of small amounts of carbon monoxide CO during ethylene polymerization has been long sought after. As anticipated in chapter one, small amounts of these keto units can impart the material with desirable photodegradability to reduce the problematic environmental persistency of mismanaged polyethylene waste.[164] Due to the strong relative binding and low insertion barriers of carbon monoxide relative to ethylene, catalytic copolymerizations usually afford strictly alternating copolymers.[165] These are high melting materials with entirely different properties and application profiles than polyethylene. Note that copolymerizations of other functionalized vinyl monomers with CO are also found to occur by an alternating mechanism.[166-167] Until a few years ago, the only known catalytic systems capable of introducing several consecutive ethylene units in addition to alternating motifs were neutral phosphinesulfonato Pd(II) complexes, the **Drent** catalyst in Scheme 6.1;[168] these are only recently complemented by cationic diphosphazane monoxide Pd(II) catalysts.[169] However, either very high carbonyl contents resulting in material properties similar to alternating polyketones (Tm ~ 200 °C) are obtained,[170] or low molecular- weight wax-like materials (Mn ≤ 3.000 g/mol) are formed, which impedes any study of material properties.[171-175] Note this picture was altered only most recently by Nozaki, who succeeded in generating higher molecular weight linear polyethylene with isolated in-chain keto units employing metal carbonyls as a source of carbon monoxide in combination with advanced phosphinesulfonato Pd(II) catalysts.[176]

Considering the possible alternative catalysts, neutral Ni(II) catalysts have long been known to be capable of ethylene chain growth reactions,[177] and recent developments pioneered by Shimizu afforded catalysts that generate high molecular weight materials.[155,98,178–179] Concerning the reactivity of neutral Ni(II) catalysts toward carbon monoxide, previous studies suggest that the phosphineenolato Ni(II) complexes investigated are sensitive for irreversible deactivation and form alternating polyketones at the most.[180] With this background, it is all the more notable that the long-sought non-alternating copolymerization is enabled by advanced phosphinephenolato Ni(II) complexes. New phosphinophenolato catalytic precursors were synthetized and the related catalytic properties tested in E-CO copolymerization by the experimental group of Prof. Mecking at the University of Konstanz (Germany), i.e. **1-OCH$_3$**, **2-OCH$_3$**, **3**, **3′** and **4** (see Scheme 6.1).[99,181] All these systems at 10 bar overall reaction pressure with low concentration of carbon monoxide (0.02 bar of ^{13}CO) yields polyethylenes with isolated keto groups, with the exception of **4** that produces in the same

reaction conditions prevalently alternating copolymers, for more details see Table S6.1 in the supplementary files. The amount of alternating *vs* non-alternating keto groups motifs (i.e. motif that have at least two consecutive ethylene units after a CO unit in the chain) varies distinctly among the polymers produced with these systems, for more details see the copolymer analysis in the supplementary files.

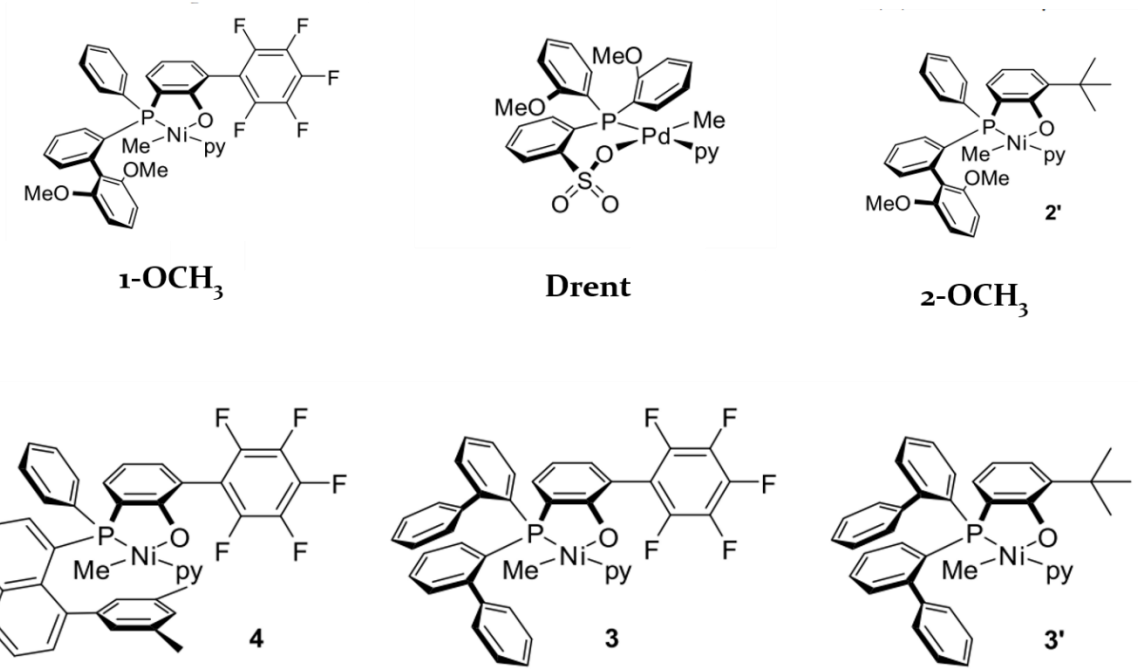

Scheme 6.1: Ni(II) Phosphinephenolate Catalysts Studied, and Phosphinesulfonato Pd(II) Reference System.

These findings prompt the question of how non-alternating ethylene–CO chain growth occurs in presence of this class of catalysts, i.e phosphine phenolate complexes reported in Scheme 6.1.

In this chapter relevant pathways and barriers identified by extensive theoretical studies are reported. This study also provides the first insights into how the active sites properties are determined by their coordination environment of the metal during this kind of reaction, in agreement with the experimental observations reported in Table S6.1 in the supplementary files.

At first, the results obtained from the in-depth mechanistic DFT study in presence of the neutral Ni(II)-phosphinephenolate catalyst **1-OCH$_3$** and the phosphinesulfonato Pd(II) reference system, i.e. **Drent** catalyst, are reported, see Scheme 6.1. Then, several different phosphinephenolato Ni(II) catalysts with different substitution patterns were explored (**2-OCH$_3$**, **3**, **3'** and **4** see Scheme 6.1). The computed free energies are expressed as ΔG_{Tol} in kcal mol^{-1} and reported in Scheme 6.2 (the computational details and the alternative pathways are reported in the supplementary files).

6.2 Results and discussion

6.2.1 Structural properties of the catalyst.

6.2.1.1 Structural analysis of the intermediate 1-cycle5-T.

Since **1-cycle5-T** intermediate is the starting point of both pathways giving access to the formation of non-alternating keto polyethylene and alternating polyketone segments, respectively, we performed an in-depth structural analysis of this species to determine the stability and the strength of the metal···O interaction depending on the nature of the metal as well as on the chelating ligand structure.

As expected, for **Drent** complex, the Pd···O interaction is weaker compared to the nickel complex **1-OCH$_3$**, as reflected by a longer Pd···O distance in **1-cycle5-T** for **Drent**, comparing the distances reported in Scheme 6.2. This effect is ascribed to the greater electron density on the palladium centre compared to the nickel site.

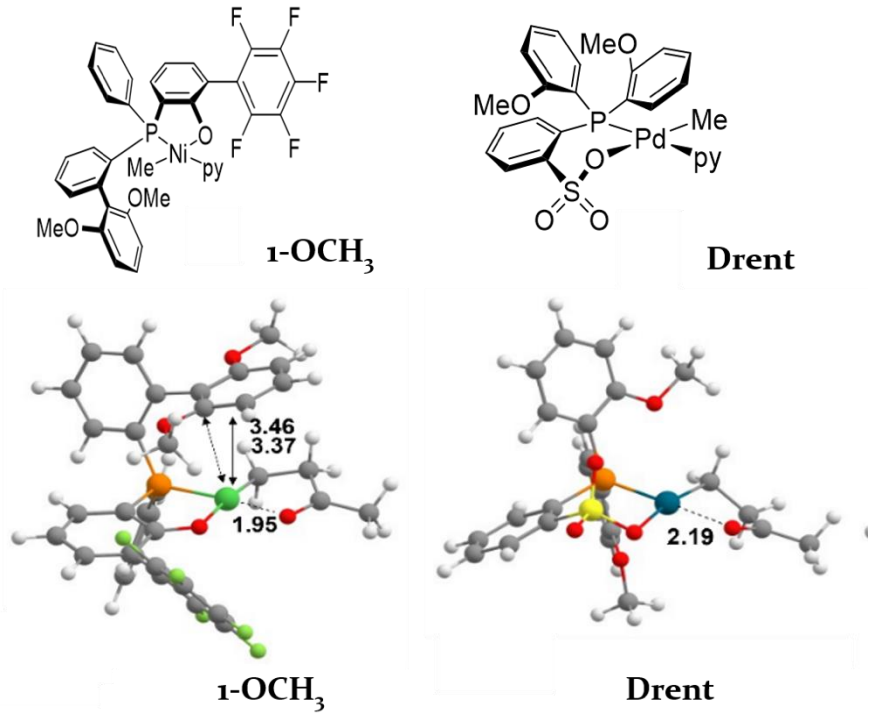

*Figure 6.2: Geometries of the catalysts **1-OCH$_3$** and **Drent** and the corresponding chelate **1-cycle5-T** intermediate for catalysts **1-OCH$_3$** (left) and **Drent** (right), distances are in Å.*

Furthermore, it is worth noting that in the case of **1-OCH$_3$** complex an η^2 interaction of the aryl ring of the bis-phenyl moiety with the metal is observed.

6.2.2 Mechanistic investigation.

For all catalysts explored (see Scheme 6.1), the intermediate **1-cycle5-T** with the alkyl chain in the *trans* position to the oxygen atom models the growing polymer chain formed after the migratory insertion of an ethylene unit into the metal–acyl bond (Scheme 6.2 and 6.3).

This stable five membered chelate is set as zero point energy for the entire ethylene and CO copolymerization pathway,[182] in line with previous calculations reported by Ziegler[107-108] on the competition between the alternating and non-alternating E-CO copolymerization catalysed by the reference **Drent** complex. Here, these mechanisms were re-evaluated at a higher level of theory to use **Drent** catalyst as a reference for the nickel-based catalysts, taking

into account a more complete reaction scenario (for more details on the competitive studied pathways, see the supplementary files).
Starting from **1-cycle5-T**, all intermediates and transition states (TSs) were calculated along the catalytic pathways involved in the formation of alternating (**alt**) and non-alternating (**non-alt**) polymer motifs for complex **1-OCH$_3$** and for the reference **Drent** complex (see Scheme 6.3).

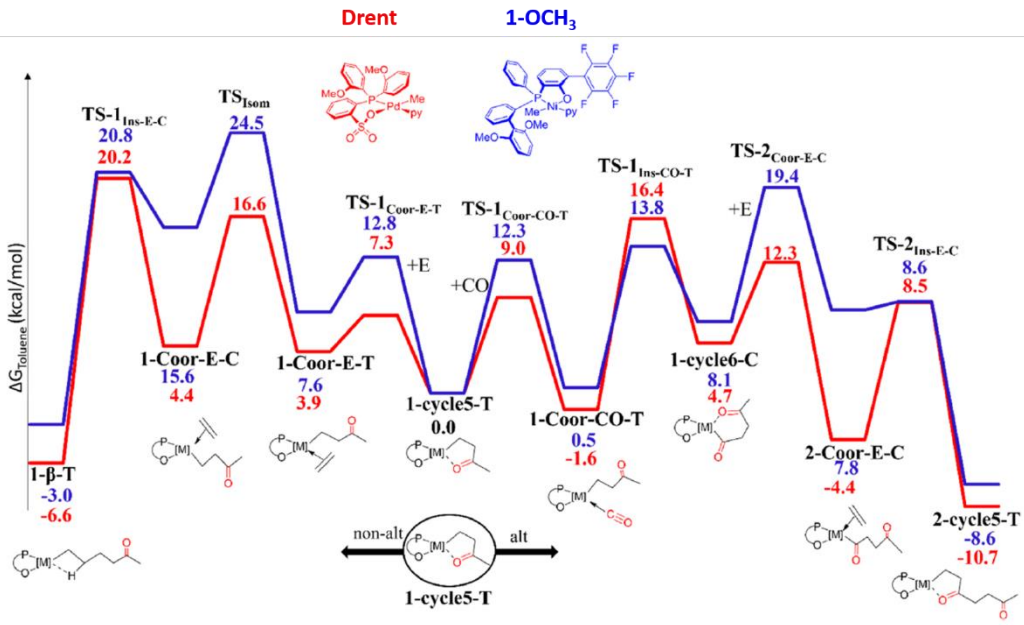

*Scheme 6.3: Free energies (ΔG_{tol} in kcal mol^{-1}) of the key steps for **non-alt** and **alt** carbon monoxide incorporation with catalysts **1-OCH$_3$** (blue) and **Drent** (red). The labels of the species in black (intermediates and TSs) refer to 1-* for species involved in monomer incorporation (E or CO) from **1-cycle5-T**, 2-* for the next second) monomer (CO + E) incorporation.*

6.2.2.1 Non-alternating chain growth (not-alt) pathway.

The results of the **non-alt** pathway are reported from **1-cycle-5-T** to the left in Scheme 6.3. Starting from the **1-cycle-5-T** intermediate, this catalytic pathway is initiated by the concerted ethylene coordination and opening of the metal···O interaction *via* **TS-1$_{Coor-E-T}$**, requiring a free energy barrier of 12.8 and 7.3 kcal mol^{-1} for **1-OCH$_3$** and **Drent** catalysts, respectively, see Scheme 6.3.
The greater electron density present on the metal centre for **Drent** clearly facilitates this step. For both complexes, the resulting **1-Coor-E-T** intermediate with the alkyl chain *trans* to the oxygen is higher in energy relative to **1-cycle5-T** + C_2H_4 considered at infinite distance, and this is more pronounced for **1-OCH$_3$** than for **Drent** (7.6 kcal mol^{-1} for **1-OCH$_3$** and 3.9 kcal mol^{-1} for **Drent**). This is likely due to the lower electron density present at the nickel centre in the neutral (*P, O*) Ni complex, which causes a weaker binding of the ethylene as a result of a reduced back-donation from the metal to the olefin.
Both complexes prefer to isomerize from **1-Coor-E-T** to the less stable **1-Coor-E-C** intermediate *via* **TS$_{Isom}$** before inserting the monomer *via* **TS-1$_{Ins-E-C}$**, for more details see supplementary files. This pathway is preferred to direct ethylene insertion from **1-Coor-E-T**,

which goes along with a significantly higher energy barrier (10 kcal mol^{-1} higher than insertion from the isomer **1-Coor-E-C**, for details see the supplementary files).
The isomerization step *via* the transition state **TS$_{Isom}$** requires a significantly higher energy barrier for the nickel complex compared to the palladium complex (24.5 and 16.6 kcal mol^{-1} for **1-OCH$_3$** and **Drent** catalysts, respectively) due to a much higher steric hindrance caused by the η^2 coordination of the aryl ring to the metal in **1-OCH$_3$**, as evidenced by the topographic steric maps reported in Figure 6.1 (compare NE and NW quadrants for **1-OCH$_3$** and **Drent** complexes).

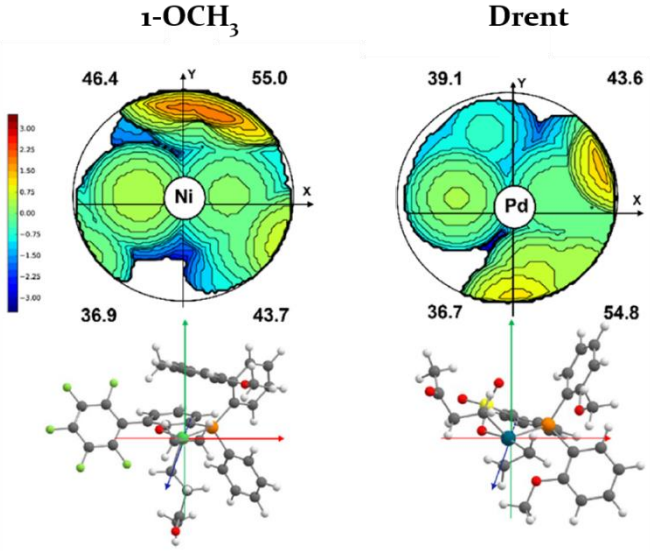

*Figure 6.1: Topographic steric maps of the transition state **TS$_{Isom}$** for catalysts **1-OCH$_3$** (top left) and Drent (top right). The complexes are oriented as shown below (bottom left and right).*[121]

Following the formation of **1-Coor-E-C**, the monomer insertion occurs *via* **TS-1$_{Ins\text{-}E\text{-}C}$** to yield the stable β-agostic complex, **2-β-T**. The overall free energy barrier from **1-cycle5-T** to **TS-1$_{Ins\text{-}E\text{-}C}$** amounts to 20.8 and 20.2 kcal mol^{-1} for **1-OCH$_3$** and **Drent** catalysts, respectively. Notably, the monomer insertion barrier is similar for both complexes; however, for **Drent** catalyst, it represents the rds of the **non-alt** pathway, while for **1-OCH$_3$**, it is lower than the *cis*/*trans* isomerization that becomes the rds for the **non-alt** chain growth pathway due to steric impediments.

6.2.2.2 Alternating chain growth (alt) pathway.

The results of the **alt** pathway are reported from **1-cycle-5-T** to the right in Scheme 6.3. Starting from **1-cycle5-T**, alternatively to ethylene coordination, CO coordination can take place, leading to the isoenergetic **1-Coor-CO-T** intermediate. The overall energy barrier for this process is, also in this case, higher for the nickel complex (12.3 kcal mol^{-1} for **1-OCH$_3$** *vs* 9.0 kcal mol^{-1} for **Drent**), in line with the greater strength of the Ni···O interaction with respect to the Pd···O one. From **1-Coor-CO-T**, CO insertion occurs *via* **TS-1$_{Ins\text{-}CO\text{-}T}$**, yielding the six-membered chelate species, **1-cycle6-C**.[183] The overall free energy barriers from **1-Coor-CO-T** to **TS-1$_{Ins\text{-}CO\text{-}T}$** amount to 13.8 and 18.0 kcal mol^{-1} for **1-OCH$_3$** and **Drent**, respectively. This difference is ascribed to a weaker σ-donation from the coordinated CO to a more electron-rich palladium centre with respect to the nickel case, as confirmed by the increased

metal–CO bond length in **TS-1**$_{Ins\text{-}CO\text{-}T}$ for **Drent** with respect to **1-OCH$_3$**, comparing the distances reported in Figure 6.2.[184]

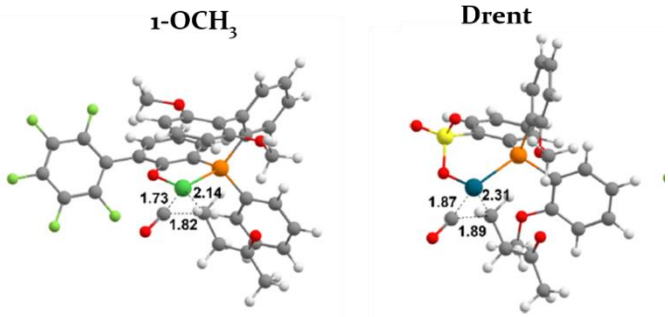

*Figure 6.2: Geometry of **TS-1**$_{Ins\text{-}CO\text{-}T}$ for catalysts **1-OCH$_3$** (left) and **Drent** (right). Distances are reported in Å.*

Notably, for **1-OCH$_3$**, the resulting chelate **1-cycle6-C** is unfavored by 8.1 kcal mol^{-1}, whereas for **Drent** catalyst, it is unfavored only by 4.7 kcal mol^{-1}. This difference is related again to the greater electron density on the Pd centre that stabilizes the metal–acyl bond in the *trans* position to the phosphorus atom to a greater extent than that for **1-OCH$_3$**. From **1-cycle6-C**, ethylene coordinates *trans* to the oxygen atom (**2-Coor-E-C**) through **TS-2**$_{Coor\text{-}E\text{-}C}$ that is about 7 kcal mol^{-1} higher in energy for **1-OCH$_3$** than for **Drent** (compare barriers of 19.4 and 12.3 and for **1-OCH$_3$** and **Drent** catalysts, respectively). This difference is related once again to the greater electron density present at the palladium centre, which favours the opening of the chelate required for ethylene coordination. For catalyst **1-OCH$_3$**, the resulting **2-Coor-E-C** intermediate is 12.2 kcal mol^{-1} less stable than the corresponding Pd intermediate (compare 7.8 kcal mol^{-1} for **1-OCH$_3$** and –4.4 kcal mol^{-1} for **Drent**, respectively). This is likely due to both the higher steric hindrance of the phosphine-bound aryl substituents and the reduced electron density on the metal centre for **1-OCH$_3$**. From **2-Coor-E-C**, the following ethylene insertion occurs *via* **TS2**$_{Ins\text{-}E\text{-}C}$ (at 8.6 and 8.5 kcal mol^{-1} for **1-OCH$_3$** and **Drent** catalysts, respectively), yielding the stable five-membered chelate complex **2-cycle5-T** at –8.6 and –10.7 kcal/mol for **1-OCH$_3$** and **Drent**, respectively.

Notably, in the case of **Drent** catalyst, the rds is the CO insertion with an energy barrier of 18.0 kcal mol^{-1}, whereas in the case of catalyst **1-OCH$_3$**, the rds is ethylene coordination with an energy barrier of 19.4 kcal mol^{-1}.

6.2.2.3 Comparison of 1-OCH$_3$ and Drent catalysts.

The pathways elucidated above underline that the five membered chelate complex **1-cycle5-T** is the key intermediate of this copolymerization catalysis, opening the route to both the **non-alt** and **alt** chain growths. The competition between these pathways determines the polymer microstructure. Starting from **1-cycle5-T**, for both catalysts considered, the two pathways are feasible and competitive with one another. Comparing the rate determining energy barriers along the two pathways, i.e., $\Delta\Delta G^{\ddagger}$ (**non-alt**)–(**alt**) of 5.1 kcal mol^{-1} for **1-OCH$_3$** and 3.8 kcal mol^{-1} for **Drent**, it emerges that overall complex **1-OCH$_3$** is similar to **Drent** complex showing a $\Delta\Delta G^{\ddagger}$ (**non-alt**)–(**alt**) higher by only 1.3 kcal mol^{-1}. This result agrees with the experimental finding of non-alternating keto groups and alternating motifs formed in pressure-reactor copolymerizations with these catalysts, for more details see the Table S6.1 in the supplementary files. The slight preference for alternating incorporation found by

theoretical methods is offset by the high ethylene-CO monomer ratio employed in the copolymerization experiments. The experimentally observed slightly higher portion of isolated keto units in the polymer obtained with **Drent** catalyst compared to **1-OCH$_3$** agrees with the slightly lower $\Delta\Delta G^{\ddagger}$ (**non-alt**)–(**alt**) determined theoretically for **Drent**; for the detailed discussion on the comparison between the theoretical and the experimental ratio of **non-alt** propagation to **alt** propagation segments, see the section S6.3.2 in the supplementary files.

The results outlined show the following: (I) Steric factors affect the **non-alt** pathway. The η^2 coordination of the aryl ring to the metal causes a greater steric hindrance for complex **1-OCH$_3$** increasing the energy of the transition state with higher steric demand, i.e., the *cis*/*trans* isomerization. (II) Electronic factors affect the **alt** pathway. The lower electron density at the Ni centre favours the CO migratory insertion into the metal–alkyl bond and reinforces the Ni···O interaction increasing the energetic barrier of ethylene coordination, which consequently becomes the decisive step.

6.2.2.4 Impact of the Structure of Chelating Phosphinephenolates on Catalysis: Phosphine Donor Substituents.

To elucidate the impact of the electronic and steric nature of chelating phosphine phenolate on the two competing pathways, catalysts **3** and **4** (see Scheme 6.1) were investigated. Since the $\Delta\Delta G^{\ddagger}$ (**non-alt**)–(**alt**) determined for **1-OCH$_3$** and **Drent** was found to correlate with the experimentally observed copolymer microstructures, these further calculations were focused on the two crucial transition states. Starting from **1-cycle5-T**, by comparing the rate-determining energy barriers along the two pathways, it emerges that $\Delta\Delta G^{\ddagger}$ (**non-alt**)–(**alt**) is 6.5 kcal mol^{-1} for **3** and 9.2 kcal mol^{-1} for **4**, which are 1.4 and 4.1 kcal mol^{-1} higher for **3** and **4**, respectively, compared to that for **1-OCH$_3$**. This trend qualitatively agrees with the experimentally observed microstructures (see the Table S6.1 in the supplementary files).

For **3**, the **non-alt** pathway suffers from the increased steric hindrance of the P-bound substituents, i.e., the additional aryl ring in the axial plane perpendicular to the coordination plane (compare SE quadrants in the steric maps of **TS$_{Isom}$** for **1-OCH$_3$** and **3** in Figure 6.3).

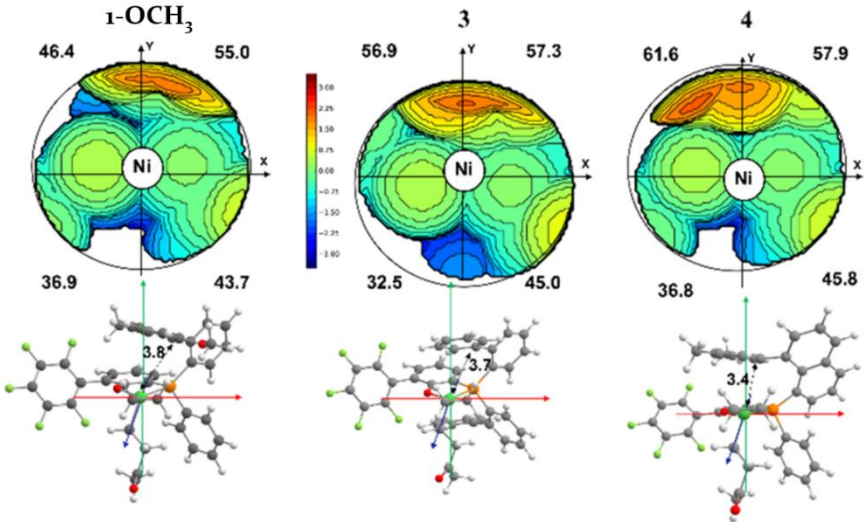

Figure 6.3: Topographic steric maps of transition state TS_{Isom} *for catalysts* **1-OCH$_3$** *(left),* **3** *(in the centre) and* **4** *(right). The Ni···C_{ipso} distances are reported in Å.*

Moreover, the absence of the methoxy groups on the aryl moiety allows the ring to be in closer proximity to the Ni in **3** than in **1-OCH$_3$** (compare Ni–aryl distances in Figure 6.3). As a consequence, the energy barrier for the *cis*/*trans* isomerization increases. On the other hand, despite the shorter Ni···aryl ring distances for **3** than that for **1-OCH$_3$**, the lack of the electron-donating groups on the aryl ring of the bis-phenyl moiety reduces the electron density transferred to the metal for **3** compared to that for **1-OCH$_3$**. As result, for **3**, the Ni···O interaction in the chelate is stronger, increasing the energy barrier for ethylene coordination, i.e., **TS-2$_{Coor\text{-}E\text{-}C}$** (for the electronic analysis, see the section 6.3.3 in the supplementary files). Overall, catalyst **3** favours the **non-alt** pathway to a lower extent with respect to **1-OCH$_3$**. Moving to **4**, the aromatic ring on the naphthyl ligand interacts even more closely with Ni (compare the aryl–Ni distance in Figure 6.3), increasing both the steric hindrance around the catalytic centre and the electron density on the metal due to the presence of the less encumbered and electron-donating methyl substituents on catalyst **4** compared to the larger methoxy groups on catalyst **1-OCH$_3$** (see electronic analysis in the section 6.3.4 in the supplementary files). As a result, the Ni···O interaction in the chelate intermediates (i.e., **1-cycle5-T** and **1-cycle6-C**) weakens, lowering the ethylene coordination TS (**TS-2$_{Coor\text{-}E\text{-}C}$**) to such an extent that the CO migratory insertion (**TS1$_{Ins\text{-}CO\text{-}T}$**) becomes the rds along the **alt** pathway. Moreover, for steric reasons (compare the Ni···C_{ipso} aryl ring distances reported in Figure 6.3 for catalysts **1-OCH$_3$** and **4**), the *cis*/*trans* isomerization rds along the **non-alt** pathway is even more penalized. Consequently, the $\Delta\Delta G^{\ddagger}$ (**non-alt**)–(**alt**) is higher for **4** than that for **3** and **1-OCH$_3$**, in line with the experimentally observed preference for alternating chain growth (for more details see Table S6.1 in the supplementary files).

6.2.2.5 Impact of the Structure of Chelating Phosphinephenolates on Catalysis: Phenolate Substituents.

As regards the impact of the substituent in the *o*-position on the phenolate moiety, for comparison to the pentafluorophenyl-substituted catalysts **1-OCH$_3$** and **3** their *tert*-butyl substituted analogues (**2-OCH$_3$** and **3′**, see Scheme 6.1) were also explored. From a steric point of view, **2-OCH$_3$** and **3′** are similar to their C_6F_5 analogues **1-OCH$_3$** and **3** as suggested by the topographic steric maps and have similar values of the buried volume (%V_{Bur}) of the quadrants (see Figure 6.4 for **1-OCH$_3$** *vs* **2-OCH$_3$** and Figure S6.4 in the supplementary files for **3** vs **3′**). Moreover, from an electronic analysis (for more details see the section 6.3.3 in the supplementary files), the nature of the substituent does not alter the charge on the metal dramatically. Indeed, the calculated $\Delta\Delta G^{\ddagger}$ (**non-alt**)–(**alt**) of 5.7 kcal mol^{-1} for **2-OCH$_3$** and 6.4 kcal mol^{-1} for **3′** are similar to those of 5.1 and 6.5 kcal mol^{-1} for the respective C_6F_5 analogues **1-OCH$_3$** and **3**, respectively. This is well in agreement with the experimentally observed smaller effect of the phenolate substitution compared to the phosphine substituents on the polymer microstructures (see Table S6.1 in the supplementary files).

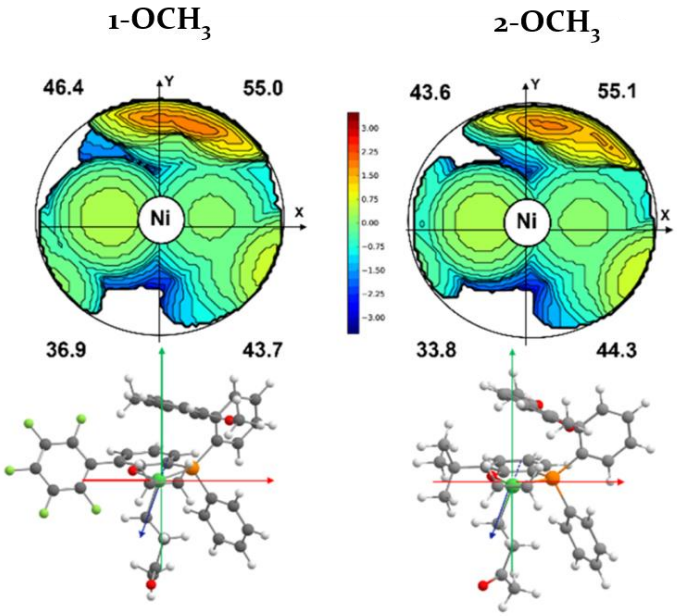

Figure 6.4: Topographic steric maps of ***TS$_{Isom}$*** *for catalysts* ***1-OCH$_3$*** *(left) and* ***2-OCH$_3$*** *(right).*

6.2.2.6 Summary and conclusion.

The non-alternating copolymerization of ethylene with carbon monoxide to obtain polyethylene materials with in-chain ketone moieties was achieved recently by means of customized Ni(II) phosphinephenolate catalysts. In this chapter the DFT study on the E- CO copolymerization mechanism was discussed. The theoretical study combined with the experimental one done by the group of Prof. Stefan Mecking reveals the mechanism of chain growth of this reaction. The rds of the pathway leading to the non-alternating incorporation of the two monomers is the *cis*/*trans* isomerization of the alkyl-olefin-intermediate. The formation of alternating motifs, instead, is determined by the opening of the six-membered chelate by ethylene coordination. The nature of the rds of either pathway differs from that of a phosphinesulfonate Pd(II) **Drent** complex, which is studied here as a reference at the same

level of theory. The pathways and barriers identified for non-alternating *vs.* alternating incorporation of ethylene and carbon monoxide agree qualitatively with experimentally observed microstructures from pressure-reactor copolymerizations with catalysts varying in the phosphinephenolates' structure. In the Ni(II) phosphinephenolate catalysts studied, the desired non-alternating incorporation is the result of a favorable combination of electronic and steric factors. (1) A moderate steric hindrance of the phosphine moiety on the ligand facilitates the **non-alt** path. (2) A balanced electronic donation to the electron-poor Ni centre is desirable to avoid the formation of a too stable five-membered chelate resting state that would reduce the catalytic activity, while an increase in the stability of the six-membered chelate disfavours the undesired **alt** path. The aromatic rings on the phosphine moieties may provide a suitable electronic contribution when apically coordinated to the metal centre, and easily clear out the catalytic site by moving away from the metal in the transition states with higher steric demand, i.e., the *cis*/*trans* isomerization and the ethylene coordination steps. In fact, the P-bound 2′,6′-dimethoxybiphenyl moiety in catalysts **1-OCH$_3$** and **2-OCH$_3$** increases the energy barrier for ethylene coordination but does not impede the linear growth of the polyethylene chain. These insights will also promote the discovery and the design of novel catalysts for this unique co-polymerization reaction, which provides in-chain-functionalized polyethylenes with a desirable property profile including lower environmental persistence.

6.3 Supplementary files.

6.3.1 Polymerization experiments.

Table S6.1: Polymerization Results.[a] All the experimental results reported herein for these complexes and experimental studies of their catalytic properties in ethylene-CO copolymerization were performed by Dr. Lukas Odenwald, Dr. Maximilian Baur and Dr. Fei Lin in the group of Prof. Stefan Mecking at the University of Konstanz (Germany).

Cat.	yield [mg]	TOF[b]	χ_{NMR}[c] [mol%]	Microstr. I / NA / A[d] [mol-%]	Insertions na/alt[e]
Drent	34	1.46	7.3	82/17/1	92/8
1-OCH$_3$	11	0.47	10.3	34/51/15	60/40
2-OCH$_3$	25	1.07	8.4	56/39/5	75/25
3	37	1.59	10.8	19/51/30	45/55
3'	31	1.33	14.4	19/53/28	46/54
4	12	0.51	36.7	0/18/82	9/91

[a] Reaction conditions: 10 μmol catalyst precursor, 200 mL of toluene 90 °C, 0.02 bar ^{13}CO, 5 min reaction time, 10 bar reaction pressure, and 1000 rpm. [b] TOF given in units of 103 mol [C_2H_4] mol^{-1} [Ni] h^{-1}. [c] Determined by ^{1}H-NMR spectroscopy. [d] I: isolated carbonyl, NA: nonalternating motifs, A: alternating motifs. Determined by ^{13}C

NMR spectroscopy (Figure S6.3). [e] Relative ratio of non-alternating and alternating carbon monoxide incorporation events, derived from the microstructure ((I + 0.5 NA)/(0.5 NA + A)).

6.3.2 Copolymer analysis.

6.3.2.1 Determination of CO incorporations from ^{1}H NMR spectra.

Compositions of ethylene-CO copolymers were determined from ^{1}H NMR spectra according to equation (1).

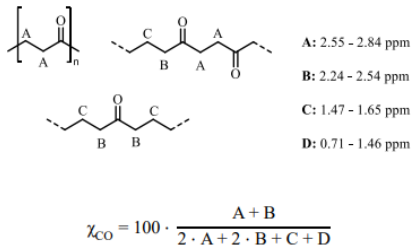

$$\chi_{CO} = 100 \cdot \frac{A + B}{2 \cdot A + 2 \cdot B + C + D} \qquad (1)$$

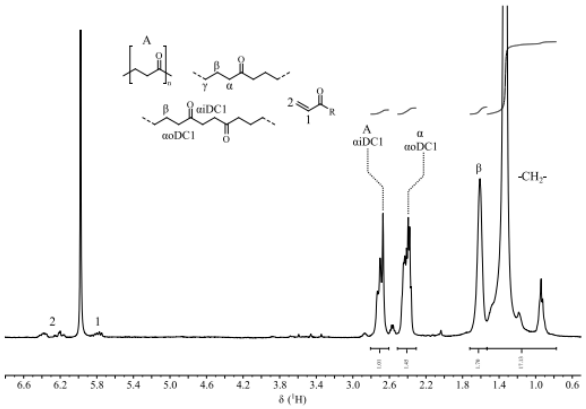

*Figure S6.1: Exemplary ^{1}H NMR spectrum of an ethylene-CO copolymer produced with catalyst **1-OCH$_3$** with assignment of typical motifs.*

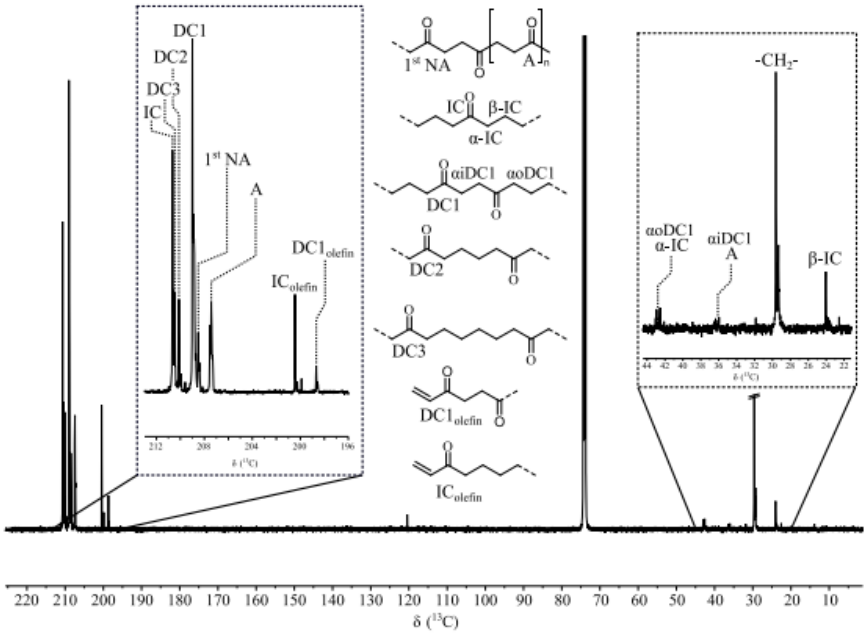

Figure S6.2: Exemplary ^{13}C NMR spectrum of an ethylene-CO copolymer produced with catalyst ***1-OCH$_3$*** with assignment of typical motifs.

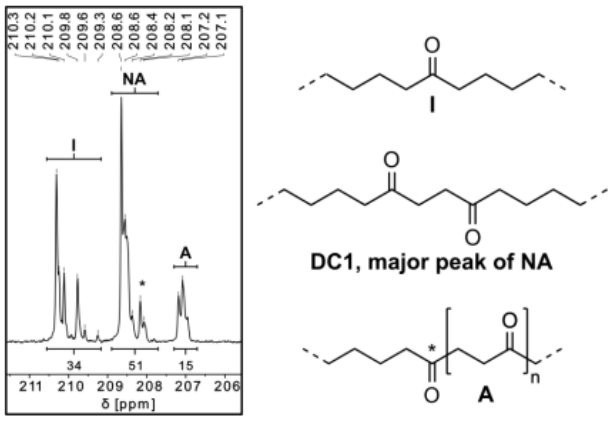

Figure S6.3: Exemplary $^{13}C\{^1H\}$ NMR spectrum of a copolymer (obtained with catalyst catalyst ***1-OCH$_3$***, Table S6.1, entry 2) with assignments of repeat unit motifs. In terms of CO incorporation events during polymerizaton, isolated motifs (I) correspond to an incorporation along the non-alternating pathway, alternating motifs (A) correspond to an incorporation along the alternating pathway, and non-alternating motifs (NA) correspond to a combination of an alt-pathway and a subsequent non-alt pathway. Thus, the relative ratio of non-alternating and alternating carbon monoxide incorporation events can be derived from the microstructure as (I + 0.5 NA) / (0.5 NA + A).

6.3.2.2 Comparison of propensity to non-alternating vs. alternating chain propagation determined by DFT methods and from experimentally observed microstructures.

In agreement with the equations reported by Ziegler[90] the theoretical ratio of non-alternating propagation to alternating propagation (f_{na}) can be evaluated as:

$$f_{na} = \frac{r_{na}}{r_a} = \left(\frac{k'_{C2H4}}{k_{CO}}\frac{[C2H4]}{[CO]}\frac{K_1}{K_2}\right)\left(1 - \frac{k_{CO}^{-1}}{K_4 * k_{C2H4} * [C2H4] + k_{CO}^{-1}}\right)^{-1} = F_B \times F_{cor}$$

In detail, r_{na} is the probability to obtain non-alternating segments, whereas r_a is the probability to obtain alternating segments.

The equilibrium and kinetic constants of the equation refer to the following scheme:

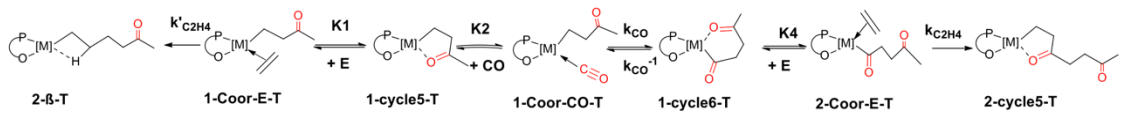

Since the CO pressure of 0.02 bar is estimated to correspond to a concentration of [CO] ≈ 1.7×10^{-4} mol L^{-1} (at 90°C in toluene)[19] and the ethylene (10 bar) concentration is estimated to [E] ≈ 0.67 mol L^{-1} (from data at 95 °C),[20] the calculated f_{na} value for catalyst **Drent** is 20.0.

It worth to note that the contribution of F_{cor} to f_{na} is negligible because k_{CO}^{-1} is << $K_4 * k_{C2H4}$ [C_2H_4] (indeed F_{cor} is 1).

In other words, the value of f_{na} corresponds to Brookhart's equation[21]:

$$f_{na} = \frac{r_{na}}{r_a} = \left(\frac{k'_{C2H4}}{k_{CO}} \frac{[C2H4]}{[CO]} \frac{K_1}{K_2}\right)$$

Moving to the Ni catalysts, from calculations it emerges that the **TS_{Isom}** shows the highest barrier along the non-alt path and the overcoming of the barrier that corresponds to the opening of the six membered chelate by ethylene is demanded for the formation of the alternating sequences (k''_{C2H4} << k_{C2H4} see the scheme below). For this reason, the f_{na} theoretical value can be calculated based on the following equation:

$$f_{na} = \frac{r_{na}}{r_a} = \left(\frac{k'_{C2H4}}{k_{CO}} \frac{[C2H4]}{[CO]} \frac{K_1}{K_2}\right)\left(1 - \frac{k_{CO}^{-1}}{k''_{C2H4} * [C2H4] + k_{CO}^{-1}}\right)^{-1} \cong \left(\frac{k'_{C2H4}}{k''_{C2H4}} \frac{1}{[CO]} \frac{K_1}{K'_2}\right)$$

where K'_2 is the equilibrium constant between of **1-cycle5-T** and **1-cycle6-T**.

This corresponds to the scheme:

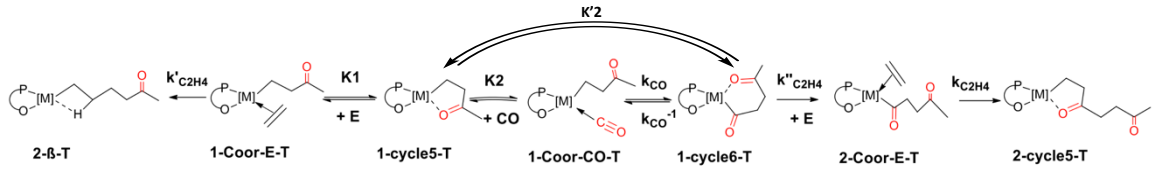

The f_{na} value obtained for catalyst **1-OCH_3**, **3** and **4** are 4.9 (mol L^{-1})$^{-1}$,0.69 (mol L^{-1})$^{-1}$and 0.15 (mol L^{-1})$^{-1}$ respectively.

Comparison of these theoretical value f_{na} to experimental values from microstructure analysis (Table 1) agrees reasonably (Table S6.2).

Table S6.2: Comparison of DFT results and experimental values derived from polymer microstructures of propensity for non-alternating vs. alternating CO incorporation.

Species	Experimentally determined f_{na}	Computed f_{na} [a](mol L^{-1}) $^{-1}$
Catalyst **Drent**	11.5	20.0
Catalyst **1-OCH_3**	1.5	(4.9) [a]
Catalyst **3**	0.8	(0.69) [a]
Catalyst **4**	0.1	(0.15) [a]

6.3.3 Steric analysis.

From a steric point of view, **2-OCH$_3$** and **3'** are similar to their C_6F_5-analogues **1-OCH$_3$** and **3** as suggested by the topographic steric maps and the similar values of the buried volume (%Vbur) of the quadrants, (see Figure 6.4 for **1-OCH$_3$** vs. **2-OCH$_3$** and Figure S6.4 for **3** vs. **3'**).

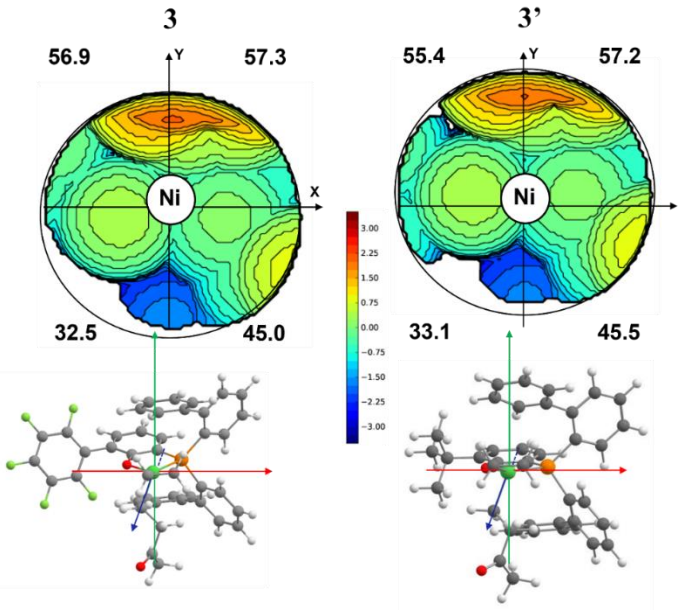

*Figure S6.4. Topographic steric maps of the transition state TS$_{Isom}$ for catalysts **3** (top left) and **3'** (top right). Thecomplexes are oriented as shown below (bottom left and right).*

6.3.4 Electronic analysis.

Table S6.3: Natural bond orbital analysis on Nickel for **TS-2$_{Coor\text{-}E\text{-}C}$** on catalysts **1-OCH$_3$** and **3** catalysts and for **TS-1$_{Ins\text{-}CO\text{-}T}$** on catalysts **1-OCH$_3$** and **4**.

Charge on Ni atom	**1-OCH$_3$**	**3**	**4**
TS-2$_{Coor\text{-}E\text{-}C}$	0.19264	0.19407	
TS-1$_{Ins\text{-}CO\text{-}T}$	0.15441		0.08933

Table S6.4: Natural bond orbital analysis on Nickel for **TS-2$_{Coor\text{-}E\text{-}C}$** on catalysts **2-OCH$_3$** and **3'**.

Charge on Ni atom	**2-OCH$_3$**	**3'**
TS-2$_{Coor\text{-}E\text{-}C}$	0.18447	0.18728

6.3.5 Computational details

We performed calculations of all important intermediates and transition states involved in the competitive linear chain growth alternating and non-alternating pathways during the ethylene and CO copolymerization (the **1-cycle5-T** intermediate was set as a reference point).

All the DFT geometry optimizations were performed at the GGA BP86[122-124] level with the Gaussian09 package. [125] The electronic configuration of the systems was described with the 6-31G(d) basis set for H, C, N, F, and O while for Ni the quasi relativistic LANL2DZ ECP effective core potential was adopted.[126] All geometries were characterized as minimum or transition state through frequency calculations. The geometry optimizations were performed without symmetry constraints. All transition-state structures were confirmed to connect corresponding reactants and products by intrinsic reaction coordinate (IRC) calculations. The reported free energies were built through single point energy calculations on the (BP86/6-31G(d)/LANL2DZ ECP) geometries using the M06 functional and the triple-ζ TZVP basis set on main group atoms while for Ni the quasi relativistic LANL2DZ ECP effective core potential was adopted.[127-129] Solvent effects were estimated with the PCM model using toluene as solvent.[130-131] To this (M06/TZVP/LANL2DZ ECP) electronic energy in solvent, thermal corrections were included from the gas-phase frequency calculations at the gas-phase level of theory (BP86/6-31G(d)/LANL2DZ ECP). The percent buried volume calculations and the steric maps were performed with the SambVca 2.1 package.[121] The radius of the sphere was fixed in the origin of the metal centre, while for the atoms, we adopted the Bondi radii scaled by 1.17, and a mesh of 0.1 Å was used to scan the sphere for buried voxels.

6.3.6 Energetic profile and Gibbs free energies for Drent and 1-OCH_3 catalysts.

6.3.6.1 Energetic profile with the alternative pathways for Drent and 1-OCH_3 catalysts.

*Figure S6.5: Gibbs free energies (ΔG_{Tol} in kcal mol^{-1}) of the competitive pathways for non-alternating and alternating carbon monoxide incorporation with catalysts Drent (red, top) and **1-OCH_3** (blue, bottom).*

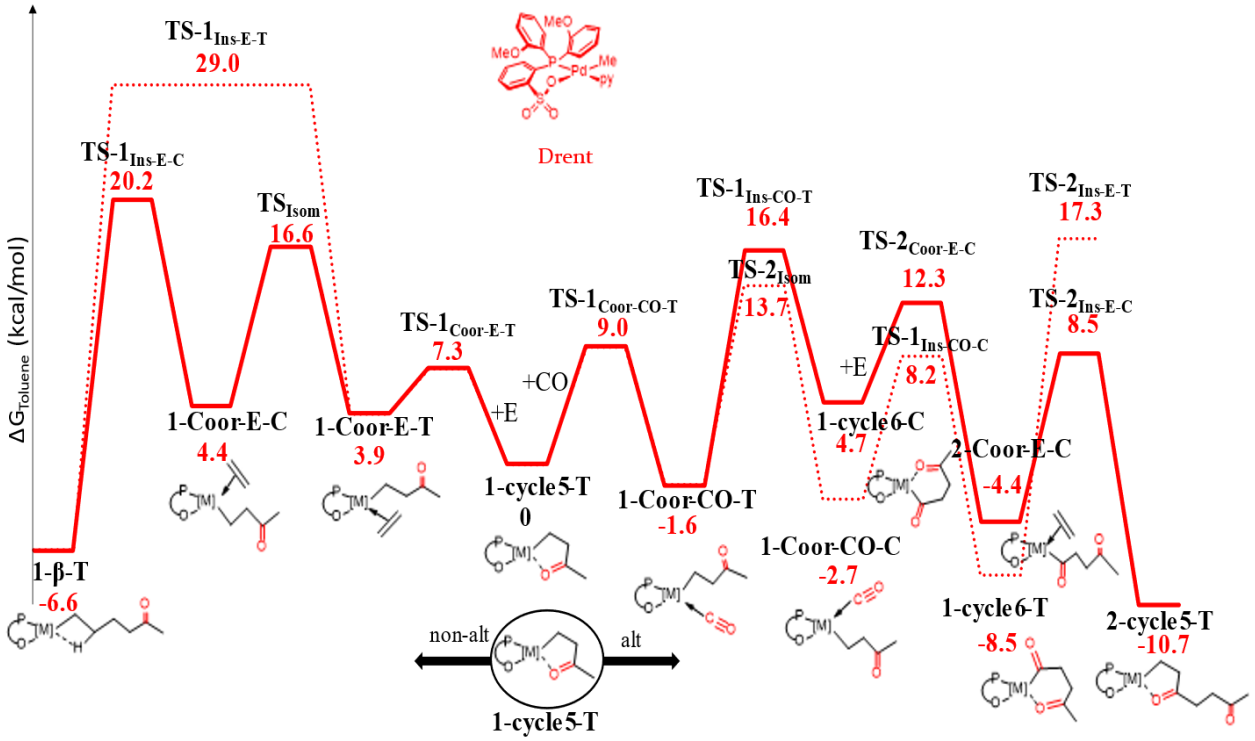

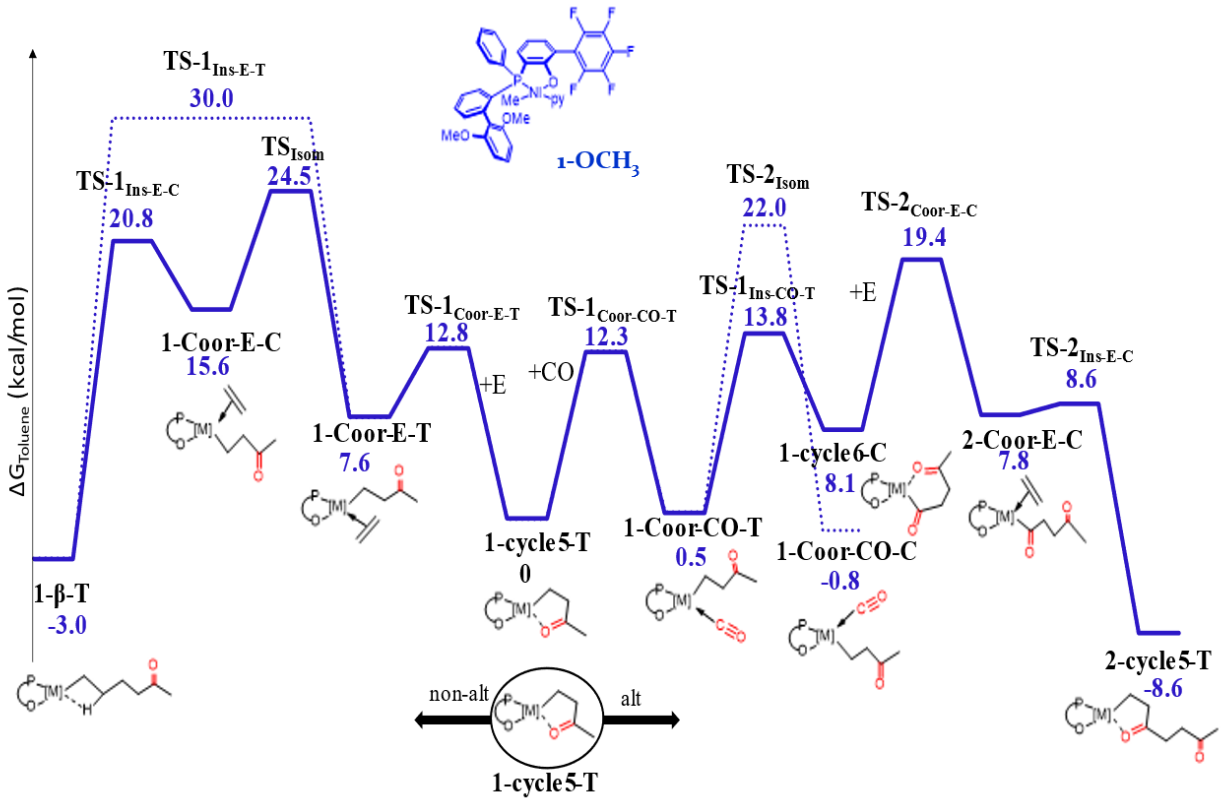

6.3.6.2 Gibbs free energies of competitive species for catalysts 3, 4, 2-OCH_3 and 3'.

Table S6.5: Gibbs free energies in Toluene (kcal/mol) of competitive species for catalysts **3** and **4**, with the same computational protocol (M06/ triple-ζ TZVP).

	Catalyst 3	Catalyst 4
1-cycle5-T	0.0	0.0
TS_{Isom}	27.1	23.8
$TS\text{-}2_{Coor\text{-}E\text{-}C}$	20.6	---
$TS\text{-}1_{Ins\text{-}CO\text{-}T}$	---	14.6
$\Delta\Delta G^{‡}$ (**non-alt**)-(**alt**)	6.5	9.2

Table S6.6: Gibbs free energies in Toluene (kcal/mol) of competitive species for catalysts **2-OCH_3** and **3'**, (M06/ triple-ζ TZVP).

	Catalyst 2-OCH_3	Catalyst 3'
1-cycle5-T	0.0	0.0
TS_{Isom}	24.5	25.9
$TS\text{-}2_{Coor\text{-}E\text{-}C}$	18.8	19.5
$\Delta\Delta G^{‡}$ (**non-alt**)-(**alt**)	5.7	6.4

Chapter 7
General conclusions

The main objective of this PhD thesis has been to provide a computational mechanistic framework in the development of advanced catalysts based on late transition metals for polymerization of ethylene and copolymerization of ethylene with CO. This in turn enables the synthesis of new materials based on polyethylene through a rational design approach.
In this context, it is important to keep in mind that in general catalysis, because of its huge influence on processes that affect daily life, is a subject of major interest in both academia and industry.
Selecting the best catalyst in a disorganized catalytic space is a challenging task often driven by trial and error, or intuition, rather than a rational science.
To this end, the role of calculations is crucial to correlate the properties of the catalytic pocket (defined as the space around the active centre) to how it behaves experimentally in order to have the tools to rationally progress towards advanced catalysts.
In this PhD project, the attention was focused on the rationalization of the catalysts' behavioursand on the design and developing of new catalysts for polyethylene-based materials, in a close collaboration with the experimental group of Professor Stefan Mecking.
In homogeneous catalysis, the steric and electronic environment of the metal centre are the fundamental parameters that define the properties of any catalytic pocket. In detail, in the field of polymerization, the properties of the products obtained such as polymer molecular weight and branching degree are strongly determined by the catalyst in use.
This thesis focused on two classes of systems, i.e. Ni(II) salicyaldiminato and Ni(II) phosphine-phenolate complexes.
In the first part of the thesis, the catalysts investigated represent an advanced and instructive version of Ni(II) salicylaldiminate motif in which the ligand skeleton was modified by means of an ancillary imine donor creating a new binding site for ethylene polymerization reactions.
From these studies it emerged that:

- the second imine donor of the neutral bis(imino)phenoxy complexes does not interfere in catalysis and thus can regarded as an innocent spectator. Catalyst with electron withdrawing substituents produces high molecular weight polymers, whereas catalyst with electron donating groups gives hyperbranched oligomers. The chain walking is promoted by a weak η^2 -coordination of the distal aryl rings to the metal center, operative only for the case of sufficiently electron-rich aryls.
- the added charge by incorporating a single proton into the $N\cdots H^+\cdots O$ bridging motif right next to the active site dramatically alters catalytic properties, yielding low molecular weight oligomers.
- the shielding of the apical sites by means of a sterically hindered ligand influences the catalytic behaviour for the neutral cyclophane complex yielding to low branched oligomers.

In the second part of the thesis, the behaviour of new complexes of the Ni(II) phosphine phenolate class was studied both in ethylene polymerization and in ethylene-CO copolymerization.
A tailored modification of the ligand structure by means of a bis phenyl group on the phosphine moiety was revealed as an effective strategy to block the apical position in order to a) suppress chain transfer reactions for obtaining linear polyethylene and b) synthesize in-chain-functionalized polyethylene with the desirable low content of CO for materials with improved properties like for example the lower environmental persistence.
From these studies it emerged that:

- the axial shielding of the catalytic site influences the polymerization behavior in the homopolymerization of ethylene, yielding linear polymers with high molecular weight in presence of electron donating remote substituents on the ligand.
- the aromatic rings on the phosphine moieties may provide both a steric and electronic contribution when apically coordinated to the metal centre affecting the catalytic behaviour of all the investigated phosphinophenolato Ni(II) catalysts in the ethylene-CO copolymerization, leading to the formation of both non-alternating and alternating copolymers.

Overall the detailed mechanistic studies performed in this thesis have offered a comprehensive understanding of the chemical reactivity beyond the (co)polymerization processes considered, an achievement almost impossible to reach only with experimental techniques. The studies described in this work demonstrated that computational techniques can be of enormous value to obtain insights that can promote the discovery and the design of novel successful catalyst architectures more rapidly and effectively.

Chapter 8
References

1) Andrady, A. L.; Neal, M. A. *Philos. Trans. R.Soc. London, Ser. B* **2009**, *364*, 1977–1984.
*2)*Plastics-the Facts **2011**.
3)Plastics-the Facts **2021**.
4) a) Whiteley, K. S. *Ullmann's Encyclopedia of Industrial Chemistry: Polyethylene*; Wiley VCH: Weinheim, **2012**. b) Omnexus **2022**. https://omnexus.specialchem.com/
5) Cantow, H. J.; Dall'Asta, G.; Ferry, J. D.; Fujita, H.; Kern, W.; Natta, G.; Okamura, S.; Overberger, C. G.; Prins, W.; Schulz, G. V. *Adv. Polym. Sci.* **1970**, 386–448.
6) Ziegler, K.; Holzkamp, E.; Breil, H.; Martin, H. *Angew. Chem.* **1955**, *67*, 541–547.
7) Chemical Recycling of Polyolefins (PE, PP): Modern Technologies and Products. **2021**
8)Ceresana **2019**. https://www.ceresana.com/de/marktstudien/kunststoffe/polyethylen-lldpe.
9) Geyer, R.; Jambeck, J. R.; Law, K. L. *Sci.Adv.* **2017**, *3*, e1700782.
10) The future of plastic. *Nat. Commun.* **2018**, *9*, 2157.
11) Pan, Z.; Guo, H.; Chen, H.; Wang, S.; Sun, X.; Zou, Q.; Zhang, Y.; Lin, H.; Cai, S.; Huang, J. *Sci. Total Environ*. **2019**, 650, 1913-1922.
12) Nielsen, T. D.; Hasselbalch, J.; Holmberg, K.; Stripple, J. *Wene*, **2020**, *9(1), 360-378*.
13) Zheng, J.; Suh, S. *Nat. Clim.Change* **2019**, *9*, 374–378.
14) Häußler, M.; Eck, M.; Rothauer, D.; Mecking, S. *Nature* **2021**, *590*, 423–427.
15) Bremer, W. P. *Polym. -Plast.Technol. Eng.* **1982**, 18 (2), 137-148.
16) Hartley, G. H.; Guillet, J. E. *Macromolecules* **1968**, 1 (2), 165-170.
17) Morgen T. O.; Baur M.; Schnetmann I.G.; Mecking S. *Nat. Commun.* **2020,** 11, 3693.
18) Ortmann P.; Wimmer F. P.; Mecking S. *ACS Macro Lett.* **2015,** 4, 704.
19) Kalay, G.; Bevis, M. J. *Polym. Sci., Part B: Polym. Phys.* **1997**, 35 (3), 415-430.
20) Mecking, S. *Colloid. Polym. Sci.* **2007**, 285 (6), 605-619.
21) Nakamura, A.; Anselment, T. M. J.; Claverie, J.; Goodall, B.; Jordan, R. F.; Mecking, S.; Rieger, B.; Sen, A.; van Leeuwen, P. W. N. M.; Nozaki, K. *Acc. Chem. Res.* **2013**, 46 (7), 1438-1449.
22) Morgen, T. O.; Baur, M.; Schnetmann, I. G.; Mecking, S. *Nat. Commun.* **2020,** 11, 3693.
23) Hartley, G. H.; Guillet, J. E. *Macromolecules* **1968**, 1, 165.
24) Andrady, A. L.; Pegram, J. E.; Song, Y. J. *Environ. Polym. Degrad*. **1993,** 1, 117.
25) Ortmann, P.; Wimmer, F. P.; Mecking, S. *ACS Macro Lett*. **2015,** 4, 704.
26) Brubaker, M. M.; Coffman, D. D.; Hoehn, H. H. *J. Am. Chem. Soc*. **1952**, 74(6), 1509–1515.
27) Coffman, D. D., Pinkney, P. S., Wall, F. T., Wood, W. H. & Young, H. S. *J. Am. Chem. Soc*. **1952,** 74, 3391–3393.
28) Nozaki K.; Ito S. *Polymer Science: A Comprehensive Reference*, **2012**, 3, 825–842.
29) Boaen, N. K.; Hillmyer, M. A. *Chem. Soc. Rev.* **2005**, *34*, 267.
30) Fodor, Z., Iring, M., Tüdos, F. & Kelen, T. J. *Polym. Sci. A Polym. Chem*. **1984,** 22, 2539–2550.
31) Bunescu, A.; Lee, S. Li, Q. Hartwig, J. F. *ACS Cent. Sci*. **2017,** 3, 895.

32) L. Chen L. ; Malollari,K. G.; Uliana, A.; Sanchez, D.; Messersmith P.B; Hartwig J.F. *Chem* **2021,** 7, 137.
33) Reppe, W.; Magin, A. US Patent **1950**.
34) Brubaker, M. M., Coffman, D. D. & Hoehn, H. H. *J. Am. Chem. Soc.* **1952**, 74, 1509–1515.
35) Wilke, G.
Angew. Chem. Int. Ed. **2003**, *42*, 5000–5008.
36) Whiteley, K. S. *Ullmann's Encyclopedia of Industrial Chemistry: Polyethylene*; Wiley-VCH: Weinheim, **2012**.
37) Hogan, J. P.; Banks, R. L. Phillips Petroleum. US2825721, **1956**.
38) Tullo, A. H. *Chem. Eng. News* **2010**, 88(42), 10– 16.
39) Baier, M. C.; Zuideveld, M. A.; Mecking, S. *Angew. Chem. Int. Ed.* **2014**, *53*, 9722–9744.
40) Keim, W. *Angew. Chem. Int. Ed.* **2013**, *52*, 12492–12496.
41) Wilke, G. *Angew. Chem. Int. Ed. Engl.* **1988**,27, 185 206.
42) Mülhaupt, R. *Macromol. Chem. Phys.* **2003**, *204*, 289-327.
43) Ittel, S. D.; Johnson, L. K.; Brookhart, M. *Chem. Rev.* **2000**, *100*, 1169-1204.
44) Mecking, S. *Angew. Chem., Int. Ed.* **2001**, *40*, 534-540.
45) Nakamura, A.; Ito, S.; Nozaki, K. *Chem. Rev.* **2009**, 109, 5215–5244.
46) Mu, H.; Pan, L.; Song, D.; Li, Y. *Chem. Rev.* **2015**, 115, 12091–12137.
48) Chen, Z.; Brookhart, M. *Acc. Chem. Res.* **2018**, 51, 1831–1839.
49) Chen, C. *Nat. Rev. Chem.* **2018**, 2, 6–14.
50) Tan, C.; Chen, C. *Angew. Chem., Int. Ed.* **2019**, 58, 7192–7200.
51) Keyes, A.; Basbug Alhan, H. E.; Ordonez, E.; Ha, U.; Beezer, D. B.; Dau, H.; Liu, Y.; Tsogtgerel, E.; Jones, G. R.; Harth, E. *Angew. Chem., Int. Ed.* **2019**, 58, 12370–12391.
52) Zhang, Y.; Kang, X.; Jian, Z. *Nat. Commun.* **2022**, 13, No. 725.
53) Mecking, S.; Schnitte, M. *Acc. Chem. Res.* **2020**, 53, 2738–2752.
54) Luckham, S. L. J.; Nozaki, K. *Acc. Chem. Res.* **2021**, 54, 344–355.
55) Mu, H.; Zhou, G.; Hu X.; Jian, Z. *Coord. Chem. Rev.* **2021**, 435, 213802.
56) Mecking, S. *Angew. Chem. Int. Ed.* **2001**, *40*, 534–540.
57) Johnson, L. K.; Killian, C. M.; Brookhart, M. *J. Am. Chem. Soc.* **1995**, *117*, 6414-6415.
58) Johnson, L. K.; Mecking, S.; Brookhart, M. *J. Am. Chem. Soc.* **1996**,*118*, 267–268.
59) Ittel, S. D.; Johnson, L.K.; Brookhart, M. *Chem. Rev*. **2000**,100, 1169-1204.
60) Deng, L.; Woo, T. K.; Cavallo, L.; Margl, P. M.; Ziegler, T. *J. Am. Chem. Soc.* **1997**, *119*, 6177-6186.
61) Froese, R. D. J.; Musaev, D. G.; Morokuma, K. *J. Am. Chem. Soc.* **1998**, *120*, 1581-1587.
62) Tempel, D.J.; Johnson, L.K.; Huff, R.L.; White, P. S.; Brookhart, M. *J. Am. Chem. Soc*. **2000**, 122, 6686–6700.
63) Gates, D.P.; Svejda, S.A.; Onate, E.; Killian, C.M.; Johnson, L.K.; White, P.S.; Brookhart, M. *Macromolecules*, **2000**, 33, 2320–2334.
64) Xie, T.; McAuley, K.B.; Hsu, J. C. C.; Bacon D.W. *Ind. Eng. Chem. Res.* **1994**, 33, 449–479.
65) Allen, K. E.; Campos, J.; Daugulis, O.; Brookhart, M. *ACS Catal.* **2015**, 5, 456–464.
66) Chen, Z.; Leatherman, M. D.; Daugulis, O.; Brookhart, M. *J. Am. Chem. Soc.* **2017**, *139*, 16013–16022.

67) Schulz, J.; Vögtle, F. Topics in Current Chemistry **1994,** 41–86, 172.
68) Diederich, F. N. Monographs in Supramolecular Chemistry; The Royal Society of Chemistry, **1991**.
69) Cram, D. J.; Cram, J. M. *Acc.Chem. Res.* **1971**, *4*, 204–213.
70) Camacho, D. H.; Salo, E. V.; Ziller, J. W.; Guan, Z. *Angew. Chem. Int. Ed.* **2004**, *43*, 1821-1825.
71) Leung, D. H.; Ziller, J. W.; Guan, Z. *J. Am. Chem. Soc.* **2008**, *130*, 7538–7539.
72) Popeney, C. S.; Levins, C. M.; Guan, Z. *Organometallics* **2011**, *30*, 2432–2452.
73) Johnson, L. K.; Bennett, A. M. A.; Ittel, S. D.; Wang, L.; Hauptman, E.; Simpson, R. D.; Feldman, J.; Coughlin, E. B. (DuPont) WO 98/30609, **1998.**
74) Wang, C.; Friedrich, S.; Younkin, T. R.; Li, R. T.; Grubbs, R. H.; Bansleben, D. A.; Day, M. W. *Organometallics* **1998**, *17*, 3149-3151.
75) Younkin, T. R.; Connor, E. F.; Henderson, J. I.; Friedrich, S. K.; Grubbs, R. H.; Bansleben, D. A. *Science* **2000**, *287*, 460-462.
76) Sun, J.; Shan, Y.; Xu, Y.; Cui, Y.; Schumann, H.; Hummert, M. *J. Polym. Sci., Part A: Polym. Chem.* **2004**, *42*, 6071-6080.
77) Godin, A.; Schnetmann, I.G.; Mecking, S. *Macromolecules* **2016**, *49*, 8825-8837.
78) Zuideveld, M.A.; Wehrmann, P.; Rohr, C.; Mecking, S. *Angew. Chem*. **2004**, *116*, 887 –887.
79) Gottker-Schnetmann, I.; Wehrmann,P.; Rohr, C.; Mecking, S. *Organometallics* **2007,** *26,* 2348-2362.
80) Bastero, A.; Schnetmann, I.G.; Röhr, C.; Mecking, S. *Adv. Synth. Catal.* **2007**, *349*, 2307–2316.
81) Wiedemann, T.; Voit, G.; Tchernook, A.; Roesle, P.; Schnetmann, I. G.; Mecking, S. *J. Am. Chem. Soc.* **2014**, *136*, 2078-2085.
82) Osichow, A.; Schnetmann, I. G.; Mecking, S. *Organometallics* **2013**, *32*, 5239-5242.
83) Wiedemann, T. Dissertation, University of Konstanz, **2017**.
84) Falivene, L.; Wiedemann, T.; Schnetmann, I. G.; Caporaso, L.; Cavallo, L.; Mecking, S. *J. Am. Chem. Soc.* **2018**, *140*, 1305–1312.
85) Drent, E.; van Dijk, R.; van Ginkel, R.; van Oort, B.; Pugh, R. I. *Chem. Commun.* **2002**, 964.
86) Drent E.; Pello, D. H. *L. Eur. Pat. Appl.,* **1995**, EP0632084;
87) a) Drent, E. Eur. Pat. Appl., **1984**, EP121965; b) Drent, E.; vanDjik, R.; vanGinkel, R.; vanOort, B.; Pugh, R.I. *Chem. Comm.* **2002**, 744-745.
88) Guironnet, D.; Roesle, P.; Rünzi, T.; Schnetmann, I. G.; Mecking, S. *J. Am. Chem. Soc.* **2009**, *131*, 422–423.
89) Noda, S.; Nakamura, A.; Kochi, T.; Chung, L.W.; Morokuma, K.; Nozaki, K. *J. Am. Chem. Soc.* **2009**, *131*, 14088–14100.
90) Haras, A.; Anderson, G. D. W.; Michalak, A.; Rieger, B.; Ziegler, T. *Organometallics* **2006**, 25, 4491.
91) Keim, W. *Angew. Chem. Int. Ed.* **2013**, *52*, 12492–12496.
92) Keim, W.; Kowaldt, F. H.; Goddard, R.; Krüger, C. *Angew. Chem.Int. Ed.* **1978**, *17*, 466–467.
93) Cornils, B.; Herrmann, W. A.; Horváth, I. T.; Leitner, W.; Mecking, S.; Olivier-Bourbigou, H.; Vogt, D. *Multiphase Homogeneous Catalysis.* Wiley-VCH: *Weinheim*, **2004**.

94) Klabunde, U.; Mülhaupt, R.; Herskovitz, T.; Janowicz, A. H.; Calabrese, J.; Ittel, S. D.*J. Polym. Sci., Part A: Polym. Chem.* **1987**, *25*, 1989–2003.
95) Ostoja-Starzewski, K. A.; Witte, J. *Angew. Chem. Int. Ed.* **1987**, *26*, 63–64.
96) Ostoja-Starzewski, K. A.; Witte, J. *Angew. Chem. Int. Ed.* **1985**, *24*, 599–601.
97) Xin, B. S.; Sato, N.; Tanna, A.; Oishi, Y.; Konishi, Y.; Shimizu, F. *J. Am. Chem. Soc*. **2017**, 139, 3611–3614.
98) Zhang,Y.; Mu, H.; Pan,L.; Wang,X.; Li Y. *ACS Catal.* **2018**, 8, 7, 5963–5976.
99) Baur,M.; Lin, F.; Morgen,T.O; Odenwald, L.; Mecking S. *Science*, **2021**, 374, 604-607.
100) Reppe, W.; Magin, A., Production of ketonic Bodies. US Patent **1950.**
101) Drent, E.; Budzelaar, P. H. M. *Chem. Re*v. **1996**, *96*, 663.
102) Ash, C. E. J. *Mater. Educ.* **1994**, 16, 1.
103) Bianchini, C.; Meli, A. *Coord. Chem. Re*V. **2002**, *225*, 35.
104) Sen, A. *Springer Science & Business Media,* **2003**, 27.
105)Hearley, A. K.; Nowack, R. J.; Rieger, B. *Organometallics* **2005**, 24, 2755.
106) Newsham, D. K.; Borkar, S.; Sen, A.; Conner, D. M.; Goodall, B. L. *Organometallics* **2007**, 26, 3636.
107) Bettucci, L.; Bianchini, C.; Claver, C.; Suarez, E. J. G.; Ruiz, A.; Meli, A.; Oberhauser, W. *Dalton Trans.* **2007**, 5590.
108) Haras, A.; Michalak, A.; Rieger, B.; Ziegler, T. *J. Am. Chem. Soc.* **2005**, 127, 8765.
109) Haras, A.; Michal ak, A.; Rieger, B.; Ziegler, T. *Organometallics* **2006**, 25, 946.
110) Piovano, A.; Zarupski, J.; Groppo, E.; J. *Phys. Chem. Lett.* **2020**, 11, 5632 2020.
111) Daugulis, O.; Roy MacArthur, A. H.; Rix, F.C.; Templeton J. F. *ACS Catal.* **2016**, 6, 1518–1532.
112) Newsham, D. K.; Borkar, S.; Sen, A.; Conner, D. M.; Goodall, B. L. *Organometallics* **2007**, *26*, 3636.
113) Mul, W. P.; Oosterbeek, H.; Beitel, G. A.; Kramer, G. J.; Drent, E. *Angew. Chem., Int. Ed.* **2000**, *39*, 1848.
114) Wang, L.; Sun, W.-H.; Han, L.; Li, Z.; Hu, Y.; He, C.; Yan, C. *J. Organomet. Chem.* **2002**,*650*, 59–64.
115) Chiu, H.C.; Koley, A.; Dunn, P. L.; Hue, R. J.; Tonks, I. A. *Dalton Trans.* **2017**, *46*, 5513–5517.
116) Na, S. J.; Joe, D. J.; S, S.; Han, W.-S.; Kang, S. O.; Lee, B. Y. *J. Organomet. Chem.* **2006**, *691*, 611–620.
117) Ohno, K.; Arima, K.; Tanaka, S.; Yamagata, T.; Tsurugi, H.; Mashima, K. *Organometallics* **2009**, *28*, 3256–3263.
118) Schiebel, E.; Voccia, M.; Falivene, L.; Caporaso, L.; Mecking, S. *ACS Catal*. **2021**, 11, 9, 5358–5368. Ph.D. Thesis Dissertation Dr. Eva Schiebel. Konstanzer Online-Publikations-System (KOPS) URL: http://nbn-resolving.de/urn:nbn:de:bsz:352-2-fstmasnarbf92
119) Bastero, A.; Schnetmann, I.G.; Röhr, C.; Mecking, S. *Adv. Synth. Catal.* **2007**, *349*, 2307–2316.
120) Zuideveld, M. A.; Wehrmann, P.; Röhr, C.; Mecking, S. *Angew. Chem. Int. Ed.* **2004**, *43*, 869–873.
121) Falivene, L.; Cao Z.; Petta A.; Serra L.; Poater A.; Oliva R.; Scarano V.; Cavallo L.; *Nat. Chem.* **2019**, *11*, 872.

122) Perdew, J. P. *Phys. Rev. B* **1986**, 33, 8822–8824.
123) Perdew, J. P. *Phys. Rev. B* **1986**, 34, 7406.
124) Becke, A. D. *Phys. Rev. A* **1988**, 38, 3098–3100.
125) Frisch, M. J.; Trucks, G. W.; Schlegel, H. B.; Scuseria, G. E.; Robb, M. A.; Cheeseman, J. R.; Scalmani, G.; Barone, V.; Mennucci, B.; Petersson, G. A.; Nakatsuji, H.; Caricato, M.; Li, X.; Hratchian, H. P.; Izmaylov, A. F.; Bloino, J.; Zheng, G.; Sonnenberg, J. L; Hada, M.; Ehara, M.; Toyota, K.; Fukuda, R.; Hasegawa, J.; Ishida, M.; Nakajima, T.; Honda, Y.; Kitao, O.; Nakai, H.; Vreven, T.; Montgomery, J. A.; Peralta, J. E.; Ogliaro, F.; Bearpark, M.; Heyd, J. J.; Brothers, E.; Kudin, K. N.; Staroverov, V. N.; Kobayashi, R.; Normand, J.; Raghavachari, K.; Rendell, A.; Burant, J. C.; Iyengar, S. S.; Tomasi, J.; Cossi, M;. Rega, N.; Millam, J. M.; Klene, M.; Knox, J. E.; Cross, J. B.; Bakken, V.; Adamo, C.; Jaramillo, J.; Gomperts, R.; Stratmann, R. E.; Yazyev, O.; Austin, A. J.; Cammi, R.; Pomelli, C.; Ochterski, J. W. R.; Martin, L.; Morokuma, K.; Zakrzewski, V. G.; Voth, G. A.; Salvador, P.; Dannenberg, J. J.; Dapprich, S.; Daniels, A. D.; Farkas, Ö.; S163 Foresman, J. B.; Ortiz, J. V.; Cioslowski, J.; Fox D. J. Gaussian 09 Revision A.1, Gaussian, Inc., Wallingford, CT, **2009**.
126) Weigend, F.; Ahlrichs, R. *PCCP* **2005**, 7, 3297– 3305.
127) Häussermann, U.; Dolg, M.; Stoll, H.; Preuss, H.; Schwerdtfeger, P.; Pitzer, R. M. *Mol. Phys.* **1993**, 78, 1211–1224.
128) Küchle, W.; Dolg, M.; Stoll, H.; Preuss, H. *J. Chem. Phys.* **1994**, 100, 7535–7542.
129) Leininger, T.; Nicklass, A.; Stoll, H.; Dolg, M.; Schwerdtfeger, P. *J. Chem. Phys.* **1996**, 105, 1052– 1059.
130) Tomasi, J.; Persico, M. *Chem. Rev.* **1994**, 94, 2027–2094.
131) Barone, V.; Cossi, M. *J. Phys. Chem. A* **1998**, 102, 1995–2001.
132) Chen, Z.; Brookhart, M. *Acc. Chem. Res*. **2018**, 51, 1831.
133) a) Keyes, A.; Alhan, H.E.B.; Ordonez, E.; Ha, U.; Beezer, D. B.; Dau, H.; Liu, Y.-S.; Tsogtgerel, E.; Jones, G. R.; Harth, E. *Angew. Chem. Int. Ed.* **2019**, 58, 12370; b) Walsh, D. J.; Hyatt, M. G.; Miller, S. A.; Guironnet, D. *ACS Catal.* **2019**, 9, 11153; c) Tan, C.; Chen, C. *Angew. Chem. Int. Ed.* **2019**,58, 7192.
134) a) Stürzel, M. Mihan, S. Mülhaupt, R. *Chem. Rev.* **2016**, 116, 1398; b) G. Wilke, *Angew. Chem. Int. Ed.* **2003**, 42, 5000.
135) Guan, Z.; Cotts, P. M.; McCord, E. F.; McLain, S. J. *Science* **1999**, 283, 2059.
136) Camacho, D. H.; Salo, E. V.; Guan, Z. *Org. Lett*. **2004**, 6, 865.
137)Popeney, C. S.; Guan, Z. *J. Am. Chem. Soc.* **2009**, 131, 12384.
138) C. S. Popeney, C. S.; Camacho, D. H.; Guan, Z. *J. Am. Chem. Soc*. **2007**, 129, 10062.
139) Camacho, D. H.; Guan, Z. *Chem. Commun*. **2010**, 46, 7879.
140) Schnitte, M.; Staiger, A.; Casper, L. A.; Mecking, S. *Nat. Commun*. **2019**, 10, 2592.
141) a) Kenyon, P.; Wçrner, M.; Mecking, S. *J. Am. Chem. Soc.* **2018**, 140, 6685; b) Mu, H.; Pan, L.; Song, D.; Li, Y. *Chem. Rev*. **2015**, 115, 12091; c) Takeuchi, D.; Chiba, Y.; Takano, S.; Osakada, K. *Angew. Chem. Int. Ed.* **2013**,52, 12536; d) Radlauer, M. R.; Buckley, A. K.; Henling, L. M.; Agapie, T. *J. Am. Chem. Soc.* **2013**, 135, 3784; f) Chen, Z.; Mesgar, M.; White, P. S.; Daugulis, O.; Brookhart, M. *ACS Catal.* **2015**, 5, 631; g) Tran, Q. H.; Brookhart, M.; Daugulis, O. *J. Am. Chem. Soc*. **2020**, 142, 7198.

142) Younkin, T. R.; Connor, E. F.; Henderson, J. I.; Friedrich, S. K.; Grubbs, R. H.; Bansleben, D. A. *Science* **2000**, 287, 460.
143) Voccia M.; Schiebel E.; Falivene L.; Schnetmann I.; Caporaso L.; Mecking, S. *Angew. Chem. Int. Ed.* **2021**, *60*, 18472–18477.
144) Chen, Z.; Brookhart, M. *Acc. Chem. Res.* **2018**, *51*, 1831–1839.
145) Johnson, L. K.; Killian, C. M.; Brookhart, M. *J. Am. Chem. Soc.* **1995**, *117*, 6414–6415.
146) Johnson, L. K.; Mecking, S.; Brookhart, M. *J. Am. Chem. Soc.* **1996**, *118*, 267–268.
147) Chen, Z.; Mesgar, M.; White, P. S.; Daugulis, O.; Brookhart, M. *ACS Catal.* **2015**, *5*, 631–636.
148) Kuhn, P.; Sémeril, D.; Matt, D.; Chetcuti, M. J.; Lutz, P. *Dalton Trans.* **2007**, 515–528.
149) Keim, W. *Angew. Chem. Int. Ed.* **2013**, *52*, 12492–12496.
150) Heinicke, J.; Köhler, M.; Peulecke, N.; He, M.; Kindermann, M. K.; Keim, W.; Fink, G. *Chem. Eur. J.* **2003**, *9*, 6093–6107.
151) Anselment, T. M. J.; Wichmann, C.; Anderson, C. E.; Herdtweck, E.; Rieger, B. *Organometallics* **2011**, *30*, 6602–6611.
152) Piche, L.; Daigle, J.-C.; Poli, R.; Claverie, J. P. *Eur. J. Inorg. Chem.* **2010**, *2010*, 4595–4601.
153) Skupov, K. M.; Marella, P. R.; Simard, M.; Yap, G. P. A.; Allen, N.; Conner, D.; Goodall, B. L.; Claverie, J. P. *Macromol. Rapid Commun.* **2007**, *28*, 2033–2038.
154) Ota, Y.; Ito, S.; Kuroda, J.; Okumura, Y.; Nozaki, K. *J. Am. Chem. Soc.* **2014**, *136*, 11898–11901.
155) Xin, B. S.; Sato, N.; Tanna, A.; Oishi, Y.; Konishi, Y.; Shimizu, F. *J. Am. Chem. Soc.* **2017**, *139*, 3611–3614.
156) Xiong, S.; Hong, A.; Bailey, B. C.; Spinney, H. A.; Senecal, T. D.; Bailey, H.; Agapie, T. *Angew. Chem. Int. Ed.* **2022**, *61*, e202206637.
157) Perrotin, P.; McCahill, J. S. J.; Wu, G.; Scott, S. L. *Chem. Commun.* **2011**, *47*, 6948–6950.
158) Fors, B. P.; Watson, D. A.; Biscoe, M. R.; Buchwald, S. L. *J. Am. Chem. Soc.* **2008**, *130*, 13552–13554.
159) Surry, D. S.; Buchwald, S. L. *Angew. Chem. Int. Ed.* **2008**, *47*, 6338–6361.
160) Barder, T. E.; Walker, S. D.; Martinelli, J. R.; Buchwald, S. L. *J. Am. Chem. Soc.* **2005**, *127*, 4685–4696.
161) Zuideveld, M. A.; Wehrmann, P.; Röhr, C.; Mecking, S. *Angew. Chem. Int. Ed.* **2004**, *43*, 869–873.
162) Bondi, A. *J. Phys. Chem.* **1964**, *68*, 441–451.
163) Differently from the salycilaldiminato Ni(II) complexes,[85] the stepwise monomer decoordination assisted by the aromatic ring in the ligand is unfavored whatever is the electronic nature of the substituents on the rings.
164) Hartley, G. H.; Guillet, J. E. *Macromolecules.* **1968**, 1, 165–170.
165) Rix, F. C.; Brookhart, M.; White, P. S. *J. Am. Chem. Soc.* **1996**, 118, 4746.
166) Nakamura, A.; Kageyama, T.; Goto, H.; Carrow, B. P.; Ito, S.; Nozaki, K. *J. Am. Chem. Soc.* **2012**, 134, 12366–12369.
167) Nakamura, A.; Munakata, K.; Ito, S.; Kochi, T.; Chung, L. W.; Morokuma, K.; Nozaki, K. *J. Am. Chem. Soc.* **2011**, 133, 6761–6779.
168) Nakamura, A.; Anselment, T.; Claverie, J.; Goodall, B.; Jordan, R.; Mecking, S.; Rieger, B.; Sen, A.; van Leeuwen, P. W. N. M.; Nozaki, K. *Acc. Chem. Res.* **2013**, 46, 1439–1449.

169) Chen, M.; Chen, C. *Angew. Chem., Int. Ed.* **2018**, 57, 3094–3098.
170) Chen, S. Y.; Pan, R. C.; Chen, M.; Liu, Y.; Chen, C.; Lu, X. B. *J. Am. Chem. Soc.* **2021**, 143, 10743–10750.
171) Drent, E.; van Dijk, R.; van Ginkel, R.; van Oorta, B.; Pugh, R. I. *Chem. Commun.* **2002**, 964–965.
172) Chen, C.; Anselment, T. M. J.; Frohlich, R.; Rieger, B.; Kehr, G.; Erker, G. *Organometallics* **2011**, 30, 5248–5257.
173) Bettucci, L.; Bianchini, C.; Claver, C.; Suarez, E. J. G.; Ruiz, A.; Meli, A.; Oberhauser, W. *Dalton Trans.* **2007**, 5590–5602.
174) Newsham, D. K.; Borkar, S.; Sen, A.; Conner, D. M.; Goodall, B. L. *Organometallics* **2007**, 26, 3636–3638.
175) Soomro, S. S.; Cozzula, D.; Leitner, W.; Vogt, H.; Müller, T. E. *Polym. Chem.* **2014**, 5, 3831–3837.
176) Tang, S.; Seidel, F. W.; Nozaki, K. *Angew. Chem., Int. Ed.* **2021**, 60, 26506–26510.
177) Keim, W. *Angew. Chem., Int. Ed.* **2013**, 52, 12492–12496.
178) Xiong, S.; Shoshani, M. M.; Zhang, X.; Spinney, H. A.; Nett, A. J.; Henderson, B. S.; Miller, T. F.; Agapie, T. *J. Am. Chem. Soc.* **2021**, 143, 6516–6527.
179) Lin, F.; Morgen, T. O.; Mecking, S. *J. Am. Chem. Soc*. **2021**, 143, 20605–20608.
180) Klabunde, U.; Ittel, S. D. *J. Mol. Catal.* **1987**, 41, 123–134.
181) Voccia, M.; Odenwald, L.; Baur, M.; Lin, F.; Falivene, L.; Mecking, S.; Caporaso, L. *J. Am. Chem. Soc.* **2022**, 144, 15111–15117.
182) Alternatively to **1-cycle-5**, a n-propyl **β-T** species modeling a polyethylenic growing chain was considered as starting point for both competitive pathways, in analogy to the previously mechanistic studies. Since the results agree with the ones referring to **1-cycle5-T** and the latter one is a resting state of the E-CO copolymerization reaction mechanism, the discussion is based on this species, for more details on **β-T** as starting species see the supplementary files.
183) It worth to note that, the alternative pathway to reach the six-membered acyl chelate complex through the isomerization of **1-Coor-CO-T** to **1-Coor-CO-C** followed by insertion of CO monomer into the metal-acyl chain bond lying trans to the phosphorus atom was ruled out for both the complexes. It is due to a high energy barrier for the isomerization step for **1-OCH_3** (almost 8 kcal mol^{-1} higher with respect to the insertion) and to the consequent formation of an energy sink along the pathway for **Drent** catalyst, for more details see the alternative pathways in the supplementary files.
184) Cavell, K. J. Coord. Chem. Rev. **1996**, 155, 209–243.

Acknowledgements

Al termine di questo percorso un ringraziamento speciale va alle persone che mi hanno accompagnato in questi anni ricchi di esperienze ed emozioni.

Innanzitutto vorrei ringraziare la Prof. Caporaso, che ha creduto in me fin dai tempi della tesi di laurea, mi ha spronata a continuare nel campo della ricerca e mi ha insegnato ad amare l'infinito mondo dei polimeri. Ha fatto sì che potessi collaborare con diversi gruppi di ricerca, facendomi crescere anche come persona oltre che lavorativamente, aiutandomi a superare insicurezze e timidezza.

Ringrazio la Dr. Falivene, che mi ha sostenuta incondizionatamente negli inevitabili momenti di scoraggiamento, guidandomi verso lo spiraglio di luce che trapelava dalle porte aperte insieme e svelandomi il mezzo più potente per risolvere i problemi della chimica computazionale.

Ringrazio il Prof. Mecking per avermi dato la possibilità di lavorare in sintonia con il suo gruppo di ricerca sulla chimica dei polimeri, interessandosi sempre allo stato di avanzamento delle mie ricerche.

Ringrazio le Dott. Ida, Rosaria, Amalia e Assunta, per avermi fatto compagnia negli innumerevoli pranzi con risate a crepapelle, sorseggiando sempre un "ottimo" caffè.

Ringrazio le Dott. Rosita, Arianna e Concetta, conosciute dal primo giorno che ho messo piede in questa Università. Nonostante le nostre strade hanno intrapreso diramazioni tutte diverse, sono sempre pronte ad appoggiarmi ed accompagnarmi in ogni mia scelta. In particolare, ringrazio la Dott. Arianna, con la quale sento di essere legata da un rapporto di profonda amicizia.

Ringrazio la mia grande Famiglia per essermi stata sempre vicina e per l'affetto dimostratomi, sostenendomi moralmente per aiutarmi a vincere le grandi scommesse della vita.

Ed infine, ma non ultimo, un ringraziamento va alla mia Famiglia, ai miei tre Uomini, per l'amore incommensurabile e incondizionato che mi dimostrano ogni giorno. Un grazie "speciale" a Carmine per avermi supportato in tutti i miei momenti di ansia e di agitazione, senza di Te, probabilmente oggi non sarei qui. A queste tre persone che saranno sempre il mio punto di riferimento dedico questa tesi.